

# **REMOTE ONLINE PERFORMANCE EVALUATION OF RADIATION MONITORS IN NUCLEAR PLANTS**

*By*

**PADI SRINIVAS REDDY**

**Enrollment No: ENGG02201104025**

**Indira Gandhi Centre for Atomic Research, Kalpakkam**

*A thesis submitted to the  
Board of Studies in Engineering Sciences*

*In partial fulfillment of requirements  
for the Degree of*

**DOCTOR OF PHILOSOPHY**

*of*

**HOMI BHABHA NATIONAL INSTITUTE**

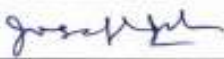



**May, 2018**

# Homi Bhabha National Institute

## Recommendations of the Viva Voce Board


As members of the Viva Voce Board, we certify that we have read the dissertation prepared by Mr Padi. Srinivas Reddy entitled "Remote Online Performance Evaluation of Radiation Monitors in Nuclear Plants." and recommend that it may be accepted as fulfilling the thesis requirement for the Degree of Doctor of Philosophy.

	21/1/19
Chairman: Prof. B. K. Panigrahi	Date:
	Jan 2, 2019
Guide/Convener: Prof. G. Amarendra	Date:
	21/1/2019
External Examiner: Prof. Joseph John, Electrical Engg. Dept., IIT Bombay	Date:
	Jan 2, 2019
Member 1: Prof. B. P. C. Rao	Date:
	21/1/19
Member 2: Prof. B. Prabhakara Reddy	Date:
	2.1.19.
Technology Advisor: Shri M. Geo Mathews	Date:

Final approval and acceptance of this thesis is contingent upon the candidate's submission of the final copies of the thesis to HBNI.

I hereby certify that I have read this thesis prepared under my/our direction and recommend that it may be accepted as fulfilling the thesis requirement.

Date: Jan 2, 2019  
Place: Kalpakkam

  
G. Amarendra  
(Guide)



## **STATEMENT BY AUTHOR**

This dissertation has been submitted in partial fulfillment of requirements for an advanced degree at Homi Bhabha National Institute (HBNI) and is deposited in the Library to be made available to borrowers under rules of the HBNI.

Brief quotations from this dissertation are allowable without special permission, provided that accurate acknowledgement of source is made. Requests for permission for extended quotation from or reproduction of this manuscript in whole or in part may be granted by the Competent Authority of HBNI when in his or her judgment the proposed use of the material is in the interests of scholarship. In all other instances, however, permission must be obtained from the author.



**(Padi Srinivas Reddy)**

## **DECLARATION**

I, hereby declare that the investigation presented in the thesis has been carried out by me.  
The work is original and has not been submitted earlier as a whole or in part for a degree/diploma at this or any other Institution / University.



**(Padi Srinivas Reddy)**

## **List of Publications arising from the thesis**

### **Journals**

- 1) "Online fault diagnostics and testing of area gamma radiation monitor using a wireless network", **Padi Srinivas Reddy**, R. Amudhu Ramesh Kumar, M. Geo Mathews and G. Amarendra, Nuclear Instruments and Methods in Physics Research A, vol. 859, pp. 23-30, 2017.
- 2) "Remote online performance evaluation of photomultiplier tube and electronics of DPCAM", **Padi Srinivas Reddy**, R. Amudhu Ramesh Kumar, M. Geo Mathews and G. Amarendra, IEEE Transactions on Nuclear Science, vol. 64, 11, pp. 2843-2853, 2017.
- 3) "Design and development of enhanced criticality alarm system for nuclear applications", **Padi Srinivas Reddy**, R. Amudhu Ramesh Kumar, M. Geo Mathews and G. Amarendra, Nuclear Engineering and Technology, vol. 50, pp. 690-697, 2018.

### **Conferences**

- 1) "Reliability enhancement of criticality alarm system in CORAL", **Padi Srinivas Reddy**, R. Anbarasan, R. Amudhu Ramesh Kumar, P. Vijayasekaran, Geo Mathews and P. Swaminathan, Proceedings of the nineteenth national symposium on Radiation Physics Research and Application of Radiation Physics, December 12-14, 2012, Mamallapuram, Tamilnadu, India.
- 2) "Integration of radiation monitors through ethernet communication with recorder and SCADA", M Swapna, Satheesh Kumar RV, **Padi Srinivas Reddy**, Sandeep PC, MS Gopikrishna, P Vijayasekaran, Reuben Daniel and Geo Mathews, CSIR sponsored Control Instrumentation System Conference (CISCON-2013), December 2013, Manipal Institute of Technology, Coimbatore, Tamilnadu, India.

- 3) "Technique to ensure the reliability of criticality alarms", Amudhu Ramesh Kumar, R. Anbarasan, **Padi Srinivas Reddy**, Geo Mathews and P. Swaminathan, Proceedings of the thirty-first IARP national conference on Advances in Radiation Measurement Systems and Techniques, March 19-21, 2014, Anushakthi Nagar, Mumbai, India.
- 4) "Fault Diagnosis Method for Area Gamma Monitors in Nuclear Facilities", **Padi Srinivas Reddy**, R. Amudhu Ramesh Kumar, M. Geo Mathews and G. Amarendra, Proceedings of the international conference on Radiological Safety in Workplace, Nuclear Facilities and Environment, February 22-25, 2016, Anupuram, Tamilnadu, India.
- 5) "Design and Development of Finite Impulse Test (FIT) Facility for Criticality Alarm System", Amudhu Ramesh Kumar. R, **Padi Srinivas Reddy**, Bineesh NT, Geo Mathews, and Swaminathan.P, Proceedings of the international conference on Radiological Safety in Workplace, Nuclear Facilities and Environment, February 22-25, 2016, Anupuram, Tamilnadu, India.
- 6) "Qualification of Data Acquisition System for Dose Alarm of Criticality Detection System", **Padi Srinivas Reddy**, R. Amudhu Ramesh Kumar, KP. Desheeb, P. Vijayasekaran, M. Geo Mathews and G. Amarendra, Proceedings of the international conference on Radiological Safety in Workplace, Nuclear Facilities and Environment, February 22-25, 2016, Anupuram, Tamilnadu, India.
- 7) "FPGA based online performance evaluation of nuclear radiation monitors", **Padi Srinivas Reddy**, Medidi Satya Rajesh, M. Geo Mathews and G. Amarendra, Research Scholars Meet on Material Science and Engineering of Nuclear Materials, May 7-9, 2018, Indira Gandhi Centre for Atomic Research (IGCAR), Kalpakkam, Tamilnadu, India.



(Padi Srinivas Reddy)

*I dedicate this thesis to my  
family and teachers*

## ACKNOWLEDGEMENTS

At the beginning, I would like to thank my research supervisor **Prof. G. Amarendra**, Senior Professor, Homi Bhabha National Institute, Director, Materials Science and Metallurgy Groups, IGCAR and my technology advisor **Shri Geo Mathews**, Head, Instrumentation & Control Section, Reprocessing Group, IGCAR for their invariable motivation, guidance, encouragement and fortitude during the course of my research. I would like to express my sincere gratitude to them for their supervision in many aspects including literature survey, investigational work, preparation of research articles and completion of the thesis.

I convey my heartiest gratitude to my doctoral committee Chairman **Prof. B. K. Panigrahi** and Committee members **Prof. B.P.C. Rao** and **Prof. B. Prabhakara Reddy** for their support and encouragement during my research work. My sincere gratitude is extended to **Prof. Anish Kumar**, Dean, Engineering Sciences, HBNI and **Prof. G. Sasikala**, former Dean, Engineering Sciences, HBNI for all the support rendered.

My heartfelt gratitude to **Prof. A. K. Bhaduri**, Director, IGCAR, **Dr. S. A. V. Satya Murty**, former Director, IGCAR and **Dr. A. Ravisankar**, Director, Reprocessing Group, IGCAR for their continuous support in providing an excellent environment for carrying out the research work.

I express my sincere acknowledgement to **Shri M. S. Illangovan**, former Head, Reprocessing Instrumentation Section (RIS), **Shri. P. Ramkumar**, former Head, Reprocessing Services Division (RPSD) and **Dr. R. Natarajan**, former Director, Reprocessing Group, IGCAR and **Prof. M. Sai Baba**, former Director, Resource Management Group, IGCAR for giving me the opportunity to carry out my research work.

My sincere thanks are owed to **Shri. M. Sivaramakrishna**, Head ISS, IGCAR for his valuable idea to select my research problem, **Shri. R. Amudhu Ramesh Kumar** for valuable technical discussion and guidance throughout my research work. I am also in-debt to **Shri. G. Prabhakara Rao**, **Shri. G. Venkata Kishore**, **Shri. T. Gokulakrishnan**, **Shri. Rajesh** and **Shri. Satya Rajesh** of Electronics & Instrumentation Group, IGCAR for their support on technical discussions related to the noise analysis, FPGAs and VHDL programming ideas.

It is my pleasure to thank ***Shri. R. Santhanam*** and ***Shri. A. Dhanasekaran*** of Health Physics Unit, Reprocessing Group for their support on technical discussions. I am filled with extreme joy to thank all my colleagues from Instrumentation and Control Section (I&CS), Reprocessing Group, IGCAR for their cooperation, assistance during the experimental works, system integration testing and measurements for my research work.

I express my sincere acknowledgement to ***Shri. V. Rajagopal*** of Health, Safety & Environment Group, ***Shri. Shekhar Kumar***, Head, Reprocessing Operations Division, ***Dr. S. Sukumar***, ***Dr. V. Satish Kumar***, ***Dr. Felix***, ***Dr. Desigan*** and ***Ms. A. L. Lavanya*** of Reprocessing Group, IGCAR for going through my research articles, thesis and giving me valuable suggestions during my Ph. D work.

I am deeply indebted to my Guru ***Shri. Kommera Devender Reddy Garu***, retired Headmaster, who taught me science and mathematics courses in my schooling. I express my sincere thanks to all my classmates and schoolmates.

Finally, I would like to thank my mother, ***Smt. Padi Durgamma***, my father, ***Shri Padi Laxma Reddy***, my wife, ***Smt. Padi Vidya***, my son, ***Mr Padi Jnanadeep Reddy***, my daughter ***Ms Padi Swarnitha Reddy***, all my brothers and sister who have been the source of constant inspiration and motivation throughout my life.

Thank you, everyone



**(Padi Srinivas Reddy)**



# CONTENTS

<b>ABSTRACT.....</b>	<b>vii</b>
<b>LIST OF FIGURES.....</b>	<b>x</b>
<b>LIST OF TABLES.....</b>	<b>xvi</b>
<b>LIST OF SYMBOLS.....</b>	<b>xviii</b>
<b>LIST OF ABBREVIATIONS .....</b>	<b>xix</b>
<b>CHAPTER 1 INTRODUCTION.....</b>	<b>1</b>
1.1 INTRODUCTION.....	1
1.2 DESCRIPTION OF NUCLEAR RADIATION DETECTORS .....	2
1.2.1 Gas-filled detectors .....	3
1.2.2 Scintillation detectors .....	4
1.3 DESCRIPTION OF RADIATION MONITORS.....	5
1.3.1 Area gamma radiation monitors (AGRM).....	5
1.3.2 Dual phosphor scintillator based continuous air monitor (DPCAM).....	5
1.3.3 Criticality alarm system (CAS).....	6
1.4 CONVENTIONAL SURVEILLANCE METHODS FOR RADIATION MONITORS.....	7
1.5 COMMUNICATION PROTOCOLS.....	7
1.5.1 Modbus protocol.....	7
1.5.2 ZIGBEE IEEE 802.15.4 Protocol.....	9
1.6 FIELD PROGRAMMABLE GATE ARRAYS (FPGA).....	10
1.7 RADIATION DATA ACQUISITION SYSTEM (RADAS).....	10
1.8 MOTIVATION FOR RESEARCH.....	12
1.9 SCOPE AND OBJECTIVE OF RESEARCH WORK.....	13
1.10 ORGANISATION OF THESIS .....	14

<b>CHAPTER 2 LITERATURE REVIEW.....</b>	<b>17</b>
2.1 LITERATURE REVIEW ONLINE SURVEILLANCE METHODS.....	17
2.1.1 Benefits of online performance evaluation methods .....	18
2.2 LITERATURE REVIEW OF ONLINE FAULT DIAGNOSTICS AND CONDITION MONITORING.....	19
2.3 ONLINE FAULT DIAGNOSTICS AND TESTING OF AREA GAMMA RADIATION MONITOR (AGRM) .....	21
2.4 ONLINE PERFORMANCE EVALUATION OF DUAL PHOSPHOR SCINTILLATOR BASED CONTINUOUS AIR MONITOR (DPCAM).....	24
2.5 ONLINE FAULT DIAGNOSTICS, TESTING AND DESIGN ENHANCEMENT OF CRITICALITY ALARM SYSTEM (CAS) .....	26
2.6 FIELD PROGRAMMABLE GATE ARRAY (FPGA) BASED ELECTRONICS FOR REMOTE ONLINE PERFORMANCE EVALUATION OF AGRAM AND DPCAM.....	30
 <b>CHAPTER 3 DEVELOPMENT OF ONLINE FAULT DIAGNOSTICS AND TESTING OF AREA GAMMA RADIATION MONITOR USING WIRELESS NETWORK.....</b>	 <b>33</b>
3.1 INTRODUCTION.....	33
3.2 SYSTEM ANALYSIS.....	35
3.2.1 GM tube and pulse processing electronics of AGRM.....	35
3.2.2 Noise analysis of GM tube and pulse processing electronics of AGRM.....	37
3.2.3 Failure modes of AGRM in an operating nuclear plant.....	41
3.3 EXPERIMENTAL STUDIES.....	45
3.3.1 Development of AGRM electronic test.....	45
3.3.2 Development of AGRM detector (GM tube) test .....	46
3.3.3 Configuration of RADAS.....	48
3.3.4 Configuration of ZigBee transceiver modules for wireless link.....	49
3.3.5 System integration.....	50

3.4	RESULTS AND DISCUSSION.....	51
3.4.1	System analysis.....	51
3.4.2	Online fault diagnostics.....	53
3.4.3	Online testing of AGRM.....	54
3.4.4	Offline testing of AGRM with a radioactive source.....	58
3.5	COMPARISON BETWEEN CONVENTIONAL AND ONLINE SURVEILLANCE METHODS OF AGRM.....	60
3.6	CONCLUSION.....	61
 <b>CHAPTER 4 DEVELOPMENT OF REMOTE ONLINE PERFORMANCE EVALUATION OF DUAL PHOSPHOR SCINTILLATOR BASED CONTINUOUS AIR MONITOR.....</b>		
4.1	INTRODUCTION.....	62
4.2	EXPERIMENTAL SETUP.....	64
4.2.1	Brief description of the experimental study.....	64
4.2.2	Transmission efficiency of scintillation material.....	65
4.2.3	Calibration of DPCAM using alpha-beta radioactive sources.....	65
4.2.4	Testing of DPCAM with LED light pulses.....	67
4.3	DESIGN AND DEVELOPMENT OF DPCAM TEST CIRCUIT.....	69
4.4	CONFIGURATION OF DEDICATED RADAS FOR ONLINE PERFORMANCE EVALUATION.....	71
4.4.1	Configuration of RADAS and system integration.....	71
4.5	ONLINE TESTING AND PERFORMANCE EVALUATION.....	74
4.5.1	Online testing of DPCAM with fresh filter paper.....	74
4.5.2	Online performance evaluation of DPCAM.....	75
4.6	RESULTS AND DISCUSSION.....	75
4.6.1	Pulse amplitude (V) versus CPM characteristics.....	75

4.6.2	Pulse width ( $\mu$ s) versus CPM characteristics.....	78
4.6.3	Selection of suitable LED.....	80
4.6.4	Frequency (Hz) versus CPM characteristics.....	80
4.7	FINE TUNING OF DPCAM TEST CIRCUIT FOR CIR LED AND PERFORMANCE EVALUATION.....	81
4.8	ONLINE TEST RESULTS OF DPCAM.....	84
4.8.1	Periodical online performance evaluation.....	85
4.9	ONLINE PERFORMANCE EVALUATION AND VALIDATION OF SYSTEM IN THE FIELD.....	85
4.10	COMPARISON BETWEEN CONVENTIONAL AND ONLINE SURVEILLANCE METHODS .....	87
4.11	CONCLUSION.....	88
 <b>CHAPTER 5 DEVELOPMENT OF ONLINE FAULT DIAGNOSTICS, ONLINE TESTING AND DESIGN ENHANCEMENT OF CRITICALITY ALARM SYSTEM.....</b>		<b>90</b>
5.1	INTRODUCTION.....	92
5.2	CONVENTIONAL CAS DESIGN.....	92
5.3	DESIGN ENHANCEMENTS IN CAS.....	93
5.3.1	FMEA of CAS.....	93
5.4	METHOD DEVELOPED FOR ONLINE CHANNEL LOOP FUNCTIONALITY TEST.....	98
5.4.1	Development of online channel loop functionality test circuit.....	99
5.5	METHOD DEVELOPED FOR DOSE ALARM TEST.....	100
5.6	DESIGN ENHANCEMENT OF EXTERNAL SYSTEMS FOR CAS.....	101
5.6.1	Reliable power supply to CAS.....	101
5.7	DESIGN OF CRITICALITY EVACUATION HOOTER CIRCUIT.....	102
5.7.1	Criticality evacuation hooter bypass facility.....	104
5.8	CONFIGURATION OF CAS FOR ONLINE MONITORING AND TESTING.....	104

5.8.1	Validation of RADAS for dose alarm.....	106
5.9	CENTRALIZED ELECTRONIC TEST AND ALARM ANNUNCIATION.....	106
5.10	RELIABILITY ASSESSMENT OF ADDITIONAL PCBS USED IN THE CAS .....	106
5.10.1	MTBF estimation methodology.....	108
5.10.2	MTBF estimation of PCBs .....	108
5.10.3	Assumptions made during the assessment.....	109
5.11	RESULTS AND DISCUSSION.....	109
5.11.1	FMEA of CAS.....	109
5.11.2	Channel loop functional test circuit output.....	109
5.11.3	Dose alarm test using electronic transient pulse.....	111
5.11.4	Centralized online electronic test and alarm annunciation facility.....	112
5.11.5	Selection of dose alarm in RADAS.....	112
5.11.6	Enhanced CAS design along with rigorous surveillance procedures.....	114
5.11.7	Failure rate and MTBF of PCBs.....	114
5.12	COMPARISON BETWEEN CONVENTIONAL AND ONLINE SURVEILLANCE METHODS OF CAS .....	116
5.13	CONCLUSION.....	117
<b>CHAPTER 6 DEVELOPMENT OF FPGA BASED ELECTRONICS FOR REMOTE ONLINE PERFORMANCE EVALUATION OF AGRM AND DPCAM .....</b>		<b>118</b>
6.1	INTRODUCTION.....	118
6.2	MATERIALS AND METHODS .....	120
6.2.1	AGRM and performance evaluation techniques .....	120
6.2.2	DPCAM and performance evaluation techniques .....	122
6.3	FPGA ARCHITECTURE.....	123
6.3.1	Two-process design method .....	123

6.4	DESIGN AND DEVELOPMENT OF FPGA BASED ELECTRONICS .....	124
6.4.1	Global clock and reset .....	126
6.4.2	Debounce block .....	126
6.4.3	Timing controller .....	126
6.5	DIFFERENT OUTPUTS OF FPGA DESIGN .....	127
6.5.1	AGRM electronic test and frequency generation .....	127
6.5.2	AGRM detector test and voltage output .....	128
6.5.3	DPCAM alpha and beta channels test and frequency generation .....	128
6.6	DEVELOPMENT OF FPGA INTERFACE CARD .....	128
6.7	CONFIGURATION OF RADAS AND SYSTEM INTEGRATION .....	131
6.7.1	Configuration of ZigBee wireless modules and performance evaluation of wireless link .....	132
6.8	RESULTS AND DISCUSSION .....	133
6.8.1	FPGA simulation results .....	133
6.8.2	FPGA synthesis report .....	134
6.8.3	Remote online performance evaluation results of AGRM .....	135
6.8.4	Remote online performance evaluation results of DPCAM .....	139
6.9	CONCLUSION .....	140
<b>CHAPTER 7 CONCLUSION AND FUTURE DIRECTIONS .....</b>		<b>141</b>
7.1	CONCLUSION .....	141
7.2	FUTURE DIRECTIONS .....	145
<b>REFERENCES .....</b>		<b>147</b>
<b>APPENDICES - A VHDL code for FPGA module (Integrated) .....</b>		<b>155</b>
<b>APPENDICES - B VHDL synthesis report .....</b>		<b>158</b>

## ABSTRACT

---

Nuclear plants handle a large inventory of radioactive substances in varying physical forms, and have potential radiation exposure to workers. Different radiation monitors are employed for monitoring the radiation levels such as area gamma radiation monitors (AGRM), dual phosphor scintillation based continuous air monitors (DPCAM), criticality alarm systems (CAS), etc. The data from these monitors is connected to the radiation data acquisition system (RADAS) for remote monitoring and recording. This thesis focuses on the failure mode and noise analysis of GM tube & pulse processing electronics of AGRM. A new method has been developed for online fault diagnostics, testing of AGRM electronics and GM tube from the control room. Two different electronic circuits are developed, one for AGRM electronic test and another for AGRM detector test. A dedicated RADAS is configured using an open platform communications (OPC) server and supervisory control and data acquisition (SCADA) software in the server computer. The Modbus RTU protocol is used on ZigBee based wireless communication to exchange data between the server computer and field device. The real-time trend and history graphs generated in RADAS help to identify the performance of AGRM electronics and GM tube in-situ. The online AGRM electronic test helps to calculate the percentage of relative intrinsic error to verify the AGRM accuracy. Online AGRM detector test is used to check the response of the GM tube below the GM threshold voltage (320 V) and verification of plateau slope (%/100 V). The plateau slope (%/100 V) of the GM tube is expected to be within 10 (as per datasheet). The time required for online testing of both AGRM electronics and GM tube of the AGRM is less than 6 minutes. The person-hours per unit per year saved using online surveillance method are 78.9% as compared with conventional methods.

The radioactive activities of airborne particulates in the operating areas of nuclear plants are monitored continuously using the instruments such as DPCAM. This thesis also focuses on a new



method developed for remote online performance evaluation of PMT along with electronics of DPCAM from the control room. Detailed experimental investigations are carried out on the response of PMT and electronics of DPCAM by subjecting to a pulsed light source of different wavelengths using light emitting diodes (LED). A suitable LED is selected based on discrimination of alpha-beta counts by pulse amplitude technique with minimum crosstalk and minimum relative intrinsic error. A DPCAM test circuit is designed and developed for the generation of test frequency to drive the LED. Based on the experimental results, colour infrared (CIR) LED is found to be the most suitable light source. The CIR LED is able to discriminate between alpha and beta radiation using pulse amplitude discrimination technique with zero crosstalk. The optimal pulse width of 10  $\mu$ s and pulse amplitudes of 2.4 V & 1.8 V (for alpha and beta respectively) are selected for performance evaluation. The relative intrinsic error for this LED is less than + 1% in both channels with fresh filter paper. The performance evaluation is also carried out in the radiation field with loaded filter paper and different alpha-beta radioactive sources along with the pulsed light source. The maximum relative intrinsic error obtained in alpha and beta channels are + 3.1% and + 6.9% respectively. The time required for online performance evaluation of both alpha and beta channels of DPCAM is around 10 minutes. The person-hours per unit per year saved using online surveillance method are 65.8% as compared with conventional methods. Wireless communication link performance is tested in terms of received signal strength indicator (RSSI) and the packet error rate (PER). The RSSI between each node has been varied between -50 and -65 dBm and 100% packet delivery is observed.

Significant quantities of strategic nuclear fissile materials are handled in nuclear plants. In these plants, there exists, the probability of occurrence of unwanted criticality. In view of the radiological consequences of such events in terms of large radiation exposures to personnel, CAS is employed for prompt detection and alarm for such criticality events. In this thesis, a novel development of online fault diagnostics, online testing and design enhancement of criticality

alarm system for maximum availability and prevention of false criticality alarms is presented. The failure modes and effect analysis (FMEA) is carried out on each element of CAS. Based on the analysis, an online fault diagnostics circuit is developed for immediate attention in the control room to prevent such false criticality alarm. Methods for online channel loop functional test and dose alarm using transient electronic pulse are developed to ensure the functional availability of CAS. Design enhancement is also performed for the external systems that are integrated with CAS. Based on experimental studies on the discharging characteristics of the RC network, the total time taken to discharge the capacitor up to 10 mGy/h is found to be 3.04 s. The voltage equivalent of 10 mGy/h dose rate output is selected for the dose alarm set-point in RADAS. The CAS incorporated with all improvements is assembled, installed, tested, and validated in the operating nuclear plant for a period of 22000 h. The system is found to operate reliably with no false criticality alarms. Enhanced CAS designs are compatible with the intended application and the person-hours per unit per year saved using online surveillance method is 78.6% as compared with that of conventional methods.

In this thesis, development of field programmable gate array (FPGA) based electronics along with in-house developed interfacing card for remote online performance evaluation of GM tube, PMT along with its electronics using ZigBee based RADAS is demonstrated. A robust two-process very high speed integrated circuit hardware description language (VHDL) coding method is utilised to provide uniform algorithm encoding with increased abstraction level and improved readability. A Digilent Atlys Xilinx Spartan 6 LX45 FPGA board along with interface card is used in this work. Relative intrinsic error and crosstalk of FPGA based system are found to be within  $\pm 10\%$  and  $\pm 1\%$  respectively. Test frequency accuracy and timing of the FPGA is better than  $\pm 0.01\%$  of full scale from 0.1 Hz to 2000 Hz at room temperature. Techniques adopted for remote online performance evaluation of GM tube and PMT along with its electronics are meeting the system requirements.

## LIST OF FIGURES

---

Figure no.	Figure description	Page no.
Figure 1.1.	Block diagram of radiation data acquisition system	11
Figure 3.1.	GM tube and pulse processing electronics of AGRM	36
Figure 3.2.	The equivalent circuit of GM tube and pulse processing electronics of AGRM.	37
Figure 3.3.	Current noise in GM tube	38
Figure 3.4.	The equivalent circuit of GM tube with parallel resistance $R_p$ .	38
Figure 3.5.	Test frequency generation circuit for AGRM electronic test.	46
Figure 3.6.	The test frequency profile applied to the AGRM counting electronics during the AGRM electronic test.	46
Figure 3.7.	The modified high voltage generating circuit for AGRM detector test.	47
Figure 3.8.	The high voltage test profile applied to the GM tube during AGRM detector test.	48
Figure 3.9.	Configuration various parameters of radio devices using X-CTU user interfaces software.	50
Figure 3.10.	Block diagram of AGRM, ZigBee transceiver modules, and RADAS.	51
Figure 3.11.	A photograph of the developed system a) The AGRM with associated components to be located in the field. b) The SCADA based Server PC (RADAS) in the control room.	51
Figure 3.12.	During AGRM electronic calibration, the test frequency profile is applied to the AGRM counting electronics.	54
Figure 3.13.	A real-time trend graph generated in SCADA during AGRM electronic calibration under the dose rate of 250 $\mu\text{Sv/h}$ .	55

<b>Figure no.</b>	<b>Figure description</b>	<b>Page no.</b>
Figure 3.14.	Real-time trend graph generated during AGRM detector test under dose rate of 500 $\mu\text{Sv/h}$ of working GM tubes.	56
Figure 3.15.	Real-time trend graph generated during AGRM detector test under dose rate of 500 $\mu\text{Sv/h}$ of a faulty GM tube (GM6).	57
Figure 3.16.	The plateau slope (%/100V) versus dose rate characteristics of GM1 to GM6.	59
Figure 3.17.	The plateau slope (%/100V) versus dose rate characteristics of GM7 to GM13.	59
Figure 4.1.	The arrangement of Mylar film, dual phosphor scintillator and its two-dimensional view.	65
Figure 4.2.	Alpha-beta pulse discrimination logic using pulse amplitude technique, the output of discrimination logic is connected to counting and display of DPCAM.	66
Figure 4.3.	a) The pulse amplifier output waveform for a $^{241}\text{Am}$ source with high pulse amplitude. b) The pulse amplifier output waveform for a $^{90}\text{Sr}$ - $^{90}\text{Y}$ source with lower pulse amplitude.	67
Figure 4.4.	a) Proposed location of LED on PMT and a ring spacer along with the perimeter of end window. b) PMT along with LED and dual phosphor scintillator are covered by single layer of Mylar film.	68
Figure 4.5.	DPCAM test frequency generation circuit.	70
Figure 4.6.	The experimental setup for online performance evaluation of DPCAM a) Field device b) RADAS in central monitoring station.	73
Figure 4.7.	Block diagram of DPCAM, DPS probe, ZigBee wireless modules and RADAS.	73
Figure 4.8.	Counts in the alpha channel using Red color LED are $23920 \pm 70$ CPM for pulse amplitude of 1.6 V to 3.6 V.	76
Figure 4.9.	Counts in the alpha channel using Green color LED are $23920 \pm 70$ CPM for the pulse amplitude of 2.2 V to 3.6 V.	77

<b>Figure no.</b>	<b>Figure description</b>	<b>Page no.</b>
Figure 4.10.	Counts in the alpha channel using Blue color LED are $23920 \pm 70$ CPM for the pulse amplitude of 2.1V to 3.6 V.	77
Figure 4.11.	Counts in the alpha channel using CIR LED are $23920 \pm 30$ CPM for the pulse amplitude of 2.1 V to 3.6 V.	78
Figure 4.12.	Alpha channel counts in CPM of RGB and CIR LEDs at pulse amplitude of 2.4 V, a pulse width from 1 $\mu$ s to 40 $\mu$ s and test frequency of 200 Hz.	79
Figure 4.13.	Beta channel counts in CPM of RGB and CIR LEDs at pulse amplitude of 1.8 V, a pulse width from 1 $\mu$ s to 40 $\mu$ s and test frequency of 200 Hz.	79
Figure 4.14.	The light wavelength of CIR LED	80
Figure 4.15.	The profile of test frequency, time and pulse amplitude applied to the LED during the online performance evaluation.	82
Figure 4.16.	Signal waveforms 1) Pulse amplifier output of DPCAM electronics. 2) Corresponding input test frequency to CIR LED with pulse amplitude at 2.4 V and a pulse width of 10 $\mu$ s.	83
Figure 4.17.	Signal waveforms 1) Pulse amplifier output of DPCAM electronics. 2) Corresponding input test frequency to CIR LED with pulse amplitude at 1.8 V and a pulse width of 10 $\mu$ s.	83
Figure 4.18.	Real-time trend graphs generated during the online performance evaluation of alpha channel with fresh filter paper.	84
Figure 4.19.	Real-time trend graphs generated during the online performance evaluation of beta channel with fresh filter paper.	85
Figure 4.20.	Relative intrinsic errors in the alpha channel using test frequency alone, loaded filter paper and three different alpha sources including counts of test frequency.	86
Figure 4.21.	Relative intrinsic errors in the beta channel using test frequency alone, loaded filter paper and three different beta sources including counts of test frequency.	87

<b>Figure no.</b>	<b>Figure description</b>	<b>Page no.</b>
Figure 5.1.	Block diagram of the CAS.	93
Figure 5.2.	Early fault detection circuit.	97
Figure 5.3.	Equivalent circuit for ionization chamber.	99
Figure 5.4.	Channel loop functional test circuit.	100
Figure 5.5.	The test profile of the high voltage applied to the ionization chamber during the channel loop functional test.	100
Figure 5.6.	Ionization chamber, RC network and preamplifier circuit. Location of test input applied during the electronic and transient test.	101
Figure 5.7.	Criticality evacuation hooter circuit consists of CAS hooter bypass switches S1 to S5, CAS alarm relays RL1 to RL5 and electronic hooters H1 to H6.	103
Figure 5.8.	The centralized online electronic test facility, alarm annunciation and RADAS architecture of CAS.	105
Figure 5.9.	Developed PCBs a) Early fault detection with channel loop functional test PCB for each channel and b) early fault detection PCB for alarm module.	108
Figure 5.10.	The RADAS historical trend graph during the online channel loop functional test for three channels of CAS.	110
Figure 5.11.	Dose alarm test using transient pulse captured in the oscilloscope.	111
Figure 5.12.	The historical trend graph generated in RADAS during the dose alarm test using a transient pulse.	112
Figure 5.13.	The historical trend graph generated during the electronic test for the three channels as red, green, and blue colors.	113
Figure 5.14.	Discharge characteristics of the RC network captured in the oscilloscope to select dose alarm set-point in RADAS.	113

<b>Figure no.</b>	<b>Figure description</b>	<b>Page no.</b>
Figure 5.15.	MTBF and FIT values of an NPN Si transistor are shown at 40°C in a ground benign environment as per MIL-217F-2 using part stress reliability prediction method.	114
Figure 6.1.	The timing diagram of AGRM electronic test, during the test, LED indication and GM tube isolation relay is activated to connect constant pulse width test frequency to AGRM electronics.	121
Figure 6.2.	Voltage test pattern used to generate different high voltage from a nominal operating voltage of GM tube from 500 V to 320 V for 40 s, 450 V for 40 s, 650 V for 40 s and back to 500 V during AGRM GM tube test.	122
Figure 6.3.	The timing diagram of test frequency of constant pulse width applied to the CIR LED during the online performance evaluation of alpha & beta channels with the LED indication.	123
Figure 6.4.	Two-process design in VHDL	123
Figure 6.5.	Design architecture of FPGA module and associated interface with digital I/O module & output signals to interface card for online testing of AGRM and DPCAM.	125
Figure 6.6.	Conceptual diagram for clock division.	127
Figure 6.7.	A timing diagram for clock division module.	127
Figure 6.8.	Interface card design for signal integration from Digilent Atlys Xilinx Spartan 6 LX45 FPGA board with radiation monitors and digital I/O module for remote online testing.	130
Figure 6.9.	Block diagram of FPGA based performance evaluation system for AGRM and DPCAM.	133
Figure 6.10.	Simulation output of Modelsim during AGRM electronic test with a frequency of 1 GHz. The design signals, test trigger input, LED indication, GM tube isolation relay activation and test frequency output are shown.	134



<b>Figure no.</b>	<b>Figure description</b>	<b>Page no.</b>
Figure 6.11.	RTL schematic view generated during the synthesis of top FPGA module. The interconnections are shown with red color and various modules in green color.	135
Figure 6.12.	Experimental setup for online performance evaluation of AGRM; the AGRM, Spartan 6 FPGA board, interface card and RADAS are connected to the RS-485 network.	136
Figure 6.13.	Real-time trend graph is generated in SCADA during AGRM electronic testing using FPGA module under the dose rate of 15 $\mu\text{Sv/h}$ .	137
Figure 6.14.	Real-time trend graph generated during AGRM detector test under dose rate of 500 $\mu\text{Sv/h}$ of working GM tubes using FPGA module.	138
Figure 6.15.	Real-time trend graph generated during AGRM detector test under dose rate of 500 $\mu\text{Sv/h}$ of a faulty GM tube using FPGA module.	138
Figure 6.16.	Experimental setup for online performance evaluation of DPCAM; The DPCAM, Spartan 6 FPGA board, interface card and RADAS are connected using ZigBee based wireless network.	139
Figure 6.17.	Real-time trend graphs are generated during the online performance evaluation of alpha channel with low background counts.	140

## LIST OF TABLES

---

Table no.	Table description	Page no.
Table 2.1.	The features available in commercial AGRMs and investigations carried out for development of online fault diagnostics and online testing of AGRM using the wireless network.	23
Table 2.2.	The features available in commercial DPCAMs and investigations carried out for development of remote online performance evaluation of photomultiplier tube and electronics of DPCAM.	26
Table 2.3.	The features available in commercial CASs and investigations carried out for development of online fault diagnostics testing and design enhancement of CAS.	29
Table 2.4.	Availability of commercial FPGA based electronics, investigations carried out for new development of remote online performance evaluation of AGRM and DPCAM using FPGAs based electronics.	32
Table 3.1.	Failure modes of AGRM components for the previous seven years from September 2011 to August 2018.	42
Table 3.2.	Various Modbus tags used for online monitoring, fault diagnostics and testing of AGRM.	49
Table 3.3.	Person-hours comparison between conventional and online surveillance methods of AGRM.	60
Table 4.1.	Various Modbus tags used for online monitoring and performance evaluation of DPCAM.	72
Table 4.2.	Percentage of relative intrinsic error of CIR LED at a pulse width of 10 $\mu$ s, the pulse amplitude of 2.4V, 1.8V.	81
Table 4.3.	Person-hours comparison between conventional and online surveillance methods of DPCAM.	88
Table 5.1.	Failure mode and effects analysis of crucial elements in CAS.	95
Table 5.2.	Different Modbus tags used for data communication and online testing of CAS.	105

<b>Table no.</b>	<b>Table description</b>	<b>Page no.</b>
Table 5.3.	PCB level component failure rate and quantity of CAS channel PCB.	115
Table 5.4.	PCB level component failure rate and quantity of CAS alarm PCB.	115
Table 5.5.	Failure rate and MTBF values of additional PCBs used in CAS.	115
Table 5.6.	Person-hours comparison between conventional and online surveillance methods of CAS.	116
Table 6.1.	Various Modbus tags used for online monitoring, fault diagnostics and performance evaluation of AGRM and DPCAM.	132
Table 6.2.	Device utilisation summary of selected FPGA.	135

## LIST OF SYMBOLS

---

s	Time in seconds
% R	Percentage of relative intrinsic error
$\mu\text{Gy}$	microGray (absorbed radiation dose)
A	Ampere
Af	Acceleration factor
$A_f$	Noise co-efficient at low frequency
Ci	Capacitance
dB	decibel
dBm	Decibels relative to one milliwatt
e	Electron charge
$e_{na}$	Equivalent noise voltage of amplifier
$e_{np}$	Equivalent noise voltage of parallel resistance
$e_{ns}$	Equivalent noise voltage of series resistance
$E_a$	Activation energy (eV)
f	Frequency
G	Gain of photomultiplier tube
GND	Ground
Gy/h	Dose rate
h	Time in hour
k	Boltzmann's constant ( $8.617 \times 10^{-5}$ )
Kbps	kilobyte per second
kHz	KiloHertz
mA	milliampere
MHz	MegaHertz
mm	millimetre
mSv/h	milliSievert per hour
mV	milli volts
N	Number of photoelectrons
nm	Wavelength
R	Resistance
$t_M$	Pulse width
$\alpha$	Confidence level
$\lambda$	Failure rate
v	Degree of freedom
$T_s$	Single exponential time constant
T	Absolute temperature in Kelvin
$Q_n^2$	Equivalent noise charge

## LIST OF ABBREVIATIONS

---

AC	Alternating Current
AES	Advanced Encryption Standard
AGRM	Area Gamma Radiation Monitor
ASCII	American Standard Code for Information Interchange
BDL	Below Detection Limits
BCC	Boron Coated Counters
Bq	Becquerel
CAM	Continuous Air Monitor
CAS	Criticality Alarm System
CIR LED	Color Infra-Red Light Emitting Diode
CPM	Counts Per Minute
CPS	Counts Per Second
CRC	Cyclic Redundancy Check
DC	Direct Current
DCR	Deficiency Clearance Report
DPCAM	Dual Phosphor scintillator based Continuous Air Monitor
DR	Deficiency Report
EDH	Equipment Device Hours
ENC	Equivalent Noise Charge
EPROM	Erasable Programmable Read-Only Memory
FET	Field-Effect Transistor
FIT	Failures in Time
FMEA	Failure Mode and Effect Analysis
FPGA	Field Programmable Gate Arrays
GM tube	Geiger-Muller tube
GUI	Graphical User Interface
HTOL	High-Temperature Operating Life
HPGe	High Pure Germanium
I&C	Instrumentation & Control

IC	Integrated Circuit
IEEE	Institute of Electrical and Electronics Engineers
IFE	Institute for Energy Technology
K-o-o-N	K out of N
LCD	Liquid Crystal Display
LED	Light Emitting Diode
LLD	Lower-Level Discriminator
LRC	Longitudinal Redundancy Check
MBAP	Modbus Application Protocol
MCR	Main Control Room
MLCC	Multilayer Ceramic Capacitors
MTBF	Mean Time Between Failure
MOSFET	Metal-Oxide-Semiconductor Field-Effect Transistor
NLOS	Non-Line Of Sight
NO	Normally Open
NPP	Nuclear Power Plant
OEM	Original Equipment Manufacturer
OLM	Online Monitoring
OPC	Open Platform Communications
OS	Operating System
PIPS	Passivated Ion-implanted Planner Silicon
PCB	Printed Circuit Board
PER	Packet Error Rate
PFD	Probability of Failure on Demand
PMT	Photomultiplier Tube
QA	Quality Assurance
QC	Quality Control
RADAS	Radiation Data Acquisition System
RPS	Reactor Protection System
RSSI	Received Signal Strength Indicator
RTU	Remote Terminal Unit

SCA	Single Channel Analyzer
SCADA	Supervisory Control And Data Acquisition
SNM	Strategic Nuclear Materials
SPI	Serial Peripheral Interface
SQL	Structured Query Language
TB	Test Bench
TCP/IP	Transmission Control Protocol/Internet Protocol
TTL	Transistor-Transistor logic
ULD	Upper- Level Discriminator
UPS	Uninterruptible Power System
V&V	Verification & Validation
VHDCI	Very High Density Cable Interconnect
VHDL	Very High-Speed Integrated Circuit Hardware Description Language
X-CTU	X-Configuration & Test Utility



## INTRODUCTION

---

*Present chapter provides an overview of nuclear radiation detectors, radiation monitors, surveillance methods, communication protocols, field programmable gate arrays and radiation data acquisition systems. The motivation, the scope of the work, objective of research work and organisation of the thesis are described in this chapter.*

---

### 1.1 INTRODUCTION

Indian nuclear program adopts a closed nuclear fuel cycle concept in which fuel fabrication, reprocessing and power generation are essential components of the cycle. These nuclear plants handle large inventory of radioactive substances in varying physical & chemical forms and have a potential for radiation exposure to the plant personnel if not handled properly [1,2]. As ionizing radiations are beyond the detecting ability of human senses, monitoring through sensitive instruments is indispensable [3,4]. Moreover, limits on exposure to ionizing radiation are defined by the international and national regulatory agencies. Handling of radioactive material not only results in external exposure to the personnel but also result in the release of radioactive materials into the operating environment, which would subsequently become a source of internal contamination for the individuals. To demonstrate compliance with the limits and to ensure that Person-mSv exposures are within the prescribed levels, a comprehensive monitoring program is mandatory.

Typically, a nuclear plant has various radiation monitoring systems [1,2] such as (i) ambient radiation level monitoring (ii) airborne radioactivity monitoring (iii) personnel monitoring (iv)

radioactive contamination monitoring (both area and personnel) (v) nuclear criticality monitoring and (vi) radioactive effluent monitoring (solid, liquid and gaseous). In addition, since large inventories of strategic nuclear materials (SNM) are involved, safety, security of such materials and the plants are also ensured using SNM monitors.

The complexity of the process and the scale of operation of the plant dictate the range of radiation monitors to be employed in the nuclear plants. Adequate numbers, sensitivity and state of the art monitoring systems are evolved in the design stage of the plant. The installation and commissioning of radiation monitors are to be carried out with due approval of the regulatory authority prior to the operation of any nuclear plant. During the lifetime of the plant, the operation of all these instruments is ensured through periodic surveillance, routine calibration and rigorous quality assurance programs. The conventional surveillance method is time-consuming and labour-intensive in plants of high capacity due to a large number of monitoring instruments. Hence, innovative procedures and techniques are to be developed without compromising the safety of the plant and the operating personnel. With the advent of innovative techniques, advanced high speed, and reliable communication electronics, efficient online surveillance methods can be implemented to achieve this goal.

### 1.2 DESCRIPTION OF NUCLEAR RADIATION DETECTORS

Three types of detectors are used to detect nuclear radiation namely gas-filled, scintillation and semiconductor. In gas-filled detector, the radiations passing through a gas medium ionization create +ve ion - electrons pairs, which are collected at respective electrodes to generate voltage/current signal. In scintillation detectors, the radiation to light conversion occurs in scintillator materials, which is further used to generate radiation detection signal in conjunction with photomultiplier tube (PMT). When an energetic particle penetrates into a semiconductor, it initiates to release electrons-holes through direct interaction with the crystal, which generates the signal.

**1.2.1 Gas-filled detectors**

The process of ionization due to the passage of radiation through a medium is used in nuclear detectors. Typically, the detector consists of a closed chamber filled with gas. The chamber is a sealed cylinder with two electrodes viz., anode and cathode. These electrodes are connected to high voltage. The gas is usually an inert gas such as argon, which produces electrons and positive ions as a result of ionization. Because of the high potential at the electrodes, residual ions are attracted towards the anode and the cathode respectively. A flow of current occurs in the circuit as indicated by a meter. For a fixed high voltage across the electrodes, the current varies depending on the intensity of radiation.

**1.2.1.1 Ionization Chambers**

Ionization chamber [3,4] operates at voltages in the ionization region. It is characterised by complete collection and without gas amplification. All the electrons liberated by the passage of the ionizing radiation are either in the form of particles or photons. The electrodes of an ionization chamber are typically cylindrical with a centre electrode. The applied voltage is selected to ensure collection of all the ions. It is high enough to prevent recombination of the ions produced but still small enough to be on the plateau where current amplification does not occur. The current pulse is proportional to the number of ionizing events produced. The output signal is proportional to the particle energy dissipated in the detector. As the output signal is small, only heavy ionizing particles such as alphas, protons, fission fragments and other heavy ions are detected.

**1.2.1.2 Geiger Muller tubes**

Geiger-Muller (GM) tube [3,4,5] operates in the GM region and is illustrated by a plateau voltage that produces an avalanche of discharge throughout the tube for each ionizing radiation. This avalanche of charge produces an electrical pulse, the amplitude of which is independent of the initial ionization. The GM tube is especially useful for counting lightly ionizing radiations such as beta particles or gamma rays and is specially designed to take advantage of this effect. GM tubes

are used mainly for more penetrating beta and gamma radiations. A GM tube usually consists of a fine tungsten electrode mounted along the axis of a tube containing the mixture of 90% argon and 10% ethyl alcohol at low pressure. A high voltage of 500 V to 1000 V is applied to the tube which depends on its size. GM tube is not capable identifying the type of radiation being detected nor its energy.

### 1.2.2 Scintillation detectors

The scintillation detectors are classified into three types inorganic, organic and plastic scintillation based. Inorganic scintillation detectors have high density, high atomic number and pulse decay time is around one microsecond. It includes zinc sulfide (ZnS), sodium iodide (NaI), caesium iodide (CsI) and lithium iodide (LiI). Organic scintillation detectors are used for the detection of beta particles. It includes stilbene, naphthalene and anthracene. The decay time of this type of scintillation detector is around ten nanoseconds. Plastic scintillation detectors are made by mixing scintillation chemicals with plastic matrixes. The decay constant of this type of scintillation detector is around one nanosecond. Normally plastic scintillation detectors have high hydrogen content, so it is advantageous to detect fast neutrons and the beta particles.

#### 1.2.2.1 Dual phosphor scintillation detectors

Dual phosphor scintillators [6,7,8] are used for the detection of both alpha and beta particles. In this case, both ZnS(Ag) and plastic scintillator are sandwiched to detect alpha and beta particles simultaneously. The alpha particles interact with the ZnS(Ag) scintillator, resulting in a PMT output pulse with higher pulse amplitude. Medium and higher energy beta particles simply pass through the ZnS(Ag) and interact with the plastic scintillator giving out a PMT pulse with lower pulse amplitude than the alpha pulse. The discriminator logic is used to distinguish alpha and beta radiation pulses based on the pulse amplitude discrimination technique.

The scintillation detectors are optically coupled to a high gain PMT which converts incident light photons into photoelectrons. The photoelectron multiplication factor of PMT is of the order of  $10^6$ .

The photocathode material used in most commercial PMTs is a compound of caesium and antimony (Cs-Sb). The operation of a scintillation process is divided into two steps. At first, absorption of incident radiation energy by the scintillator and production of light photons in the visible region part of the electromagnetic spectrum. Second, multiplication of the photoelectrons from PMT is utilised for the production of the pulse output.

### 1.3 DESCRIPTION OF RADIATION MONITORS

#### 1.3.1 Area gamma radiation monitors (AGRM)

The ambient gamma radiation levels in active areas of nuclear plants are monitored continuously by wall mounted AGRM [9]. The AGRM is GM tube based monitor and provides the dose rate measurement in the range of 0.1 to 1000  $\mu\text{Sv/hr}$  with an accuracy of  $\pm 10\%$ . The AGRM is a microcontroller based counting electronics, interfaced with liquid crystal display (LCD), alarm set keypad, visual & audio alarm, detector probe, and an RS-485 communication port. The detector probe contains a GM tube, high voltage circuit, and pulse processing electronics enclosed in a thin SS enclosure. It displays the radiation dose rate locally and enables the visual & audio alarm if the dose rate level crosses the alarm-preset level. The dose rate information is also connected to the RADAS via serial communication (RS-485) for remote monitoring in the control room and recording. Presently there is no provision for online fault diagnostics and remote online performance evaluation of this system.

#### 1.3.2 Dual phosphor scintillator based continuous air monitor (DPCAM)

The radioactive nuclides of airborne particulates in the operating areas of nuclear plants are monitored continuously using DPCAM [10], in which a dual phosphors scintillator is used as a detector. In this case, both a ZnS(Ag) and a plastic scintillator are sandwiched to detect alpha-beta particles simultaneously using a single integrated filter head cum detector assembly. The DPCAM is used to detect artificial radionuclides  $^{239}\text{Pu}$ ,  $^{241}\text{Am}$ ,  $^{90}\text{Sr}$ ,  $^{90}\text{Y}$ ,  $^{131}\text{Ce}$ ,  $^{60}\text{Co}$ ,  $^{36}\text{Cl}$  along with

natural radioactivity due to short-lived radon and thoron progeny. The DPCAM electronics comprises of alpha-beta pulse discrimination logic module and microcontroller based independent counting channels. The alpha and beta pulse discrimination logic consists of pulse amplifier followed by two single channel analysers (SCA) for pulse amplitude based discrimination. The counts of alpha-beta channels are displayed independently on local display as well as remotely in control room using the RS-485 network. Presently there is no provision for remote online performance evaluation of this system.

### 1.3.3 Criticality alarm system (CAS)

CASs [11] are mandatory in nuclear plants for prompt alarm in the event of any criticality incident. CAS consists of three independent channels, and it generates criticality alarm based on 2 out of 3 logic. Each channel contains an ionization chamber, preamplifier and electronic module. The ionization chamber is a gamma-based detector, and it has a sensitivity of  $3 \times 10^{-8} \text{ A/Sv/h}$  for an operating voltage of 200 to 1000 V. The current signal from the detector is connected to RC network for equivalent voltage output. The voltage is applied to the preamplifier for further amplification up to 1 to 5 V for the dose rate display of 0.01 to 100 mGy/h. The preamplifier is an integrated FET based amplifier, and its output is connected to the electronic module. The electronic module consists of low voltage power supply, high voltage, processing electronics, display, channel visual & audio alarm indications and channel alarm relay contacts. An electronic test/reset facility is provided in the electronic module in which a test voltage of one volt is applied to the input stage of the preamplifier. It provides an equivalent dose rate of 40 mGy/h on display and testing of channel alarm. Presently, online fault diagnostics, online testing and design enhancement of CAS are not available for reliable operation and genuine criticality alarms.

### 1.4 CONVENTIONAL SURVEILLANCE METHODS FOR RADIATION MONITORS

Purpose of surveillance is to test the functionality and to verify the alarm set points of the different radiation monitors. Conventional surveillance method [12,13] of radiation monitors is performed manually, and it requires physical access to each radiation monitor performed at a different period between, once a shift to once in the year. Hence, the duration of surveillance test ranges anywhere from few minutes to several hours depending on the plant and complexity of equipment. Conventional surveillance methods adopt manually in radiation field with an electronic pulse generator, oscilloscope, multimeter, radioactive sources and mechanical tools test/calibrate the radioactive monitors. These methods suffer from a long time requirement, more person-days, high cost, loss of precision, and downtime of the instrument. It is also burden on radiological safety in terms of high person-mSv expenditure and contamination. These testing procedures detect faults after they have occurred. Sometimes, the radiation monitors remain unattended for a longer periods that lead to a reduction in safety of the plant and personnel.

### 1.5 COMMUNICATION PROTOCOLS

#### 1.5.1 Modbus protocols

Modicon developed Modbus communication protocol [14] in 1979. It applies to industrial automation and control systems. It is universal as open protocol. Industrial products such as a programmable logic controller, radiation monitors and digital I/O modules are used for the system communication. The main advantage of Modbus protocol is that it runs on all types of communication medium including twisted pair wires, Ethernet, fibre optics and wireless. The Modbus devices are provided with inbuilt memory where the plant information is stored. The memory is divided into four different parts as discrete input, discrete coil, input register and holding register. The discrete input and coil are of one bit while input register and holding register are of 16-bit size. The most commonly used communication protocols are Modbus remote

terminal unit (RTU), Modbus American standard code for information interchange (ASCII) and Modbus transmission control protocol/internet protocol (TCP/IP).

#### ***1.5.1.1 Modbus RTU protocol***

Modbus RTU [15] is a point to point open serial communication protocol. It is used as master-slave or server-client communication between the devices. In Modbus RTU, RS-232, RS-422 or RS-485 are used as a physical layer. RS-232 is a full duplex topology, which transmits and receives data simultaneously. RS-485 is a half / full duplex topology, in this case, the data transmission and receiving process carried one right after another. In Modbus RTU, the physical layer is meant for slave address, start bit and stop bit in data and cyclic redundancy check (CRC). The data link layer is intended for function code recognition or rejection and busy or resend data. Modbus RTU function code is the 32-bit floating point, and integer formats are used. In Modbus, an RTU master device sends a query to slave devices, and slave devices send a response to the query of the master according to specified code.

The format for each byte in RTU mode is 8-bit binary, hexadecimal 0–9, A–F two hexadecimal characters contained in each 8-bit field of the message. There are two types of error codes in Modbus, one is CRC and another one is longitudinal redundancy check (LRC). The CRC is used in Modbus RTU whereas LRC is used in Modbus ASCII.

#### ***1.5.1.2 Modbus TCP***

Modbus TCP [16] is client-server communication over Ethernet TCP/IP. Modbus TCP is similar to Modbus RTU that runs over Ethernet interface. In 1<sup>st</sup> step, the client sends a query request to the server, in 2<sup>nd</sup> step, this query is acknowledged or accepted by the server. In 3<sup>rd</sup> step, server decodes the request, sends responses for function code and during the 4<sup>th</sup> step, the client gives confirmation signal to the server for disconnection of TCP.



The message frame consists of MBAP (Modbus application header) of seven bytes including transaction ID, protocol ID, length of message and client ID. In Modbus TCP for server connects ID port number of the server are required to establish communication, and for a client, an IP address of the server, client ID and port number are required in the message format.

### **1.5.2 ZIGBEE IEEE 802.15.4 protocol**

In nuclear plants, the wireless networks are a novel technology with potential to enable distributed sensor tasks, especially online monitoring and control. The wireless network provides easy installation, substantial cost reduction, redundancy path for real-time nuclear systems and where processing time is one primary requirement of instrumentation & control (I&C) system design. The ZigBee [17,18] based wireless communication is preferred in this work over the other technologies like Wi-Fi, Bluetooth, Wibree, and Ultrawideband. It is mainly because of its low power consumption, considerable long range and low cost. The commercial ZigBee transceivers are provided with an integrated antenna, media access control, and physical layer inside the module. The physical layer and data link layer of ZigBee are approved by IEEE 802.15.4 standard. The primary specification of 802.15.4 is low cost and low power. It provides low complexity and simplicity. ZigBee has two different data rates, for high speed, it is 250 Kbps, and for slow-speed, it is 20 Kbps. The ZigBee transceiver modules are to be added to the wireless network using X-Configuration & Test Utility (X-CTU) software. Various parameters like 16-bit source, destination address, baud rate and encryption details are configured for 2.4 GHz of IEEE 802.15.4 Standard ZigBee transceiver modules before employing in the network. The wireless communication and signal strength between these modules are to be tested with X-CTU software. Usually, the nuclear plants are constructed with thick walls of high-density concrete to ensure the containment of radiation levels. The wireless signal penetration is tested between the wireless sensor node and the base station. The repeater nodes are to be added to the network for the robust wireless link.

**1.6 FIELD PROGRAMMABLE GATE ARRAYS (FPGA)**

In nuclear power plants, computer-based I&C systems are safety-related, subject to verification & validation (V&V) in regulations and standards. However, abundant functions and resulting complexity of software make the V&V of computer-based I&C systems time-consuming and expensive. Computer-based systems use microprocessors produced in the semiconductor industry that has shorter product life cycle compared with nuclear industry. Most microprocessors may be obsolete within few years. FPGA [19,20] has been developed in semiconductor industry in 1990. Unlike ordinary semiconductor devices, the FPGAs can be programmed after they are shipped from manufactures. Therefore, it is suited for low volume applications such as nuclear plants.

An FPGA is a semiconductor device, the HDL code embedded in the device determining its function. FPGAs operate without an operating system (OS) or complex applications that are necessary for computer-based I&C systems. FPGA based I&C systems are simpler than computer-based I&C systems, which makes V&V efforts simpler and being resolved. The FPGA vendors tend to offer long-term support of their products compared with microprocessor vendors. Considering these benefits, FPGA as a next-generation device for nuclear power plants I&C that could succeed the microprocessor systems. FPGAs are employed in radiation monitors for the non-safety and safety-related systems.

**1.7 RADIATION DATA ACQUISITION SYSTEM (RADAS)**

Supervisory control and data acquisition (SCADA) software used in this work is a standard product of M/s Iconics. Configuration of Modbus tags, alarms, and communication are carried out through a single software. The SCADA software supports 500 tags with the scan time of 100 ms. On integration, it is capable of providing fast real-time performance and accurate process monitoring and control. Parameter display is possible in the form of screen objects like a bar graph, trends, historical, displays, alarm windows, message boxes, numeric readouts, etc. Ethernet

LAN connectivity in Modbus RTU, and Modbus TCP/IP protocol is possible. Alarm annunciation is provided with colour changes, automatic report generation of alarm history with date/time sorting, alarm logging, display etc. The real-time database is capable of managing and storing all process data. The data is stored in standard database formats like Microsoft structured query language (SQL) server or Oracle. The database supports sufficient number of discrete, real, integer and string variable Modbus tag names. The database can export to/import from spreadsheets, Microsoft SQL, etc. Data logging provides for event logging of set-point adjustments. The robust, stand-alone script work facility allows the creation and management of visual basic for applications scripts. Multiple level security with username and password facilities is provided to lock the executables to prevent unauthorised modification.

In nuclear plants, the RADAS [21] is configured using OPC server and SCADA software in a server computer as shown in Figure 1.1. The data from AGRMs, WGRMs, DPCAMs, CASs, etc. are connected to the RADAS via RS-485/Ethernet/wireless for live data monitoring and recording.

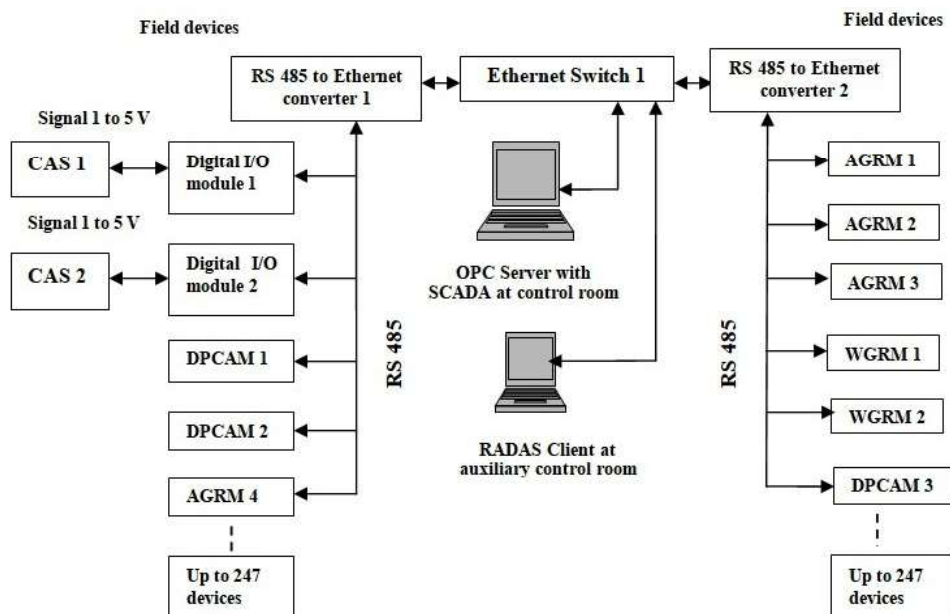


**Figure 1.1** Block diagram of radiation data acquisition system

The serial communication parameters such as device ID, port address, data bits, baud rate parity, and stop bits are configured in OPC server for communication with the field device. Different Modbus RTU tags used in field device are configured in OPC server software to update the engineering values.

### 1.8 MOTIVATION FOR RESEARCH

Nuclear plants require a large number of radiation monitoring instruments, and they spread over different zones of the plant. These instruments continuously monitor the radiological status of the plant and not only display them locally in the field but also communicate the data to the RADAS through a dedicated network for storage and archival of the data. The performance of the radiation monitors is likely to degrade over the period due to the adverse ambient conditions like temperature, humidity, radiation, shock & vibration, failure of detectors, failure of electronic components, etc. Hence, they require periodic testing and calibration. Conventionally these checks and calibrations are done manually in the radiation field [12,13] and this is highly operator dependent. In case of large plants with intense radiation monitoring systems, such works are not only labour intensive, time-consuming, involving handling of radiation sources, but also prone to operator errors. As the online performance evaluation features are not available in different commercial radiation monitors mentioned in Tables: 2.1, 2.2, 2.3 and 2.4, development of automated online performance evaluation techniques in a single step from a single point using a communication network is beneficial and becomes necessary in the view of nuclear safety [22,23,24,25,26]. With this motivation, the research work on remote online performance evaluation of radiation monitors in nuclear plants has been undertaken to meet the requirements and validated the same in the operating nuclear plant.

**1.9 SCOPE AND OBJECTIVE OF RESEARCH WORK**

The scope of the present work is to evolve engineering solutions for the remote online performance evaluation of radiation monitoring systems employed in nuclear plants. The present thesis aims at new developments that are proposed for remote online performance evaluation of different radiation monitors from the control room using emerging technologies. It includes 1) online fault diagnostics and online testing of AGRM electronics and Geiger-Muller tube using a wireless network. 2) remote online performance evaluation of photomultiplier tube along with electronics of DPCAM using the wireless network. 3) online fault diagnostics, online testing and design enhancement CAS and 4) FPGA based electronics developed for remote online performance evaluation of AGRM & DPCAM using the wireless network. The objectives of the present research work are as follows:

- To ensure continuous availability of the field radiation monitors in the nuclear plant.
- To ensure that field radiation monitors are operating as per design intent of the nuclear plant.
- To reduce the time requirement and for accurate calibration during all the states of the nuclear plant.
- To avoid field electronic calibrations using pulse generators.
- To reduce the frequency of handling of radioactive sources for calibration, thereby minimising the radiation exposure.
- To develop & qualify the off-field testing, calibration and performance evaluation techniques.
- To minimize human intervention during the surveillance of field radiation monitors.
- To qualify wireless sensor networks for deployment in the nuclear plants.
- To adapt FPGA technology for online performance evaluation of radiation monitors.

Unless such highly reliable, robust, automated, remote techniques are devised, tested and employed in operating nuclear plants, it would be difficult to meet the ever-increasing surveillance requirements by the regulatory bodies. This problem would be more severe in high throughput, integrated nuclear plants wherein large numbers of radiation monitoring systems are installed for ensuring radiological safety of the personnel and the environment. This thesis highlights the works carried out towards meeting these objectives.

### 1.10 ORGANISATION OF THESIS

The proposed thesis is divided into seven chapters. **Chapter 1** depicts a brief introduction, description of nuclear radiation detectors, radiation monitors, conventional surveillance methods, communication protocols, field programmable gate arrays and radiation data acquisition systems. The motivation, the scope of the work, the objective of research work and organisation of thesis are also discussed towards the end of this chapter.

**Chapter 2** focuses on literature review of online surveillance, benefits of online performance evaluation methods, online fault diagnostics and condition monitoring. Features available in commercial radiation monitors and novel investigations for development of remote online performance evaluation techniques for GM tube, PMT and ionization chamber based radiation monitors are also described in this chapter.

**Chapter 3** explains the new development of fault diagnostics and remote online performance evaluation techniques for GM tube based AGRM. The vital concepts of high voltage characteristics of GM tubes like a) GM threshold voltage, b) Plateau length, c) Plateau slope (% of count rate/100 V) and d) Background count rate for online performance evaluation is described. Development of electronic & detector test circuits and configuration of ZigBee based wireless network for RADAS are explained in this chapter. Descriptions of the experimental setup, online

testing of 13 GM tubes including faulty and working are discussed. Validation of the techniques using conventional radioactive source test is also described.

**Chapter 4** describes the novel development of remote online performance evaluation techniques for DPCAM. A detailed experimental investigation on the response of DPCAM subjected to a pulsed light source of different wavelengths using LEDs is presented. Development of DPCAM test circuit and configuration of ZigBee based wireless network RADAS is explained. Online performance evaluation of the prototype DPCAM using pulse amplitude discrimination technique with a light source and loaded filter paper is elaborated. The real-time trend graphs evaluation with five-point calibration, verification of relative intrinsic error and verification of crosstalk between alpha-beta channels are explained. Validation of the technique using conventional alpha-beta radioactive sources is also described.

**Chapter 5** explains the new developments of online fault diagnostics and remote online performance evaluation techniques for ionization chamber based CAS. The failure mode and effect analysis of the crucial element of CAS, techniques for early detection to prevent false criticality alarm and reliability assessment of additional PCBs used in the CAS are discussed. Development of two novel methods for channel loop functionality test and dose alarm test using electronic transient pulse are elaborated. Unique design enhancement techniques are also developed for the external systems that are integrated with CAS include a DC power supply to CAS, criticality evacuation hooter, integration & provision of different soft alert alarm set-points in RADAS and incorporation of the centralised online electronic test facility are explained in this chapter.

**Chapter 6** deals with the new development of FPGA based electronics for remote online performance evaluation of AGRM and DPCAM. The benefits of application of FPGAs in nuclear plants, the introduction of AGRM, DPCAM and performance evaluation methods are explained in

this chapter. Two-process design method, FPGA architecture and development of in-house made interface card are discussed. Simulation, synthesis and validation of VHDL code for the intended function are explained. Pin configuration of Spartan 6 LX45 FPGA development board, configuration of dedicated RADAS using ZigBee based wireless network and validation of design for the intended application is also described.

**Chapter 7** summarises the results of online performance evaluation of AGRM, DPCAM and CAS in nuclear plants. Directions for further work that needs to be carried out for research in this area are also discussed in this chapter.



## LITERATURE REVIEW

---

*The present chapter provides literature review of online surveillance methods, benefits of online performance evaluation methods, fault diagnostics and condition monitoring. Features available in commercial radiation monitors and new investigations to be carried out for development of remote online performance evaluation techniques for Geiger-Muller tube, photomultiplier tube and ionization chamber based radiation monitors are also described in this chapter.*

---

### 2.1 LITERATURE REVIEW OF ONLINE SURVEILLANCE METHODS

Online surveillance [22,24] is an automated method intended to evaluate the performance of radiation monitor from the control room and assessing its performance while the plant is operating without disturbing the monitoring channels. During evaluation, different test signals are injected to the radiation monitor based on its type through radiation data acquisition system (RADAS). The response against each test signal is compared with expected values. Performance of both electronics and detector of the radiation monitor is evaluated in terms of early fault detection, online fault diagnostics, online testing and online calibration. Three different approaches deal with early failure detection of radiation monitors 1) based on feature extraction and status classification, 2) based on time series modeling and 3) based on anomaly detection. Among these methods, anomaly detection method can quickly identify the significant deviation as compared to the expected values. Online fault diagnostic indications are provided for failure of high voltage, low voltage, detector fault, electronics fault, cable fault, etc. using Modbus tags. Online testing has ensured the functionality of the radiation monitors whereas online calibration is used to verify the accuracy within its limits. The performance evaluation metrics are different from one type of

radiation monitor to another. In case of Geiger-Muller (GM) tube based area gamma radiation monitor (AGRM), these metrics are GM threshold voltage, plateau length, plateau slope [5] and relative intrinsic error, etc. The duration of evaluation in this case is less than 6 minutes and it is based on go/no-go basis.

### **2.1.1 Benefits of online performance evaluation methods**

The proposed methods for online performance evaluation of radiation monitors present a methodology to maintain the nuclear plant safety and productivity with respect to the current calibration practices. The method reduces the number of field radioactive source calibrations required during the life of the nuclear plant. The benefits [22] of online performance evaluation techniques are as follows.

1. Continuous availability of assessment of the radiation monitor calibration status
2. Reduced duration and the person-hours required for calibration activities.
3. Reduced or no radiation exposure due to the elimination of field calibrations using pulse generator and minimize the radioactive source calibrations.
4. Reduced possibility of instrument damage during calibration.
5. Identification of abnormal plant conditions through monitoring sensor interrelationships.
6. Evaluation of radiation monitor components such as detector and counting electronics are tested for its degradation or failure.
7. Instant identification of unusual or unexpected anomalies in the process parameters of nuclear plants is possible.
8. Efficient validation of radiation monitor outputs using computer software tools.

## 2.2 LITERATURE REVIEW OF ONLINE FAULT DIAGNOSTICS AND CONDITION MONITORING

Research of online monitoring was started in the mid-years of 1980 in nuclear power plants after the invention of operating system based computers for development of fault diagnosis method, condition monitoring of instrument channels, assessment of instrument performance, etc. Later, the online testing and performance evaluation techniques are used for inspection of condition-based maintenance strategies, automating testing activities and numerous other applications. Some of the established applications of online assessment of instrument performance techniques are listed below.

P. F. Fantoni *et al.* [23] explained, online monitoring of instrument channel performance in a nuclear power plant using PEANO. PEANO is a client-server architecture, the server is connected to the process through a TCP/IP communication protocol, and the results of the validation activity are transferred to the client programs. PEANO system is an online calibration monitoring system developed in the years 1995-2001 at the Institute for energy technology (IFE), Norway. PEANO was used for online monitoring at the HBWR reactor in Halden. Online monitoring of instrument channels provide information about the condition of the monitored channels through accurate, more frequent monitoring of each channel's performance over time. This type of performance monitoring is a methodology that offers an alternative approach to traditional time-directed calibration. Online monitoring of these channels can provide an assessment of instrument performance and provide a basis for determining when adjustments are necessary. Elimination or reduction of unnecessary field calibrations can reduce associated labour costs, reduce personnel radiation exposure and reduce the potential for mis-calibration.

H.M. Hashemian [24] proposed online monitoring (OLM) technologies, new diagnostic and prognostic methods are developed to anticipate, identify, resolve equipment and process problems. The OLM techniques are used to ensure plant safety, efficiency, and immunity to

accidents. These applications include monitoring the calibration of pressure transmitters online, cross-calibrating temperature sensors in-situ, assessing equipment condition and performing predictive maintenance of reactor internals which are discussed in this work.

Jianping Ma *et al.* [13] research work mainly dealt with fault diagnosis in nuclear power plants (NPP), the framework that integrates equipment condition monitoring, and diagnostic reasoning based on pattern analysis. The research has a particular focus on applications where data collected from the existing supervisory control and data acquisition (SCADA) system is not sufficient for the fault diagnosis system. A fault diagnosis method based on semi-supervised pattern classification is developed. It is a promising tool for applications in NPPs, where it is usually difficult to obtain training data under fault conditions for a conventional fault diagnosis model.

Yong-kuo Liu *et al.* [25] stated different types of faults can occur in a nuclear power plant, and there was no direct connection between a specific fault and its symptoms. The hybrid intelligence approach is proposed for the fault diagnosis at a nuclear power plant. Different fault diagnosis technologies, such as artificial neural network, data fusion and signed directed graph, could be combined as appropriate to detect and identify different faults at a local or global level in nuclear power plants. The effectiveness of hybrid intelligence approach in improving the fault diagnosis efficiency in nuclear power plants was verified through simulation experiments.

IAEA Nuclear energy series No. N.P-T-1.1 [22] described online monitoring for improving the performance of nuclear power plants, process and component condition monitoring and diagnostics. The online monitoring data routinely collected in nuclear power plants for a variety of purposes. These data are not often trended or used for long-term predictive maintenance purposes. This report promotes the idea of trending such data and provides guidance on how this trending is performed to yield a new maintenance tool for nuclear power plants.

Mikhail Yazikov *et al.* [26] proposed a method for online fault diagnosis of analogic channels of the VVER1000/440 monitoring systems. The method is based on the analysis of the amplitude fluctuations of electrical signals at the output of analogic channels. The advantage of this method is the possibility to perform online fault diagnosis of the monitoring system during the normal operation of the nuclear power plant.

Placid Rodriguez *et al.* [27] presented an overview on some of the developments for In-Service Inspection (ISI) of nuclear power plant components using magnetic, electromagnetic and acoustic NDT methods. The potential of some of the newer techniques and philosophies to enhance the reliability of ISI are explored. Significant developments in ISI, which can be used in near future, were discussed.

Most of the online testing and performance evaluation applications encompass fault diagnosis method, condition monitoring instrument channels, assessment of instrument performance. Several researchers attempted for development of several approaches based on the above applications.

### **2.3 ONLINE FAULT DIAGNOSTICS AND TESTING OF AREA GAMMA RADIATION MONITOR (AGRM)**

Periodical surveillance, checking, testing, and calibration of the installed AGRM in the nuclear plants are mandatory. The online functional testing of AGRM counting electronics and online testing of GM tube are to be monitored periodically. Several researchers have reported the development of GM tube based radiation monitoring instruments and offline testing of GM tubes. A new remote online testing method is to be developed to meet the above requirements.

ANSI N42.3-1999 [5] IEEE standard described the test procedures, performance evaluation techniques using GM threshold voltage and plateau characteristics. Similarly, Morin. D [28] explains the investigation into the causes for the short lifetimes of GM tubes.

A.R. Jones *et al.* [29] had shown how the counts from GM tube output can be used to convert dose rate  $D$ , considering the sensitivity ( $S$ ) parameter. It is beneficial to calculate plateau slope of GM tube if the counts obtained for the fixed time, in case of the online testing method.

Marc Abilama *et al.* [30] described GM tube failures and operational characteristics. Preserving the halogen gas helps maintain the operating lifetime of the detectors. Such halogen gases are highly corrosive, and the small quantities within a gas-filled detector can deplete rapidly via interactions with surrounding materials.

IAEA Safety reports series No. 16 [12] is meant for calibration of radiation protection monitoring instruments. This safety report provides guidance on the operation of calibration facilities for radiation monitoring instruments. It reflects the current internationally accepted principles and recommended practices in calibration procedures, taking into account the significant changes and developments that had occurred over the past decade.

Rao Kalapatapu [14] explained the SCADA protocols and communication trends used for implementation of online fault diagnostics and testing GM tube based radiation monitor.

Rania Ibrahim Gomaa *et al.* [17] described the design and development of a practical small-scaled wireless sensor network (WSN) that allows smart real-time monitoring of radiation levels at nuclear facilities. GM tube used as a reliable detector for the radioactive particulates in the gaseous effluent vented from nuclear facilities. The WSN allows the operators to record and control the radiation levels emitted to the environment and it is supported by a warning system for the early detection of radiation release.

A detailed and systematic literature survey was carried out in the area of online fault diagnostics, online testing, calibration and performance evaluation techniques of AGRM from the control

room. A few commercial AGRM are provided with single frequency to test the electronics of AGRM locally. However, details related to online testing of installed AGRM electronics with three/five-point calibration and performance evaluation of its GM tube using a) GM threshold voltage, b) Plateau length, and c) Plateau slope techniques are not available in the open literature. Hence, there is a strong need to develop an online fault diagnostics and testing of AGRM to address difficulties of conventional surveillance methods. The features available in commercial AGRMs and new developments carried out are mentioned in Table 2.1.

**Table 2.1.** The features available in commercial AGRMs, investigations carried out for new development of online fault diagnostics and online testing of AGRM using wireless network.

S. No	Feature description	Features in commercial AGRMs
1	Online monitoring of dose rate	Available
2	Online alarm set-point selection	
3	Online alarm set-point monitoring	
4	Online adjustment of the calibration factor	
5	Online acknowledgement and reset	
6	Online low voltage failure diagnostics	
7	Online high voltage failure diagnostics	
8	Online cable fault diagnostics	
9	Online normal operation	
10	Configuration of fault diagnostics with RADAS	Not available  Hence, investigations are carried out for new development of online fault diagnostics and online testing of AGRM using wireless network.
11	Online three/five-point electronic test	
12	Online GM tube performance evaluation wrt plateau slope and GM threshold voltage	
13	AGRM data communication with RADAS using the wireless network	

## 2.4 ONLINE PERFORMANCE EVALUATION OF DUAL PHOSPHOR SCINTILLATOR BASED CONTINUOUS AIR MONITOR (DPCAM)

Continuous monitoring of ambient air for the presence of airborne radioactivity is a mandatory requirement in nuclear plants to be able to initiate prompt action for the protection of personnel from internal exposures. The DPCAM is an instrument to measure airborne of alpha and beta radioactivities. It is important to study different methods to ensure the reliable functionality of the PMT along with electronics of DPCAM. A unique remote online method to be developed to meet the above requirements. The following literature is available for PMT based CAMs and testing of PMTs.

L. C. Cadwallader *et al.* [31] discussed the operating experience of continuous air monitors (CAM) used in the nuclear facilities. All modes average failure rate of conventional CAMs are  $2.65 \times 10^{-5}$ /unit-h considering the power losses, faults of electronic circuits, PMT, human-related errors and mechanical faults.

Hamamatsu photonics [32] described the PMT characteristics, sensitivity and dark current are susceptible to environmental conditions such as ambient temperature, humidity and magnetic fields. To obtain the complete capabilities from a PMT, it is necessary to know how environmental conditions affect the PMT and to take corrective actions are discussed.

J.T.M. de Haas *et al.* [33] proposed three different methods to determine the intensity of weak light pulses measured with various PMTs. The methods rely on a precise determination of the response of the PMTs to the detection of a single photon. The single photon response spectra provide information on the performance of the tested PMTs during the manufacturing stage.

B. K. Seo *et al.* [8] explained the development of phoswich detector for convenient monitoring of alpha and beta contamination. There is a single detector composed of both a ZnS(Ag) scintillator



for counting alpha particles and a plastic detector for beta particles. Preparation procedure of dual phosphor for simultaneous alpha and beta counting was developed.

Subramanian Muthu *et al.* [34] described the LED light source made of red, green, and blue LEDs (RGB-LEDs) that can provide unique feature of color variability, allowing the user to select the desired color point of the lamp. The variation in lumen output and wavelength for nominally identical LEDs was discussed. Change in these parameters with temperature and time result in unacceptably high variability in the color point of white light from RGB-LEDs is also discussed.

Statewide mapping advisory committee *et al.* [35] provides a guide for understanding, interpreting and benefiting of color infrared (CIR) imagery. The light wavelength of CIR imagery varies between 500 to 900 nm, and its peak wavelength is 850 nm. CIR imagery has better penetration through atmospheric haze than normal color imagery. It can detect how an object responds to near-infrared light.

Rania Ibrahim Gomaa *et al.* [36] explained the configuration of ZigBee transceiver modules used for wireless communication and performance evaluation of wireless link. Performance of wireless link was tested in terms of the received signal strength indicator (RSSI) and the packet error rate (PER).

From the literature, the failure rate of CAM and PMT, testing of PMT with a light source, different light wavelength from RGB and CIR LEDs, Dual phosphor scintillator, performance evaluation of wireless link are discussed. The quality assurance testing of PMT, during its manufacture stage using pulsed light source is available. However, the online performance evaluation of PMT and downstream electronics of DPCAM using a pulsed light source from LED are not available. Hence, considering difficulties in conventional periodic surveillance methods, it is essential to focus research on the unique development of online performance evaluation of PMT

and electronics of DPCAM from the control room using wireless network. The features available in commercial DPCAMs and investigations carried out are mentioned in Table 2.2.

**Table 2.2.** The features available in commercial DPCAMs, investigations carried out for new development of remote online performance evaluation of PMT and electronics of DPCAM using wireless network.

S. No	Feature description	Features in commercial DPCAMs
1	Online monitoring of CPM in alpha and beta channels	Available
2	Online alpha and beta alarm set-point selection.	
3	Online alpha and beta set-point monitoring	
4	Online adjustment of the calibration factor	
5	Online acknowledgement and reset	
6	Online low voltage failure diagnostics	
7	Online high voltage failure diagnostics	
8	Online cable fault diagnostics	
9	Online normal operation indication	
10	Online testing/calibration of alpha channel	Not available  Hence, investigations are carried out for new development of remote online performance evaluation of PMT and electronics of DPCAM using wireless network.
11	Online testing/calibration of beta channel	
12	Online verification of relative intrinsic error	
13	Online verification of crosstalk between two channels	
14	DPCAM data communication with RADAS using the wireless network	

## 2.5 ONLINE FAULT DIAGNOSTICS, TESTING AND DESIGN ENHANCEMENT OF CRITICALITY ALARM SYSTEM (CAS)

CAS is mandatory in nuclear plants for prompt alarm in the event of any criticality incident. CAS generates criticality alarm based on 2 out of 3 voting logic using a relay that operates in a fail-safe

mode, i.e., the alarm relay de-energises on criticality alarm condition. Several researchers have reported the development of CAS and associated literature as mentioned below.

N. Tsujimura *et al.* [37] explained that the installation of criticality accident detectors in nuclear facilities. The detector, the Toshiba RD120, is composed of a plastic scintillator coupled to a PMT, and an operational amplifier. The alarm triggering point was set at 1.0 – 3.6 mGy/h for photon dose rate to detect the minimum accident of concern.

Y. Naito *et al.* [38] described the history of criticality research in the 50 years for accurate methods to obtain the effective multiplication factor ( $k_{eff}$ ). The main tasks were (1) the development of numerical calculation methods, (2) the enhancement of criticality safety evaluation methods, and (3) the collection of subcritical, supercritical, and critical experiment data.

V. Meenakshisundaram *et al.* [39] reported operational experiences in radiation protection in the fast reactor fuel reprocessing facility. CAS installed at CORAL is based on the detection of prompt gamma emission during a criticality incident, and it is capable of detecting criticality accidents even when detectors are placed at a distance of 30 m from an unshielded source of an accident. Each CAS comprises of three criticality monitors (ionization chamber) connected to alarm annunciation system. When any two of the three monitors of a CAS (2/3 logic) detect the dose levels exceeding the preset values for an alarm condition, criticality alarm is actuated.

B. Greenfield [40] described the purpose of a CAS to promptly detect a criticality accident and immediately trigger an audible evacuation warning to personnel. It has been shown that rapid evacuation of occupants away from the area of criticality accident can considerably reduce the dose received by personnel. Because these criticality alarm systems can save the potential lives, it is of utmost importance that they are rigorously designed. It provides instructional guide for a robust CAS design that will perform its functions with the highest reliability.

S. Sravanthi *et al.* [41] elaborated an inherently fail-safe electronic logic circuit. A failure mode effect analysis (FMEA) was performed for the circuit to systematically ensure that failure of components in postulated modes result in the fail-safe state. A prototype circuit was built to verify the results obtained from FMEA.

From the literature, it is reported that the plastic scintillation based CAS, alarm trigger point, detection of prompt gamma emission, capable of detecting criticality accidents and rapid evacuation of occupants can considerably reduce the dose received by personnel to save lives. CAS is the most important system that needs to be rigorously designed.

Similarly, maintaining such system with maximum availability and minimum false criticality alarm probability is a challenging task. Design of CAS is meant for a continuous operation such that it neither fails to detect even single criticality event nor it triggers false criticality alarm due to system failure. However, failures associated with low voltage power supply, high voltage, system on battery, battery charging/isolation diode and single channel alarm are found as primary causes for system unavailability that generates false criticality alarms. False criticality alarm not only creates a panic amongst radiation personnel but also erodes the credibility of the system, failing to react to criticality alarms promptly. Hence, there is a strong need to focus research in this area for early failure detection, online testing and design enhancing of CAS. The features available in commercial CASs and investigations carried out are mentioned in Table 2.3.

**Table 2.3.** The features available in commercial CASs and investigations carried out for new development of online fault diagnostics, online testing and design enhancement of CAS.

S. No	Feature description	Features in commercial CASs
1	Three criticality monitoring channels	Available
2	Channel mains failure indication	
3	Channel high voltage indication	
4	Channel normal operation indication	
5	The offline electronic test facility	
6	Independent battery back up	
7	Criticality alarm based on 2/3 logic	
8	Online dose rate monitoring and recording	
9	Early fault detection for the failure of CAS components	Not available  Hence, investigations are carried out for new development of online fault diagnostics, online testing and design enhancement of CAS.
10	Reliability assessment of early fault detection PCBs	
11	Online channel loop and functionality test	
12	Dose rate alarm test using transient pulse	
13	Reliable power supply to CAS	
14	Criticality evacuation hooter and bypass facility	
15	Validation of dose alarm in RADAS	
16	Centralized online test facility and alarm annunciation	

## 2.6 FIELD PROGRAMMABLE GATE ARRAY (FPGA) BASED ELECTRONICS FOR REMOTE ONLINE PERFORMANCE EVALUATION OF AGRM AND DPCAM.

The functionality of the GM tube, PMT along with its electronics is to be tested online at periodic intervals to ensure reliability. Design and development of these methods using conventional discrete electronics are time-consuming, labour intensive and low product life cycle. The development of remote online performance evaluation of GM tube, PMT along with its electronics using advanced high speed, stable, accurate, reliable electronics and higher levels of automation has become mandatory. Literature available on these area researchers is mentioned below.

Ibrahim Ahmed *et al.* [42] described safety-critical instrumentation and control (I&C) system in a nuclear power plant (NPP) and implemented on programmable logic controllers (PLCs), which plays a vital role in the safe operation of the plant. The challenges such as fast obsolescence, the vulnerability to cyber-attack, and other related issues of software systems have currently led to the consideration of FPGAs as an alternative to PLCs because of their advantages and hardware related benefits. However, safety analysis for FPGA based I&C systems and V&V assessments remain important issues to be resolved, which are now become a global research point of interests. A systematic design and verification strategies are ready-to-use in the form of model-based approaches for FPGA-based reactor protection system (RPS) that can lead to the enhancement of the design verification and validation processes.

IAEA Nuclear energy series No. NP-T-3.17 [43] reported that FPGAs are gaining increased global attention for their application in nuclear power plant I&C systems, particularly for safety, safety-related and non-safety applications. On comparing with microprocessor-based systems, FPGA based solutions are simpler, more testable, less reliant on complicated software and more comfortable to qualify for safety and safety-related applications. Also, they can offer acceptable

solutions to diversity requirements and new opportunities for cost-effective, long-term support over extended plant lifetimes.

Toshiba Corporation, Japan [44] has designed the radiation monitoring systems (RMS) using the FPGA-based circuits. The FPGA-based circuits process signals by hardware only. Hence, these system does not required a microprocessor. A hardware description language called very high speed integrated circuit hardware definition language (VHDL) is used to design the FPGA logic. If the supply of a certain type of FPGA is stopped, a different FPGA can be used. The same processing can be implemented by using the same VHDL logic. Toshiba offers radiation monitoring equipment for both non-safety and safety related applications. Available detector types are ionization chamber, scintillation counter, and solid-state. Toshiba has also developed both single channel and multi-channel FPGA-based RMS.

Jiri Gaisler [45] proposed a new 'two-process' VHDL coding method to overcome the limitations of the data flow design style. The method applies to any synchronous single-clock design, which represents the majority of all designs. The goal of the two-process method is to provide increased abstraction level with uniform algorithm encoding, clear identification of sequential logic, improved readability, simple debugging and improved simulation speed of the design. FPGAs are volatile devices, and their programming code is usually stored in dedicated flash memories for proper configuration during module power-on.

S.A.V.Satya Murty *et al.* [18] describes the hardware and software of wireless sensor network (WSN) node, deployment details of the and observations derived for the future permanent deployment. The throughput and packet drop ratio have been analysed during the normal working of the reactor. For security, 128 bit AES is enabled and tested. The results are satisfactory and give confidence to authors for further research and development of WSN technology for future nuclear reactors.

From the literature, it is reported that the challenges such as fast obsolescence, the vulnerability to cyber-attack, and other related issues of software systems have currently led to the consideration of FPGAs as an alternative to PLCs because of their advantages and hardware related benefits. FPGA based solutions can be made simpler, more testable, less reliant on complicated software and more comfortable to qualify for safety and safety-related applications. In addition, they can offer acceptable solutions to diversity requirements and new opportunities for cost-effective, long-term support over extended plant lifetimes. Availability of commercial FPGA based electronics and development of online performance evaluation of AGRM and DPCAM are mentioned in Table 2.4.

**Table 2.4.** Availability of commercial FPGA based electronics, investigations carried out for new development of remote online performance evaluation of AGRM and DPCAM using FPGA based electronics.

S. No	Feature description	Features in commercial FPGA based electronics
1	FPGA based radiation monitors	Available
2	FPGA based electronics for online performance evaluation of radiation monitors.	Not available  Hence, investigations are carried out for new development of remote online performance evaluation of AGRM and DPCAM using FPGAs based electronics.
3	FPGA based electronics for online performance evaluation and data communication with RADAS using the wireless network.	

The goal of the two-process VHDL coding method is to provide simple debugging and improved simulation speed of the design. Observations are to be noted for future permanent deployment of wireless networks of nuclear plants. Hence, focusing research on the development of FPGA based electronics for online performance evaluation of radiation monitors is beneficial.



## DEVELOPMENT OF ONLINE FAULT DIAGNOSTICS AND TESTING OF AREA GAMMA RADIATION MONITOR USING WIRELESS NETWORK

---

*The present chapter highlights the development of online fault diagnostics, testing of area gamma radiation monitors (AGRM) electronics and Geiger-Muller (GM) tube from the control room using the wireless network. The failure mode and noise analysis of GM tube & pulse processing electronics of AGRM are presented. The experimental setup, development of AGRM test circuits, the configuration of radiation data acquisition system (RADAS) using ZigBee network and system integration are discussed. Remote online testing of AGRM electronics with 13 GM tubes, offline radioactive source test for verification of accuracy, the percentage of relative intrinsic error and plateau slope are elaborated. Person-hours requirement analysis of conventional and online surveillance methods of AGRM are also described.*

---

### 3.1 INTRODUCTION

Area gamma radiation monitors (AGRM) are Geiger Muller (GM) tube based instruments for continuous monitoring of gamma radiation in and around the nuclear plants. After the invention of GM tube in 1928, the electronic technology of radiation monitors evolved from vacuum tube-based electronics to the transistor, microprocessor, microcontroller and field programmable gate array based electronics. Similarly, data communication technologies from field radiation monitor to the control room has been advanced from 4-20 mA current loop, RS-232, RS-485, Ethernet and wireless networks [17,46]. In nuclear plants, the wireless networks are a novel technology with the potential to perform distributed sensor tasks, especially online monitoring and control. The wireless network provides easy installation, substantial cost reduction, redundancy path for real-

time nuclear systems and where processing time is one primary requirement of I&C system design. The ZigBee based wireless communication is preferred in this work over the other technologies viz., Wi-Fi, Bluetooth, Wibree, and Ultra wideband. It is mainly because of its low power consumption, considerable long range coverage and low cost. The commercial ZigBee transceivers are provided with an integrated antenna, media access control, and physical layer inside the module. The AGRM provides the dose rate measurement range from 0.1 to 1000  $\mu\text{Sv/h}$  with an accuracy of  $\pm 10\%$ . The conventional method of manual surveillance of AGRM suffers from high Person-mSv expenditure, contamination, more time consumption, high cost, lack of precision and downtime of the instrument [22]. The upcoming technologies can be used for the complete fault diagnostics, online testing, and calibration [13,24] of AGRM.

The failure mode and noise analysis of GM tube & pulse processing electronics of AGRM are carried out. A new method is developed for online fault diagnostics, testing of AGRM electronics and GM tube from the control room. Two different electronic circuits are developed, one for AGRM electronic test and another for AGRM detector test. These circuits are installed in prototype AGRM. The online AGRM electronic test detects the faults associated with the pulse processing and counting electronics of the AGRM. It includes the functionality of passive components, amplifier, sensitivity [47], pulse shaping, and digital circuits. The three-point electronic calibration provides checking of the accuracy of the AGRM. The percentage of relative intrinsic error [12] is calculated at these points to verify the accuracy. The online AGRM detector test is designed based on count-rate versus applied high voltage characteristics of the GM tube. The high voltage characteristics of GM tube gives the information [5] about i) GM threshold voltage, ii) Minimum operating voltage, iii) Maximum operating voltage and iv) Recommended operating voltage. The life of GM tube depends on [30,48,49] a) GM threshold voltage, b) plateau length, c) plateau slope (% of count rate/100V) and d) background count rate. The state of the GM tube in the installed AGRM cannot be judged easily based on the background, due to the

continuous background variations in nuclear plants. The GM threshold voltage and plateau slope play a crucial role to decide the life of the GM tube. These parameters are expected to change due to vibration, high temperature, age, the chemical reaction of the primary gas, and loss of quenching mechanism [3,28] inside the GM tube.

A dedicated radiation data acquisition [21] system (RADAS) is configured using an open platform communications (OPC) server and supervisory control and data acquisition (SCADA) software in the server computer. The Modbus RTU protocol [15] is used on ZigBee based wireless communication to exchange data between server computer and field device. The Modbus protocol address tags are configured for real-time data monitoring, testing and recording in a structured query language database for every 100 ms interval. The database is used to generate reports, history trend graphs for post-analysis of radiation data and checking healthiness of AGRM. The online testing of AGRM detector test is nothing but verification of the GM threshold voltage and plateau slope in the limits. The online AGRM detector test is conducted under the dose rate of 500  $\mu\text{Sv/h}$  on thirteen GM tubes depicted as GM1 to GM13. The dose rate patterns of GM tubes, GM1, GM2, GM3, GM4, GM5, GM7, GM8, GM9, GM10, GM11, and GM12, are a similar type of working characteristics, whereas GM6 and GM13 are found to be the faulty GM tubes. Thus, real-time trend and history graphs generated in RADAS helps to identify the performance of AGRM electronics and GM tube in-situ. Person-hours requirement analysis are also carried out for conventional and online surveillance methods of AGRM.

## **3.2 SYSTEM ANALYSIS**

### **3.2.1 GM tube and pulse processing electronics of AGRM**

AGRM is a microcontroller based on counting electronics, interfaced with LCD, keypad, visual & audio alarm, detector probe, and an RS-485 communication port. The detector probe contains a GM tube, high voltage (DC) circuit, pulse amplifier, pulse height discriminator and pulse shaper

electronics enclosed in a thin stainless steel enclosure. The pulse shaper output is TTL, which is fed to the microcontroller for counting, display and remote monitoring. The GM tube and pulse processing electronics of AGRM are shown in Figure 3.1.

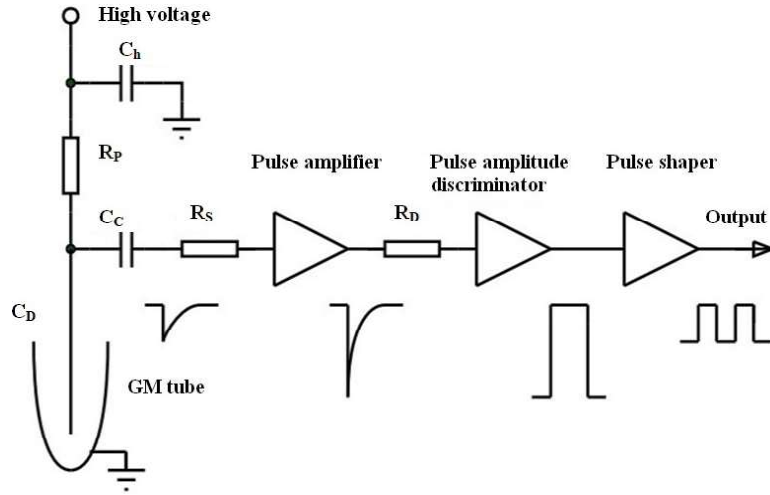


**Figure 3.1.** GM tube and pulse processing electronics of AGRM.

High voltage is applied through the resistor  $R_P$  for biasing GM tube. The bypass capacitor  $C_h$  serves as a short circuit to ground for any external high-frequency interference in the high voltage line. The coupling capacitor  $C_C$  blocks the high voltage to the input of a voltage-sensitive amplifier. If the time constant  $R_P C_D$  is very small compared to the shaping time of pulse shaper then the inherent GM tube capacitance ( $C_D$ ) is discharged through  $R_P$ . The charge  $Q_s$  is collected at GM tube and the signal voltage [50] is given by  $Q_s / (C_D + C_i)$ , where  $C_i$  is the input capacitance of pulse amplifier added with external & stray capacitances. The signal voltage of GM tube varies from few mV to hundreds of mV and it is amplified with tens of voltage gain using a pulse amplifier. Pulse amplitude discriminator is a two input level comparator. One input is connected to the pulse amplifier output and another input is connected to a reference voltage. Normally, the reference voltage is set just above the noise voltage contributed from both internal noise voltage generated in electronic components and external high-frequency noise. The output of the pulse

discriminator is the rectangular pulse of different pulse widths. Subsequently, it is shaped to TTL output with a fixed pulse width of 10  $\mu\text{s}$  using pulse shaper circuit.

### 3.2.2 Noise analysis of GM tube and pulse processing electronics of AGRM

Noise analysis [50,51,52] is carried out to quantify the signal to noise ratio of the system. Figure 3.2 shows the equivalent circuit of GM tube and pulse processing electronics of AGRM using a voltage-sensitive amplifier.

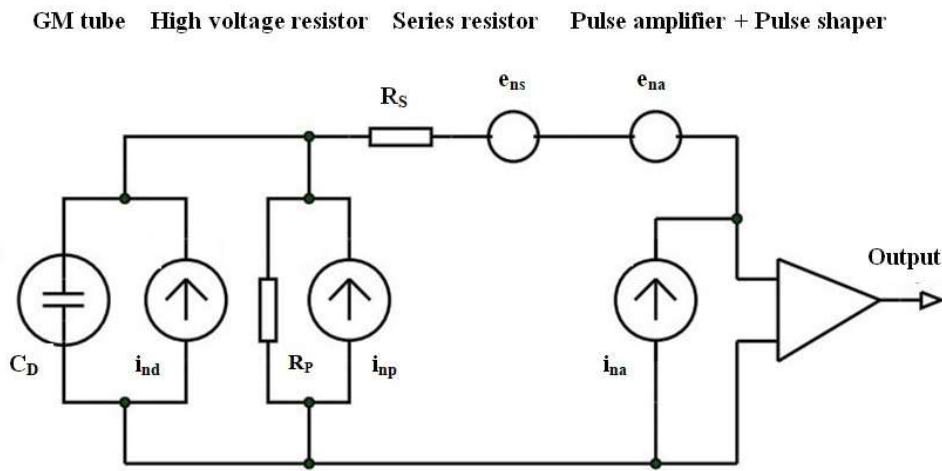


**Figure 3.2.** The equivalent circuit of GM tube and pulse processing electronics of AGRM.

The noise contributions of all the components are calculated in terms of the noise voltage at the input of the pulse amplifier. The current noise fluctuations due to the high voltage resistance ( $R_P$ ) are grounded through GM tube capacitance ( $C_D$ ). The series resistor ( $R_S$ ) represents the total resistance present in the connection from the GM tube to the output. The electronic noise of the pulse amplifier is described by a combination of voltage and current source at its input as  $e_{na}$  and  $i_{na}$  separately. The noise voltage contributed by the pulse discriminator circuit will not have any effect at the input of the pulse amplifier and hence, such noise contribution is considered as negligible. It is assumed that the input impedance of the pulse amplifier is infinite and the parallel resistance of  $R_P$  (including high voltage resistance and other shunt resistances) is much larger than

the capacitive reactance of the GM tube in the output frequency range of the pulse amplifier.

Noise analysis is carried out as per the following steps.

1. Determine the frequency distribution of the noise voltage which is available at the input of pulse amplifier from all individual noise sources.
2. Integrate over the frequency response for total noise voltage.
3. Determine the equivalent noise charge and noise voltage.

### 3.2.2.1 Noise contributions

#### A. GM tube bias current

Figure 3.3 shows the current noise (shot noise) of the GM tube represented by a current source ( $i_{nd}$ ) in parallel with  $C_D$ .

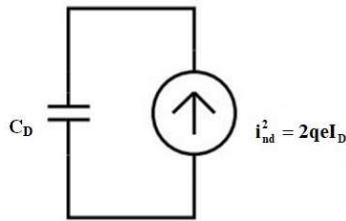


**Figure 3.3.** Current noise in GM tube.

$$i_{nd}^2 = 2qeI_D \quad (3.1)$$

#### B. Parallel resistance

The parallel resistance  $R_P$  acts as a noise current source. Figure 3.4 shows the equivalent circuit of the GM tube with  $R_P$ . The noise current flows through both the  $R_P$  and the GM tube capacitance  $C_D$ .

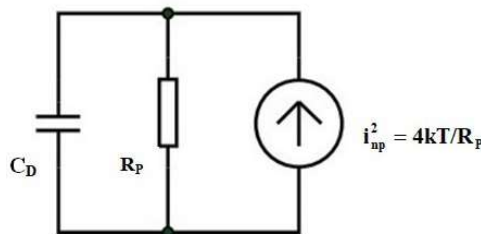


**Figure 3.4.** The equivalent circuit of GM tube with parallel resistance  $R_P$ .

$$i_{np}^2 = \frac{4kT}{R_P} \quad (3.2)$$

The noise voltage applied to the pulse amplifier input is

$$e_{np}^2 = \frac{4kT}{R_P} \left[ \frac{R_P \frac{-i}{\omega C_D}}{R_P - \frac{i}{\omega C_D}} \right]^2 \quad (3.3)$$

$$e_{np}^2 = 4kTR_P \frac{1}{[1 + (\omega R_P C_D)]^2} \quad (3.4)$$

Integrating this result overall frequencies

$$\int_0^\infty e_{np}^2(\omega) d\omega = \int_0^\infty \frac{4kTR_P}{[1 + (\omega R_P C_D)]^2} d\omega = \frac{kT}{C_D} \quad (3.5)$$

The result is independent of  $R_P$ . It is referred to as kTC noise, this contribution is often interpreted as the noise of the  $C_D$ . An ideal capacitor has no thermal noise and all noise originates in the resistors only. As  $R_P$  increases, its thermal noise increases but the noise bandwidth decreases which makes the total noise independent of  $R_P$ . On integration,  $e_{np}$  over a bandwidth-limited system, the total noise decreases with increasing  $R_P$ .

$$E_n^2 = \int_0^\infty 4kTR_P \left| \frac{G(i\omega)}{1 - i\omega R_P C_D} \right|^2 d\omega \quad (3.6)$$

### C. *Series resistance*

The equivalent input noise voltage associated with the series resistance  $R_S$  is in series with the other noise sources,

$$e_{nr}^2 = 4kTR_S \quad (3.7)$$

### D. *Pulse amplifier input noise*

The pulse amplifier noise [53] originates within the amplifier and appears at the output. It is referred to the input by dividing the output noise by the amplifier gain, where it appears as equivalent input noise voltage ( $e_{na}$ ).

$$e_{na}^2 = e_{nw}^2 + \frac{A_f}{f} \quad (3.8)$$

Where  $e_{nw}$  represents the high-frequency white noise,  $\frac{A_f}{f}$  term referred to the high frequency  $\frac{1}{f}$  noise. The amplifier noise is also added in series with the other noise sources in the circuit. Amplifiers also exhibit input current noise ( $i_{na}$ ) and its effect is the same as for the GM tube bias current.

### E. Equivalent noise charge

Two different equivalent noise sources represent the electronic noise. They are parallel & series noise sources and these are transferred to the input of pulse amplifier. The noise performance of the voltage-sensitive amplifier is usually described by the equivalent noise charge (ENC) [50,51], which is expressed in Coulombs or number of electrons. The general formula for ENC ( $Q_n^2$ ) of pulse processing electronics is

$$Q_n^2 = \left[ 2q_e I_D + \frac{4k}{R_p} + i_{na}^2 \right] * \tau_s * F_i + C_i^2 * (4kTR_s + e_{na}^2) * \frac{F_v}{\tau_s} + 4 * A_f * C_D^2 \quad (3.9)$$

Where in the first term  $q_e$  is the electron charge =  $1.6 \times 10^{-19}$ ,  $I_D$  is the GM tube current =  $4.54 \times 10^{-5}$  A,  $k$  is the Boltzmann constant =  $1.38 \times 10^{-23}$ ,  $T$  is absolute temperature in Kelvin (K),  $R_p$  is the input parallel resistance =  $1 \text{ M } \Omega$  and  $\tau_s$  is the shaping time constant =  $10 \text{ } \mu\text{s}$ . Similarly, in the second term  $C_i$  is the total input capacitance ( $C_D + C_a + C_{ei}$ ), where  $C_D$  is the GM tube capacitance =  $3 \text{ pF}$ ,  $C_a$  is the pulse amplifier input capacitance =  $4 \text{ pF}$  and  $C_{ei}$  is the external input capacitance including stray capacitances =  $100 \text{ pF}$ .  $R_s$  is the series resistance =  $2 \text{ K } \Omega$ ,  $e_{na}$  is the equivalent input noise voltage of pulse amplifier (IC CA 3140) =  $40 \text{ nV/Hz}^{1/2}$  and  $i_{na}$  is the current noise in the amplifier, which is negligible as it is a MOSFET input operational amplifier. In the third term,  $A_f$  is the noise co-efficient at low frequency =  $10^{-10} \text{ V}^2$ , the shape factors  $F_i$  &  $F_v$  are considered as 0.923 as the GM tube based systems have simple CR-RC with equal time constants. Total ENC of GM tube and pulse processing electronics of AGRM is calculated as follows.



**i) Noise current sources**

$$\text{a) GM tube current} = i_{nh}^2 = 2q_e I_D = 1.45 \times 10^{-23},$$

$$\text{b) High voltage resistor (R}_P\text{)} = i_{nP}^2 = \frac{4kT}{R_P} = 1.65 \times 10^{-26}.$$

**ii) Noise voltage sources**

$$\text{a) Series resistance (R}_S\text{)} = 4kTR_S = 3.31 \times 10^{-17},$$

$$\text{b) Pulse amplifier} = e_{na}^2 = e_{nw}^2 = (40 \times 10^{-9})^2 = 1.6 \times 10^{-15}$$

On substituting these values in the Eqn. 3.9 then the total ENC is

$$\begin{aligned} Q_n^2 = & [1.45 * 10^{-23} + 1.65 * 10^{-26}] 10 * 10^{-6} * 0.923 \\ & + 1.15 * 10^{-20} [3.31 * 10^{-17} + 1.60 * 10^{-15}] \frac{0.923}{10 * 10^{-6}} + 4 * (10^{-10}) * (3 \\ & * 10^{-12})^2 \end{aligned}$$

$$Q_n^2 = 1.35 * 10^{-28} \text{ C}$$

$$Q_n = 1.16 * 10^{-14} \text{ C}$$

$$Q_n = 72547 \text{ electrons}$$

$$\text{Noise voltage at the input of pulse amplifier (V}_n\text{)} = \frac{Q_n}{C_D + C_i} = \frac{1.16 * 10^{-14}}{107 * 10^{-12}} = 108 \mu\text{V}$$

**3.2.3 Failure modes of AGRM in an operating nuclear plant**

AGRMs are used to detect gamma dose rate in the nuclear plants. There are 25 no. of AGRMs used in an operating nuclear plant. These systems were installed in 2005 and are continuously operating 24x7 hours. During the manual surveillance, if any faults are observed in the performance of such systems, they are reported using a deficiency report (DR). A DR provides information about system ID, location, nature of the fault and maximum allowable time for rectification. Subsequently, the fault is attended within a specified period, and the actual fault is recorded on deficiency clearance report (DCR). The different failure modes of AGRM are

recorded based on the information available in DRs and DCRs for the past seven years from September 2011 to August 2018 as mentioned in Table 3.1.

**Table 3.1.** Failure modes of AGRM components for the previous seven years from September 2011 to August 2018.

S. No	Fault description	Sub-component fault or error	Fault count
1	Low voltage power supply	DC Regulators	6
2	High voltage power supply	HV Capacitor	13
3	Utility power supply	Tripping	4
4	Display	LCD Connector	5
5	Data communication	System Hang	4
6	Visual and audio alarm	Relay / LED	5
7	Electronic hardware	ICs / Components	9
8	System firmware	EPROM	2
9	Detector	GM tube	5
Total fault count			53

The upper band of all mode failure rates of similar such radiation monitors is  $1.99 \times 10^{-05}$ /unit-h and  $3.31 \times 10^{-05}$ /unit-h [31]. All mode failure rate of AGRM is calculated (as per the Table 3.1) to be  $3.2 \times 10^{-05}$ /unit-h, in this case, the failures of the utility power supply are not considered for calculation. Consider a nuclear plant using 100 AGRM units with the average failure rate of  $3.2 \times 10^{-05}$ /unit-h times 100 units, inverting the result gives approximately 313 hours for mean time between AGRM failures. It indicates that there must be a failure in every 313 hours or 13 days and it demands stringent periodical surveillance plans for early detection of such faults in favor of maximum availability of the system.

### 3.2.3.1 Failure modes of GM tubes

GM tube is a gas-filled detector used for radiation monitoring applications. A GM tube consists of a fine tungsten electrode mounted along the axis of a tube containing the mixture of 90% noble gas and 10% halogen used as a polyatomic self-quenching gas at low pressure. A high voltage of 500 V to 1000 V is applied to the tube, depending on its size. After the gas molecules in the GM tube are ionized by incident radiation, the positive ions formed will drift towards the negative cathode (wall). On reaching the cathode, the ions will then interact with the cathode and return to their neutral state by acquiring an electron. This process leaves the atom in an excited state. The atom can emit a photon having sufficient energy to cause further gas ionization. The quenching mechanism interrupts the emission of further secondary photons to reduce the spurious counting occurring to an insignificant level.

In GM tubes, the depletion of the quenching gas governs the lifetime of the detector [28,54,55]. Initially, organic quenching gas-based detectors have a limited life due to irreversible dissociation. In case of halogen quenching gas-based detectors, the gas molecules can recombine after each quench event and provides extended life. A typical GM tube initially contains approximately  $10^{20}$  polyatomic molecules [54] in the quenching gas. In this about  $10^{10}$  of molecules are ionized in each discharge and dissociate when they reach the cathode. The maximum life counts that can be detected are about  $10^{10}$  counts for a self-quenched GM tube. The drawback of using halogen gases is it gives highly reactive species on dissociation. It might deplete through interactions with surrounding materials or contamination. The different failure modes of the GM tube is discussed below.

1. Most of the self-quenching GM tubes exhibit symptoms of ageing, decrease in the GM threshold voltage, decrease in plateau length, increase in plateau slope, and multiple pulses at lower operating voltages. Some GM tubes may be brought into self-sustained discharge

above the plateau voltage and these GM tubes are not recovered when returned to the operating voltage, whereas others GM tubes are permanently damaged if brought into continuous discharge even for a moment. Most of these observations are indicate the decomposition of the quenching gas.

2. The GM tubes fail because the halogen gas gets depleted. This loss is due to reactions with the cathode and anode electrodes of GM tube. The impurities cause these reactions on materials that are not basically halogen resistant. The abrasions increase the rate of these reactions on the anode electrode caused by the vibrations.
3. Plateau starting voltage is defined as the minimum operating voltage that must be applied to the GM counter in order to detect pulses with heights of 20 mV. If this voltage is monitored during the ageing of the tube, a decrease in pulses height would be noted. This decrease is thought to be caused by a depletion of the halogen gas through reactions with the internal surfaces of the GM tube.
4. If a GM tube fails due to ageing, it means that the quench gas has exhausted in the tube. Subsequently, the GM tube goes into a continuous discharge mode. In this condition, once the GM tube starts ionization, it stays on and does not turn off. This sort of failure will happen with a long enough radiation exposure to the GM tube and go into the continuous discharge mode. The GM threshold voltage decreases with age, the plateau starts and ends at lower voltages, and its slope increases with age, and oscillations [28] are detected when the halogen content is very small.
5. The thin window ( $1$  to  $2 \text{ mg/cm}^2$ ) of the GM tube is damaged easily by contact with anything that is a sharp tool, nail or even with swarf material. It is also deteriorating or

inadvertently gets removed due to corrosive effect from the vapours of nitric acid and other organic solvents. Vibration [28] and physical impact on GM tube will damage the central anode electrode to one side, which leads to a non-uniform electric field in the tube that will affect its performance.

### 3.3 EXPERIMENTAL STUDIES

#### 3.3.1 Development of AGRM Electronic test circuit

The AGRM electronic test circuit is designed using discrete electronic components as shown in Figure 3.5. The PCB is developed as per IPC-2221A [56] and it is accepted as per IPC-A-610F [57]. The circuit contains two relays, the timer, decade counter, and an oscillator to generate test frequency. The frequency accuracy of the circuit is  $\pm 0.2\%$  of full scale from 100 Hz to 2000 Hz at room temperature. The circuit is fine-tuned for required Transistor-Transistor Logic (TTL) output, frequency, pulse width, and timing. The test frequency is applied at the input stage of AGRM counting electronics. The frequency is selected based on the sensitivity (180 CPS/ $\mu\text{Sv/h}$ ) of the GM tube. Three dose rate points are selected at 100  $\mu\text{Sv/h}$ , 500  $\mu\text{Sv/h}$ , and 900  $\mu\text{Sv/h}$ . The equivalent test frequencies at these points are 180 Hz, 900 Hz and 1620 Hz. The time interval is approximately 30 s at each step for stable dose rate on AGRM display. During the online calibration, two relays energise simultaneously, a two-pole relay (RL1) to latch the test frequency oscillator. Another single pole relay (RL2) is to disconnect the GM tube temporarily from the counting electronics. It is to avoid the background dose rate during the calibration for better accuracy. At the end of calibration test, the circuit automatically connects the GM tube for normal operation. In Figure 3.6, the profile of TTL test frequency applied to counting electronics of AGRM is shown.

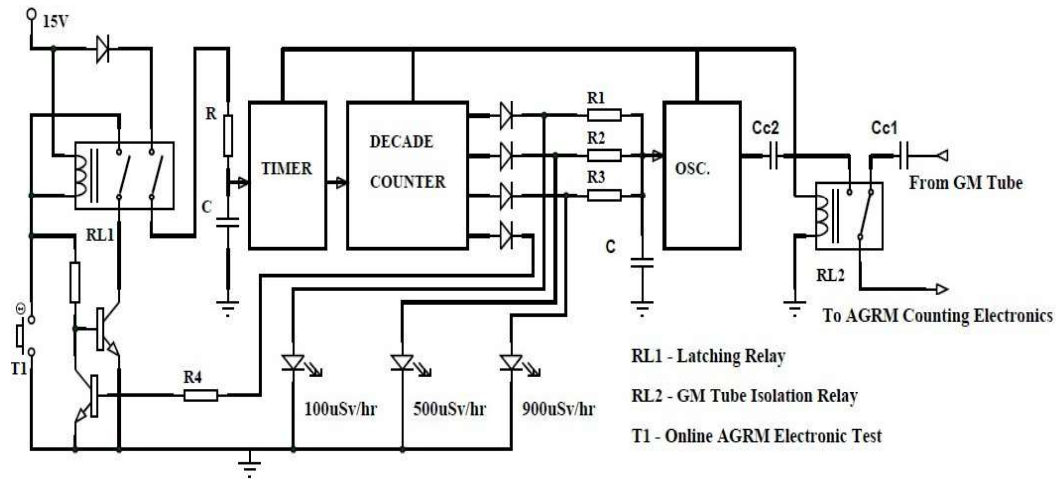


**Figure 3.5.** Test frequency generation circuit for AGRM electronic test.

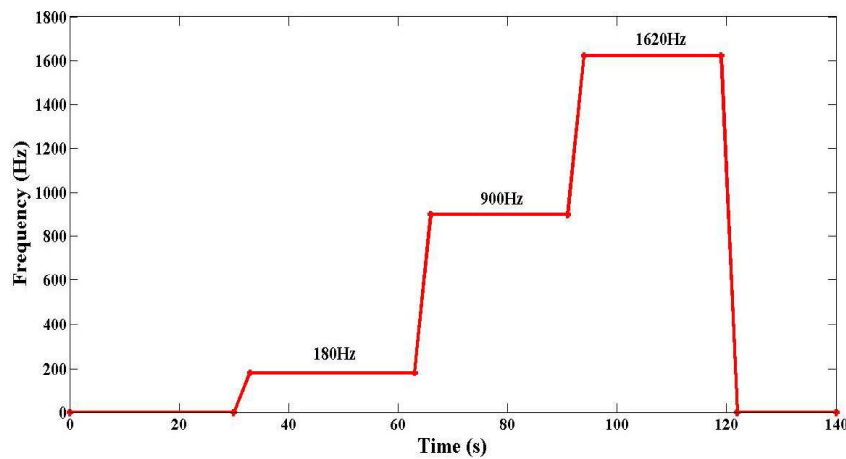


**Figure 3.6.** The test frequency profile applied to the AGRM counting electronics during the AGRM electronic test.

### 3.3.2 Development of AGRM detector (GM tube) test circuit

The state of health of GM tube in the AGRM is tested using high voltage characteristics. The conventional high voltage circuit is a DC-DC converter and provides a constant 500VDC to the GM tube for normal operation. The high voltage circuit is modified so that it generates three different high voltage outputs as per the electrical specifications of GM tube during the test. An AGRM detector test circuit is designed using discrete electronic components as shown in Figure 3.7. The PCB is developed as per IPC-2221A [56] and it is accepted as per IPC-A-610F [57]. Design of

additional electronic circuits is provided with proper protection, isolation and fail-safe features. It is also ensured that the failure of additional circuits does not degrade the performance of AGRM.

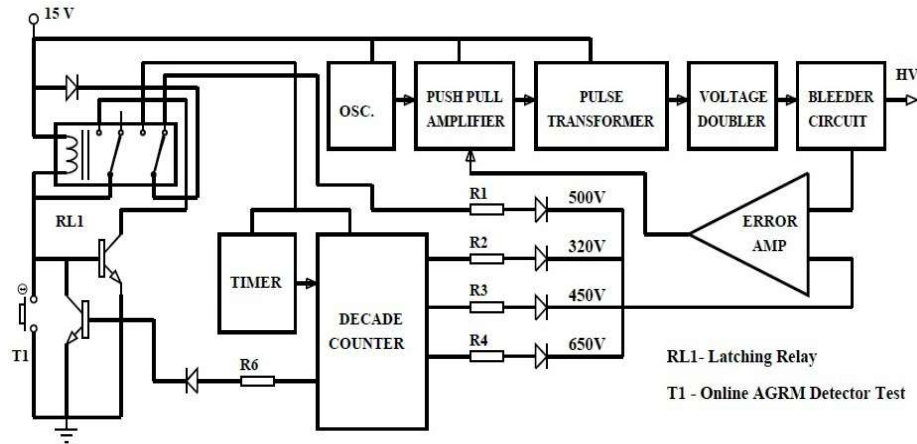


**Figure 3.7.** The modified high voltage generating circuit for AGRM detector test.

The AGRM detector test circuit consists of a two-pole relay, timer, and decade counter. The output of this circuit is connected to error amplifier to control the output high voltage. During the online AGRM detector test, a relay (RL1) is latched to activate the timer. The output of error amplifier is connected to the input of the pulse transformer through the push-pull amplifier. It is to obtain the output high voltages of 320 V, 450 V, and 650 V for the time interval of 30 to 80 s at each step. The accuracy of high voltage output is  $\pm 0.5\%$  of full scale from 320 V to 650 V at room temperature. The high voltage at 320 V is just below the GM threshold voltage (325 V), where ideally no counts are expected for a working GM tube. The high voltage at 450 V is the minimum operating voltage, and 650 V is the maximum operating voltage. At the end of the test, the circuit will automatically connects to 500 V (fail-safe design), which is the standard operating voltage of the GM tube. The mean dose rate value of the AGRM at each step is used to calculate the percentage of plateau slope. In Figure 3.8, the high voltage test profile applied to GM tube is shown.

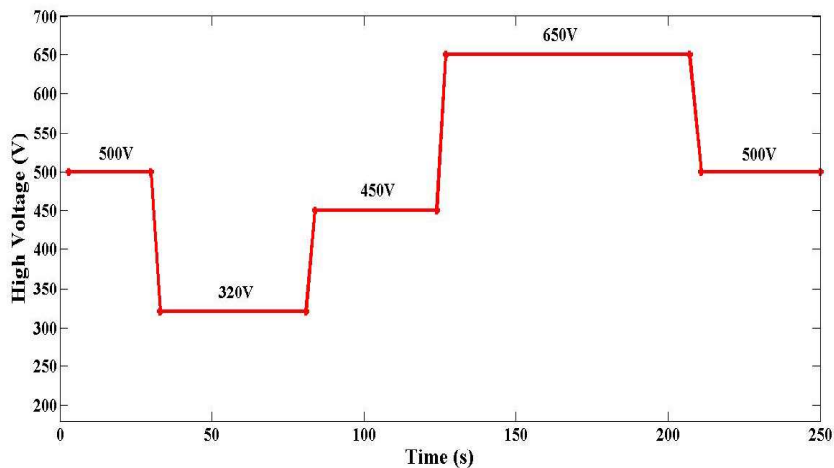


**Figure 3.8.** The high voltage test profile applied to the GM tube during AGRM detector test.

### 3.3.3 Configuration of RADAS

A dedicated RADAS is developed using OPC server and SCADA [14] software in the server computer. The prototype AGRM with test circuits is linked to the OPC server using Modbus RTU on RS-485. The required serial communication parameters like device ID, port address, baud rate, data bits, parity, stop bits are configured in OPC server for communication with the field device. A Modbus protocol supported digital output module is used to activate both AGRM electronic test and AGRM detector test circuits from RADAS. This module can be waived if the AGRM is provided with two Modbus digital outputs. Different Modbus tags are configured in OPC server software to update the current engineering values as mentioned in Table 3.2. These values are displayed as a real-time trend and recorded in the database for every 100 ms. Graphical user interface screens are developed against each Modbus tag address in SCADA. The trend graphs are created in SCADA for displaying, charting of high voltage and dose rate. The equations of the percentage of relative intrinsic error and plateau slope (%/100V) are written in SCADA for real-time numerical representation.



**Table 3.2** Various Modbus tags used for online monitoring, fault diagnostics and testing of AGRM

S. No	Tag Description	Modbus Tag Address	Data type	Client Access
1	Low voltage	300030	Word	Read Only
2	High voltage	300031	Word	Read Only
3	Dose rate	300032	Word	Read Only
4	Reset	100003	Boolean	Read/Write
5	Acknowledgement	100002	Boolean	Read/Write
6	Calibration factor	400015	Word	Read/Write
7	Alarm level	400030	Word	Read/Write
8	Alarm active	100007	Bit	Read Only
9	AGRM electronic test	400001	Boolean	Read/Write
10	AGRM detector test	400002	Boolean	Read/Write

### 3.3.4 Configuration of ZigBee transceiver modules for the wireless link

The ZigBee transceiver modules are added to the wireless network using X-Configuration & Test Utility (X-CTU) software as shown in Figure 3.9. Various parameters [58] like 16-bit source, destination address, baud rate, encryption details, etc. are configured for 2.4 GHz of IEEE 802.15.4 Standard ZigBee transceiver modules before employing in the network. The wireless communication and signal strength between these modules are tested with X-CTU software. Usually the nuclear plants are constructed with thick walls of high-density concrete to ensure the containment of radiation levels. The wireless signal penetration is tested indoor up to 20 meters from the location of the wireless sensor node and the base station.

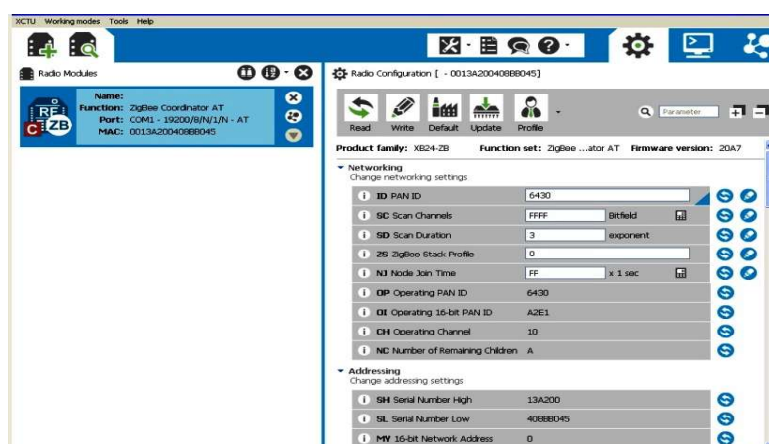


**Figure 3.9.** Configuration various parameters of radio devices using X-CTU user interfaces software.

### 3.3.5 System integration

The AGRM, digital output module and a server computer connected to an RS-485 wired network. The communication between these devices is checked in the network. The real-time updates of AGRM functionality and fault diagnostic information are checked. Both the AGRM electronic test and AGRM detector test circuits are tested online using SCADA in RADAS. The real-time trend graphs of high voltage and dose rate are generated successfully during online electronic calibration and testing of the GM tube. For wireless communication, one ZigBee transceiver module connected to AGRM via RS-485 to RS-232 converter works as a wireless sensor node. Another ZigBee transceiver module, which is connected to SCADA based server computer works as a base station as shown in Figure 3.10. The port address is configured in the server computer for communication between ZigBee transceiver modules. The AGRM transmits the data to RADAS vice-versa through the wireless communication [59,60]. The AGRM with associated components to be located in the field is shown Figure 3.11(a). The SCADA based server computer (RADAS) at the control room is shown in Figure 3.11(b).

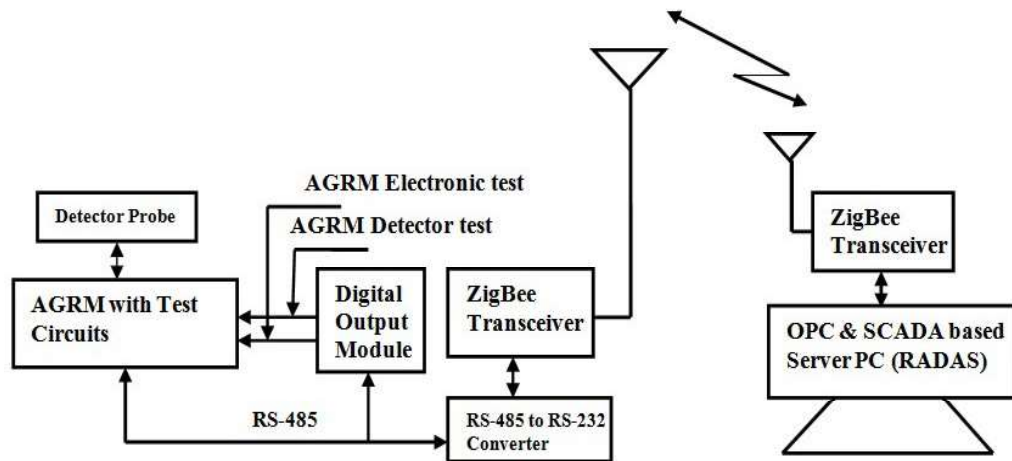


**Figure 3.10.** Block diagram of AGRM, ZigBee transceiver modules, and RADAS.

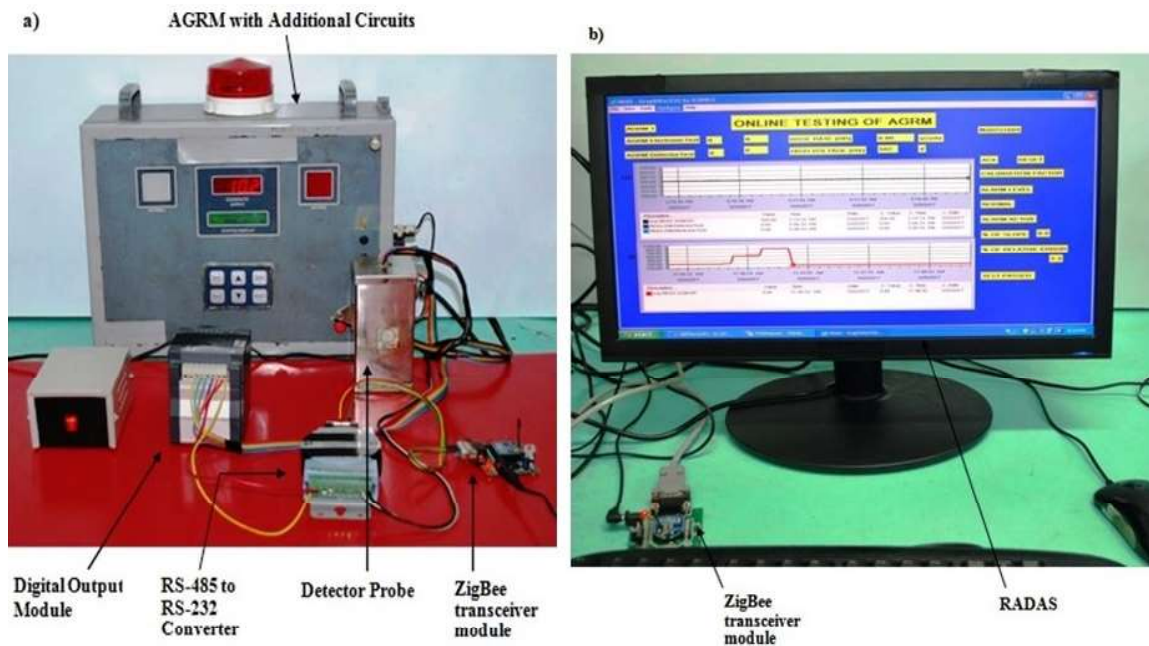


**Figure 3.11.** A photograph of the developed system a) AGRM with associated components are located in the field. b) The SCADA based server computer (RADAS) in the control room.

### 3.4 RESULTS AND DISCUSSION

#### 3.4.1 System analysis

##### 3.4.1.1 Noise analysis of GM tube and pulse processing electronics of AGRM

The noise voltage at the pulse amplifier output with a gain of eleven becomes 1.2 mV for the input noise voltage of 108  $\mu$ V. This noise voltage is further reduced by reducing  $C_{ei}$  value from

100 pF to 200 pF across the input terminals of the pulse amplifier. In this configuration, the noise voltage at the input of the pulse amplifier becomes 57  $\mu$ V. Subsequently, the noise voltage at the pulse amplifier output with the same gain becomes 0.63 mV. The pulse amplifier output signal voltage of a GM tube based system varies in the range from few mV to few hundred mV. In the pulse discrimination stage, the reference voltage of few mV is selected to discriminate such noise voltages.

From the Eqn. 3.9, it is found that the equivalent noise charge is directly proportional to the noise current contribution from GM tube and high voltage / parallel resistance ( $R_p$ ). Similarly, it is also directly proportional to the noise voltage contributions from series resistance ( $R_s$ ) and the pulse amplifier. The parameters drift of such components due to ageing results in a drastic increase in the equivalent noise charge.

#### ***3.4.1.2 Failure mode analysis of AGRM in operating nuclear plant***

##### ***3.4.1.2.1 Failure mode analysis of the HV capacitor***

From Table 3.1 it is observed that there are different modes of failure of AGRM hardware components. Out of which maximum failures are observed in the high voltage power supply wherein the 0.1  $\mu$ F/2 KV rated ceramic capacitors fail in DC voltage doubler circuit. From the study of the failure modes, it is found that the failures of such ceramic capacitors are due to electrical overstress. It is an inappropriate component selection due to which self-heating and micro-cracking within the ceramic material. Subsequently, increased leakage current causes decreased internal resistance leading to short or open. Alternately, the lower loss dielectric multilayer ceramic capacitors (MLCC) are replaced in place of existing ceramic capacitor. After that, no such failures were observed for previous  $3.2 \times 10^5$  AGRM-hours of operation.

#### **3.4.1.2.2 Failure mode analysis of the GM tubes**

The total number of GM tubes failed from September 2011 to August 2018 is five as mentioned in Table 3.1. All mode failure rate of GM tube is calculated to be  $3.26 \times 10^{-6}$ /unit-h. The failed GM tubes were analysed, and it is found that two GM tubes were failed because of the failure of the quenching mechanism due to ageing and continuous oscillations were observed. One GM tube failed due to overexposure to the radiation. In this case, it was observed that the GM tube operated in a continuous discharge mode. This GM tube was continuously working 24x7 for six years at a dose rate of 700  $\mu\text{Sv/h}$  and survived up to a maximum count of  $2.38 \times 10^{11}$ . Another two GM tubes failed in a vibration environment in which no dose rate was recorded. These GM tubes did not survive for considerable counts due to radiation. In this environment, there are six no. of industrial electric motors with exhaust fans operating with the capacity of class II (18.5kW to 75kW) and RMS vibration velocity of each motor varies from 1.8 mm/s to 2.8 mm/s (continuous operation) in the frequency bandwidth of 10 Hz - 1000 Hz.

An increased periodical surveillance helps to detect the failures of different AGRM components including ICs, DC regulators, EPROMs, HV capacitors and GM tubes. Similarly, abnormal equivalent noise charge generated in the system will also be detected. Remote online performance evaluation techniques will help to detect such component failures and bring down the system failures on demand in the nuclear plants.

#### **3.4.2 Online fault diagnostics**

In RADAS, real-time information is available for high voltage, low voltage, dose rate, reset, acknowledgement, calibration factor, alarm level, alarm active, etc. These parameters are stored in database periodically. The real-time trend graphs are generated during online calibration/test help to identify the failures in AGRM on go/no-go basis. The real-time trend graphs can also be compared with the periodical history graphs to predict the early failure and determine the

performance of AGRM. Reliable wireless communication link observed between AGRM and RADAS during the test.

### 3.4.3 Online testing of AGRM4

#### 3.4.3.1 AGRM electronic test results

The online AGRM electronic test is conducted on prototype AGRM. The real-time dose rate trend graph generated during AGRM electronic test is compared with expected dose rate. The percentage of relative intrinsic error (R) is calculated as per the Eqn. (3.10).

$$R = \left[ 1 - \frac{O}{E} \right] * 100 \quad (3.10)$$

Where O is the observed dose rate, and E is the expected dose rate. The series of average observed dose rates recorded at expected dose rates (100  $\mu$ Sv/h, 500  $\mu$ Sv/h and 900  $\mu$ Sv/h) are 109  $\mu$ Sv/h, 510  $\mu$ Sv/h and 850  $\mu$ Sv/h respectively as shown in Figure 3.12. The values of R calculated at these points are -9.8%, -2% and +5.5% respectively. The deviation in the observed dose rate can be minimised by adjusting the sensitivity (calibration factor) of the AGRM.

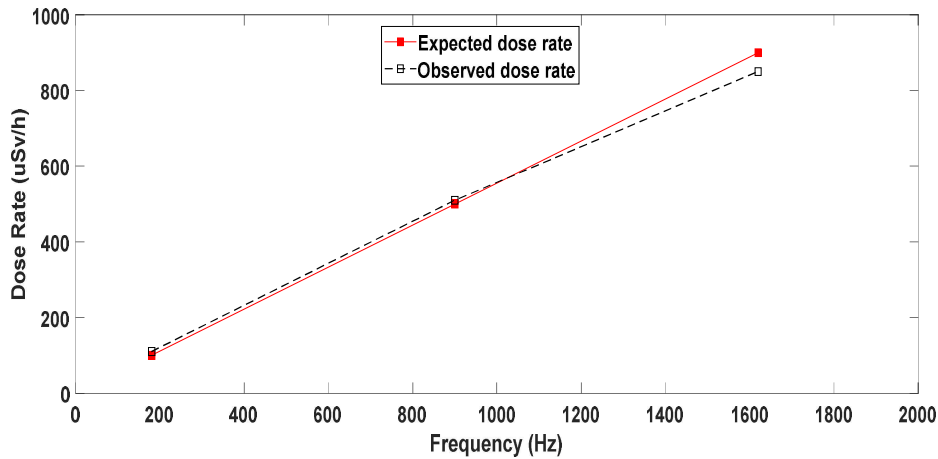


**Figure 3.12.** During AGRM electronic calibration, the test frequency profile is applied to the AGRM counting electronics. The expected dose rate corresponding to 180 Hz, 900 Hz and 1620 Hz is 100  $\mu$ Sv/h, 500  $\mu$ Sv/h and 900  $\mu$ Sv/h. The observed dose rate at these points is 109  $\mu$ Sv/h, 510  $\mu$ Sv/h and 850  $\mu$ Sv/h respectively.

The AGRM electronic calibration is studied under different dose rates using Caesium-137 gamma source at 50  $\mu\text{Sv/h}$ , 250  $\mu\text{Sv/h}$ , 500  $\mu\text{Sv/h}$  and 900  $\mu\text{Sv/h}$ . In all these cases, the real-time trend graph patterns generated are similar. The RL2 is disconnected the GM tube temporarily and re-connected at the end of the AGRM electronic calibration. A real-time trend graph generated in RADAS during AGRM electronic calibration under the dose rate of 250  $\mu\text{Sv/h}$  is shown in Figure 3.13. The maximum percentage of relative intrinsic error among three expected dose rates is displayed as a numeric value in SCADA. The high voltage graph (top graph) shows the constant 500V. In dose rate graph, after initiation of AGRM electronic test on SCADA, the GM tube is temporarily disconnected during the test, and test frequency output is connected to AGRM counting electronics. The dose rate changed (bottom graph) from 250  $\mu\text{Sv/h}$  to 100  $\mu\text{Sv/h}$ , 500  $\mu\text{Sv/h}$  and 900  $\mu\text{Sv/h}$  in the span of 30 s. At the end of the test, GM tube re-connected automatically and the dose rate observed is 250  $\mu\text{Sv/h}$ .

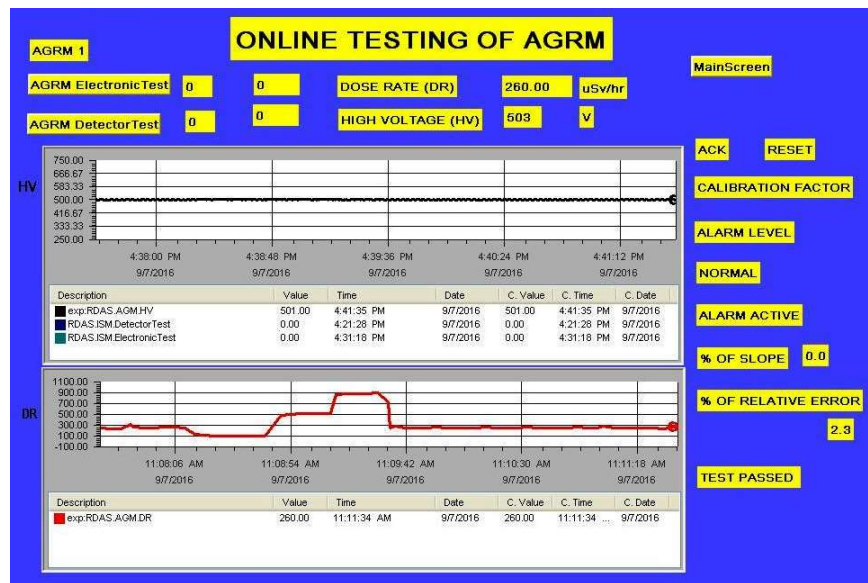


**Figure 3.13.** A real-time trend graph generated in SCADA during AGRM electronic calibration under the dose rate of 250  $\mu\text{Sv/h}$ . The high voltage graph (top graph) shows the constant 500V. The dose rate changed (bottom graph) from 250  $\mu\text{Sv/h}$  to 100  $\mu\text{Sv/h}$ , 500  $\mu\text{Sv/h}$  and 900  $\mu\text{Sv/h}$  in the span of 30 s.

### 3.4.3.2 AGRM detector test results

The online AGRM detector test is conducted under the dose rate of 500  $\mu\text{Sv/h}$  on LND 7121 GM tubes depicted as GM1 to GM13. In Figure 3.14 shows the real-time trend graph of dose rate under high voltage test profile. It is observed that the dose rate at 500V (high voltage) is 500  $\mu\text{Sv/h}$ . When high voltage (top graph) is changed to 320V (below GM threshold voltage), the dose rate (bottom graph) is zero. High voltage is increased further to 450 V, 650 V and then 500 V, the dose rate is constant at 500  $\mu\text{Sv/h}$ . It is the ideal characteristics of a working GM tube. At the end of the test, the numerical value of plateau slope displayed on SCADA is 1.5%. The dose rate patterns of GM tubes, GM1, GM2, GM3, GM4, GM5, GM7, GM8, GM9, GM10, GM11, and GM12, are a similar type of working characteristics.

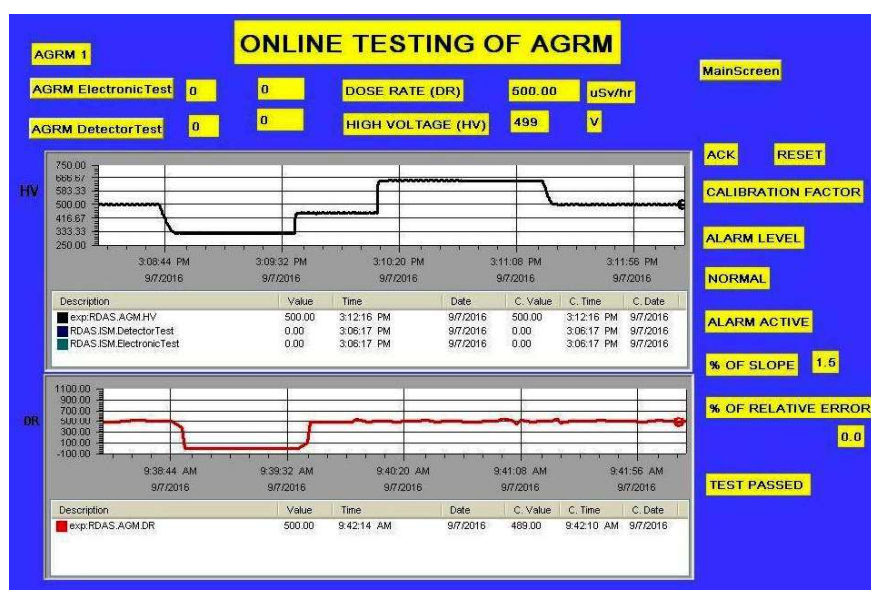


**Figure 3.14.** Real-time trend graph generated during AGRM detector test under dose rate of 500  $\mu\text{Sv/h}$  of working GM tubes. When high voltage (top graph) is changed to 320V (below GM threshold voltage), the dose rate (bottom graph) is zero. The high voltage is increased further to 450 V, 650 V and then 500 V, the dose rate is constant at 500  $\mu\text{Sv/h}$ . It is the ideal characteristics of a working GM tube.

The real-time trend graph in Figure 3.15 shows the dose rate pattern of GM6. When high voltage (top graph) is changed to 320V and up to 450 V, the dose rate (bottom graph) is constant at 100  $\mu\text{Sv/h}$  (whereas dose rate is expected to be zero for working GM tube). High voltage is changed



from 450 V to 650 V, dose rate suddenly raised to 1000  $\mu\text{Sv/h}$  (GM tube is saturated). As high voltage decreased from 650 V to 500 V, the dose rate is fallen to 500  $\mu\text{Sv/h}$ . This type of dose rate patterns indicates that it is a faulty GM tube. The plateau slope displayed on SCADA is 90.3%. The reason behind this type of fault is due to failure of quenching gas mechanism [28,48] inside the GM tubes.

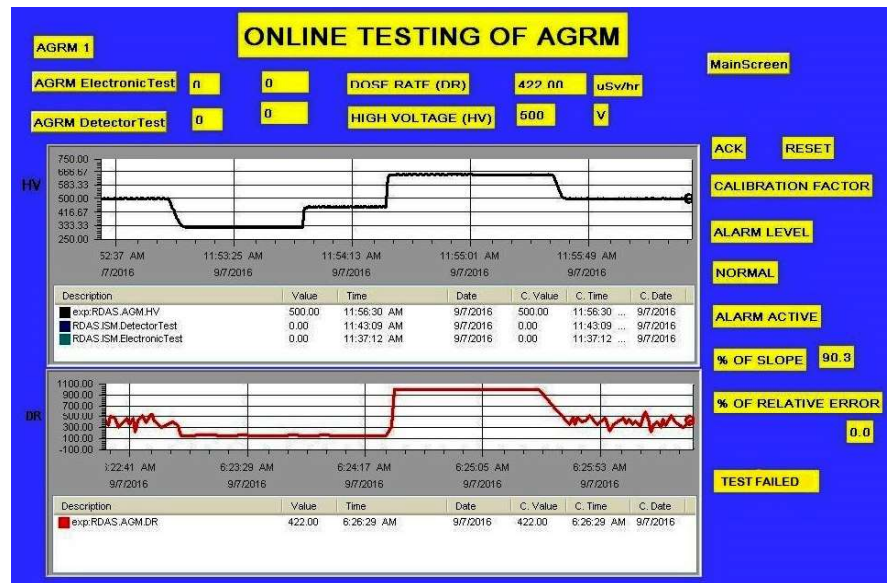


**Figure 3.15.** Real-time trend graph generated during AGRM detector test under dose rate of 500  $\mu\text{Sv/h}$  of a faulty GM tube (GM6). When high voltage (top graph) is changed to 320V and up to 450 V, the dose rate (bottom graph) is constant at 100  $\mu\text{Sv/h}$  (whereas dose rate is expected to be zero for working GM tube). High voltage is changed from 450 V to 650 V, dose rate suddenly raised to 1000  $\mu\text{Sv/h}$  (GM tube is saturated). As high voltage decreased from 650 V to 500 V, the dose rate is fallen to 500  $\mu\text{Sv/h}$ .

### 3.4.3.3 Periodical online test

Periodical online testing methods enable trend analysis of AGRM electronics and detector tests for its early failure detection. Many different techniques available [61,62,63] for trend analysis such as anomaly detection, qualitative trend analysis, shape based on a linear piece-wise time-invariant model, etc. to estimate the downtime of the system.

### 3.4.4 Offline testing of AGRM with a radioactive source

The detailed experimental study is made on the plateau slope of GM tubes GM1 to GM13 at different dose rate levels in the stable background environment. The experiments are conducted at 5  $\mu\text{Sv/h}$ , 50  $\mu\text{Sv/h}$ , 100  $\mu\text{Sv/h}$ , 500  $\mu\text{Sv/h}$  and 900  $\mu\text{Sv/h}$  using the Caesium-137 gamma radioactive source in the calibration room.

As per technical specifications of LND 7121 GM tube,

Plateau length  $(V_2 - V_1) = 650\text{V} - 450\text{V} = 200\text{V}$

Sensitivity = CPS/mR/h = 18 or

$$= \text{CPS}/\mu\text{Sv/h} = 180$$

Then

Dose rate ( $\mu\text{Sv/h}$ ) = CPS /180 for the response time of AGRM

Dose rate ( $\mu\text{Sv/h}$ ) = Counts /180

$$S = 100 \left[ \frac{D_2 - D_1}{\frac{(D_1 + D_2)}{2}} \right] \left[ \frac{1}{\frac{(V_2 - V_1)}{100}} \right] \quad (3.11)$$

Here S [47] is the plateau slope (%/100V),  $D_1$  is the dose rate at the  $V_1$  voltage, and  $D_2$  is the dose rate at  $V_2$  voltage.

$$S = 100 \left[ \frac{D_2 - D_1}{D_1 + D_2} \right] \quad (3.12)$$

The average dose rate of GM tubes, GM1 to GM13 is recorded at 450V and 650V. The plateau slopes of each GM tube are calculated as per the Eqn. (3.12). Figure 3.16 and Figure 3.17 show the plateau slope versus dose rates of GM tubes GM1 to GM13. The plateau slope variation of GM1, GM2, GM3, GM4, GM5, GM7, GM8, GM9, GM10, GM11, and GM12 GM tubes is found to vary from 0.07 to 7.6. These values are statistically inconsistent because of low counting time (30 to 80s), and the accuracy of AGRM is  $\pm 10\%$ . The acceptance criterion of the percentage of plateau slope per 100 V shall be less than 10 (as per OEM). It includes the maximum allowable plateau slope variation of LND 7121 (+6% per 100 V). From online and offline experimental

studies, the plateau slopes of GM6 and GM13 GM tubes deviated more than 10% per 100 V at all dose rate levels. These GM tubes are identified as faulty. Eqn. (3.10) and Eqn. (3.12) are written in SCADA for real-time numerical representation of the maximum percentage of relative intrinsic error and plateau slope (%/100 V).

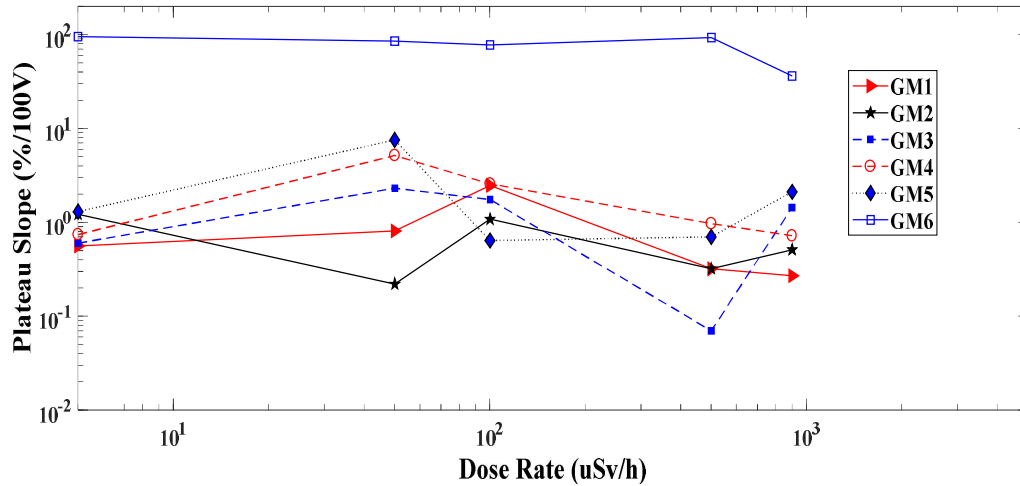


**Figure 3.16.** The plateau slope (%/100V) versus dose rate characteristics of GM tubes, GM1 to GM6 is shown. The plateau slope variation of GM1 to GM5 is from 0.07 to 7.6 (working), and the plateau slope of GM6 is 90.3% (faulty).

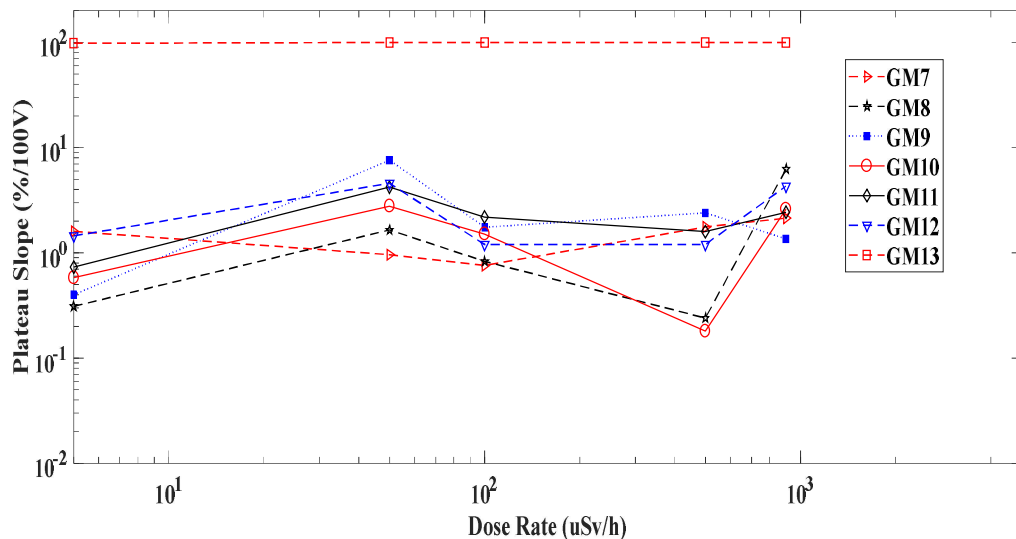


**Figure 3.17.** The plateau slope (%/100V) versus dose rate characteristics of GM tubes, GM7 to GM13 is shown. The plateau slope variation of GM7 to GM12 is from 0.07 to 7.6 (working), and the plateau slope of GM13 is 100.0% (faulty).

### 3.5 COMPARISON BETWEEN CONVENTIONAL AND ONLINE SURVEILLANCE METHODS OF AGRM

The periodical surveillance of AGRM is carried out as per the typical technical specification of a nuclear plant. Detailed person-hours requirement analysis of conventional and online surveillance methods of AGRM are shown in Table 3.3. The radioactive source calibration is performed using conventional surveillance method. Hence, there is no change in the requirement of Person-hours per year. The person-hours per unit per year saved [64] using online surveillance method are 78.9% even after radioactive source calibration considered as mandatory.

**Table 3.3.** Person-hours comparison between conventional and online surveillance methods of AGRM.

S. No	Surveillance plan as per the technical specification of the plant	Surveillance type	Conventional surveillance			Remote online surveillance		
			Average time (h) per year	No. of persons	Person-hours	Average time (h) per year	No. of persons	Person-hours
1	Continuous monitoring	RADAS readings checking	(No change)			(No change)		
2	Monthly	Checking	0.25x12	2	9	0.1x12	1	1.2
3	Quarterly	Radioactive source testing	0.33x4	3	3.96	0.1x4	1	0.4
4	Half year	Radioactive source calibration	0.42x2	3	2.52	0.42x2	3	2.52
5	Yearly	Electronic calibration	0.5x1	3	1.50	0.1x1	1	0.1
Total no. of person-hours per unit per year			19.98			4.22		
Total no. of person-hours per 100 units per year in a nuclear plant			1998			422		
Person-hours per unit per year saved using online surveillance method.			78.9% (Including radioactive source calibration)					

### 3.6 CONCLUSION

In this chapter, the failure mode and the noise analysis of GM tube & pulse processing electronics of AGRM are presented. All mode failure rate of AGRM is calculated to be  $3.2 \times 10^{-05}$ /unit-h. The noise voltage at the output of the pulse amplifier is reduced from 1.2 mV to 0.62 mV by reducing  $C_{ei}$  value from 100 pF to 200 pF. A newly developed online testing of AGRM electronics and GM tube from the control room using the wireless network is presented. The real-time trend and history graphs generated in RADAS help to identify the performance of AGRM electronics and GM tube in-situ. The online AGRM electronic test helps to calculate the percentage of relative intrinsic error to verify the AGRM accuracy. The accuracy of a working system is expected to be within  $\pm 10\%$ . This is acceptable and lies well within the applicable International Standards (ANSI N42.17A-2003 and ISO 4037-3). Online AGRM detector test is used to check the response of GM tube below GM threshold voltage (320 V) and verification of plateau slope (%/100 V). Ideally, no dose rate is expected for a working GM tube below GM threshold voltage. The plateau slope (%/100 V) of GM is expected to be within 10 (as per datasheet). Reliable wireless communication link observed between AGRM and RADAS during the test. The time required for online testing of both AGRM electronics and GM tube of the AGRM is less than 6 minutes. The person-hours per unit per year saved using online surveillance method are 78.9% as compared with conventional methods. The proposed method is applicable for testing of all GM tube based radiation monitors in the nuclear plants. The online surveillance method reduces the radiation exposures received by the maintenance crew and facilitates quick testing with minimum downtime of the instrument.

## DEVELOPMENT OF REMOTE ONLINE PERFORMANCE EVALUATION OF DUAL PHOSPHOR SCINTILLATOR BASED CONTINUOUS AIR MONITOR

---

*The present chapter describes the development of remote online performance evaluation techniques for dual phosphor scintillator based continuous air monitor (DPCAM). A detailed experimental study on the response of DPCAM subjected to a pulsed light source of different wavelengths using LEDs is presented. Development of DPCAM test circuit and configuration of ZigBee based wireless network based RADAS is explained. Online performance evaluation of the prototype DPCAM using pulse amplitude discrimination technique with a light source and loaded filter paper is elaborated. The real-time trend graphs evaluation with five-point calibration, verification of relative intrinsic error and verification of crosstalk between alpha-beta channels are explained. Validation of the technique using alpha-beta radioactive sources is elaborated. Person-hours requirement analysis of conventional and online surveillance methods of DPCAM are evaluated.*

---

### 4.1 INTRODUCTION

The radioactive activities of airborne particulates in the operating areas of nuclear plants are monitored continuously using the instruments such as the two-channel (alpha-beta) conventional continuous air monitor (CAM) [31,65], the plutonium in air monitor, and the dual phosphor scintillator [6,7,8,66,66,67] based continuous air monitor (DPCAM). The conventional CAM is provided with two filter head cum detector assemblies with independent detectors to detect alpha and beta activities. A ZnS(Ag) detector is used to detect alpha particles, and a GM tube is used

for beta particles. In DPCAM, a dual phosphors scintillator is used as a detector. The DPCAM is used to detect artificial radionuclides  $^{239}\text{Pu}$ ,  $^{241}\text{Am}$ ,  $^{90}\text{Sr}$ ,  $^{90}\text{Y}$ ,  $^{131}\text{Ce}$ ,  $^{60}\text{Co}$ ,  $^{36}\text{Cl}$  along with natural radioactivity due to short-lived radon and thoron progeny. The alpha-beta pulse discrimination logic consists of pulse amplifier followed by two single channel analyzers (SCA) for pulse amplitude based discrimination to identify alpha-beta radiations.

The performance of photomultiplier tube (PMT) degrades [69,70] due to the adverse ambient conditions like temperature, humidity, shock and vibration. PMTs suffer from long time gain drifts [32,71,72] even under normal ambient conditions if the anode current is more than 1  $\mu\text{A}$ . It affects the measurement due to a reduction of gain up to 85% to 60% over the period of  $10^4$  h. An average failure rate of conventional CAM and DPCAMs is  $2.65 \times 10^{-5}/\text{unit-h}$  [31] and  $2.28 \times 10^{-5}/\text{unit-h}$ , respectively. In case of 100 DPCAMs in the plant, the mean time between failures is once in every 18 days. Hence, conventional periodic field calibrations [13,22] using radioactive sources and pulse generator are mandatory. These methods suffer from a long time requirement, more person-days, high cost, and loss of precision and downtime of the instrument. It is also burden on radiological safety in terms of high Person-mSv expenditure and contamination.

A new method is developed for remote online performance evaluation of PMT along with electronics of DPCAM from the control room. Detailed experimental investigations carried out on the response of PMT and electronics of DPCAM subjected to a pulsed light source of different wavelengths using LEDs. A suitable LED is selected based on discrimination of alpha-beta counts by pulse amplitude technique with minimum crosstalk and minimum relative intrinsic error. A DPCAM test circuit is designed and developed for the generation of test frequency to drive the LED. A dedicated radiation data acquisition system (RADAS) is configured using an open platform communication server and data acquisition software. Modbus

RTU protocol on ZigBee based wireless communication is used for real-time monitoring and testing of prototype DPCAM. The graphical user interface screens are configured for each Modbus tag address in supervisory control and data acquisition (SCADA) system for remote online evaluation. This technique improves the system reliability by early failure detection, reduces the frequency of field radioactive source calibration and avoids field electronic calibration using pulse generators. The failures detected in DPCAM include passive electronic components, pulse-processing electronics, digital circuits and drifts in PMT gain, amplifier gain & discrimination levels. Person-hours requirement analysis are also carried out for conventional and online surveillance methods of DPCAM.

## 4.2 EXPERIMENTAL SETUP

### 4.2.1 Brief description of the experimental study

The response of the PMT depends upon the input pulsed light source and the nature of the output signal depends upon the time profile of the input. The light source follows exponential profile Eqn. (4.1) and the current  $i(t)$  in PMT for single exponential time constant  $T_s$  is

$$i(t) = \frac{N e G}{T_s} \exp\left(\frac{-t}{T_s}\right) \quad (4.1)$$

Here  $N$  is the number of photoelectrons generated for the incident light source,  $e$  is the electron charge, and  $G$  is the gain of the PMT. When  $t \gg T_s$ , it is voltage mode operation Eqn. (4.2) and in this case, the pulse height is proportional to the total input charge  $C$ . The output voltage [69]  $v_0(t)$  is

$$v_0(t) = \frac{N e G}{C} \left[ \exp\left(\frac{-t}{T_s}\right) - 1 \right] \quad (4.2)$$

$v_0(t)$  is directly proportional to the number of photoelectrons. This concept is used to evaluate PMT along with electronics of DPCAM using pulse amplitude discrimination technique. The value of  $v_0(t)$  varies from zero to 500 mV in practical scenarios, and it depends on the incident photon intensity.  $v_0(t)$  is applied to the input of pulse amplifier for amplification and pulse counting. Similarly, the intensity of photons emitted from LED depends on the current flowing



through it [73]. The LED is preferred [33] in this work as applied voltage controls the current that in-turn control the intensity of light photons. Moreover, LEDs are cheap, compact and its light wavelength matches with the spectral response of the PMT. A technique for remote online performance evaluation of PMT and electronics of DPCAM using the pulsed light source from LED is proposed.

#### 4.2.2 Transmission efficiency of scintillation material

Figure 4.1 shows the thickness of Mylar film, dual phosphor scintillator and its two-dimensional view. During the scintillation process, light photons are absorbed in scintillation material by statistical processes [3,74] it leads to exponential absorption Eqn. (4.3). The photons that do not get through the scintillation material is either absorbed or scattered. In this case, all the photons interact with the scintillation material.

$$I = I_0 * \exp^{-\left(\frac{\mu}{\rho}\right)\rho t} \quad (4.3)$$

Where  $I_0$  is the number of photons of incident energy,  $\rho t$  is the mass thickness of the scintillator,  $I$  is the number of photons that are passed through a scintillation material, and  $\mu/\rho$  is the mass attenuation coefficient of the material for photon energy.

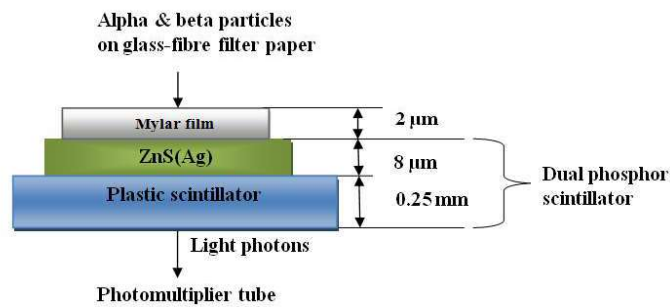


**Figure 4.1.** The arrangement of Mylar film, dual phosphor scintillator and its two-dimensional view.

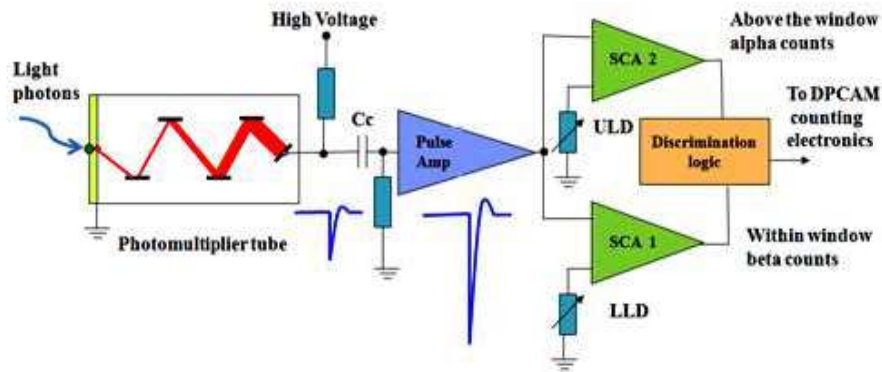
#### 4.2.3 Calibration of DPCAM using alpha-beta radioactive sources

In a dual phosphor scintillator, alpha particles interact with the ZnS(Ag) scintillator, resulting in a PMT output pulse with high amplitude. Medium and higher energy beta particles simply pass

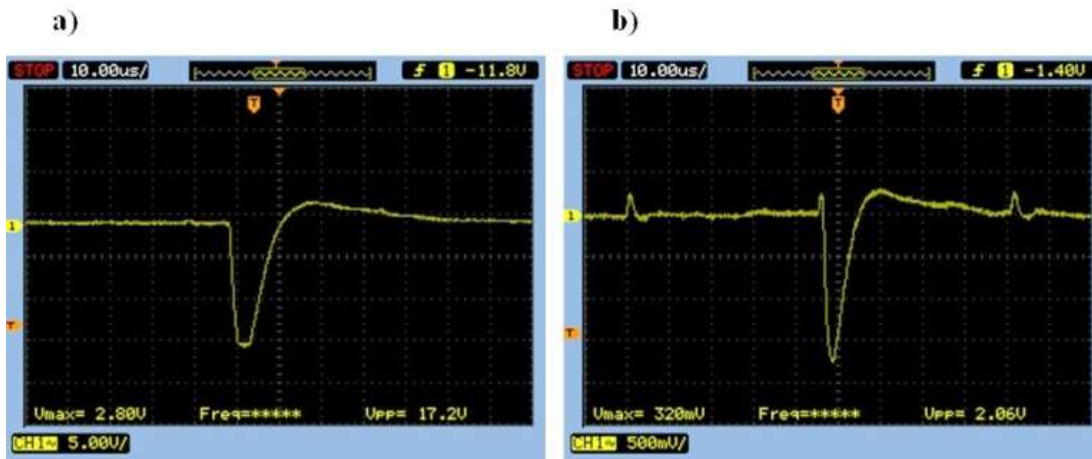
through the ZnS(Ag) and interact with the plastic scintillator giving out a PMT pulse with lower amplitude than the alpha pulse. The pulse amplifier output is fed to the inputs of SCA 1 and SCA 2 as shown in Figure 4.2. The second input of SCA 1 to lower-level discriminator (LLD) and similarly, the second input of SCA 2 to upper-level discriminator (ULD). The LLD reference voltage level is adjusted to eliminate the power supply and other pickup noise signals. The ULD reference voltage is adjusted for beta discrimination. The discriminator logic is used to distinguish alpha and beta radiation pulses based on the pulse amplitude discrimination technique.

Figure 4.3(a) shows the pulse amplifier output captured in an oscilloscope with  $^{241}\text{Am}$  alpha source and Figure 4.3(b) shows the pulse amplifier output with  $^{90}\text{Sr}$ - $^{90}\text{Y}$  beta source. The pulse amplifier gain, LLD and ULD of alpha-beta discrimination logic are fixed accordingly for the maximum counting efficiency Eqn. (4.4) and minimum crosstalk between alpha-beta channels before starting the experiment. The expected counting efficiencies ( $\eta$ ) are 25-30% in alpha channel with  $^{241}\text{Am}$  source and 28-35% in the beta channel with the  $^{90}\text{Sr}$  -  $^{90}\text{Y}$  source. The acceptable crosstalk is up to 0.01% counts in alpha channel with beta source and up to 1% counts in the beta channel with alpha radioactive source.

$$\% \eta = \left[ \frac{\text{Counts per second} - \text{Background per second}}{\text{No. of disintegrations per second}} \right] * 100 \quad (4.4)$$



**Figure 4.2.** Alpha-beta pulse discrimination logic using pulse amplitude technique, the output of discrimination logic is connected to counting and display of DPCAM.



**Figure 4.3.** a) The pulse amplifier output waveform for a  $^{241}\text{Am}$  source with high pulse amplitude. b) The pulse amplifier output waveform for a  $^{90}\text{Sr} - ^{90}\text{Y}$  source with lower pulse amplitude.

#### 4.2.4 Testing of DPCAM with LED light pulses

The PMT [75] (Electron Tubes make, Model No: 9256B) used in this work has a nominal diameter of 51mm, no. of dynodes as 10 (LF), Sb-Cs based dynodes, Bialkali photocathode material and spectral response of 290-680 nm. The PMT along with electronics of DPCAM is subjected to different photon wavelengths using LEDs [76]. These LEDs are a transparent commercial grade of 5 mm dia., Red color (620-720 nm), Green color (500-570 nm), Blue color (450-500 nm) and colour [35] infrared (CIR, 500-900 nm). A ring spacer of 52 mm diameter with the thickness of 6 mm is fixed to maintain a uniform gap between dual phosphor scintillator and surface of the PMT. Figure 4.4 shows the proposed location of LED on PMT and a ring spacer. The LED is connected to the output of pulse generator through a 100-Ohm resistor. The experiment is conducted for each LED independently for optimum pulse amplitude, pulse width, different frequencies to achieve minimum crosstalk and minimum relative intrinsic error Eqn. (4.5) for the full range of 50000 CPM.

$$\% \text{ of Relative Intrinsic Error} = \left[ 1 - \frac{\text{Observed counts}}{\text{Expected counts}} \right] * 100 \quad (4.5)$$

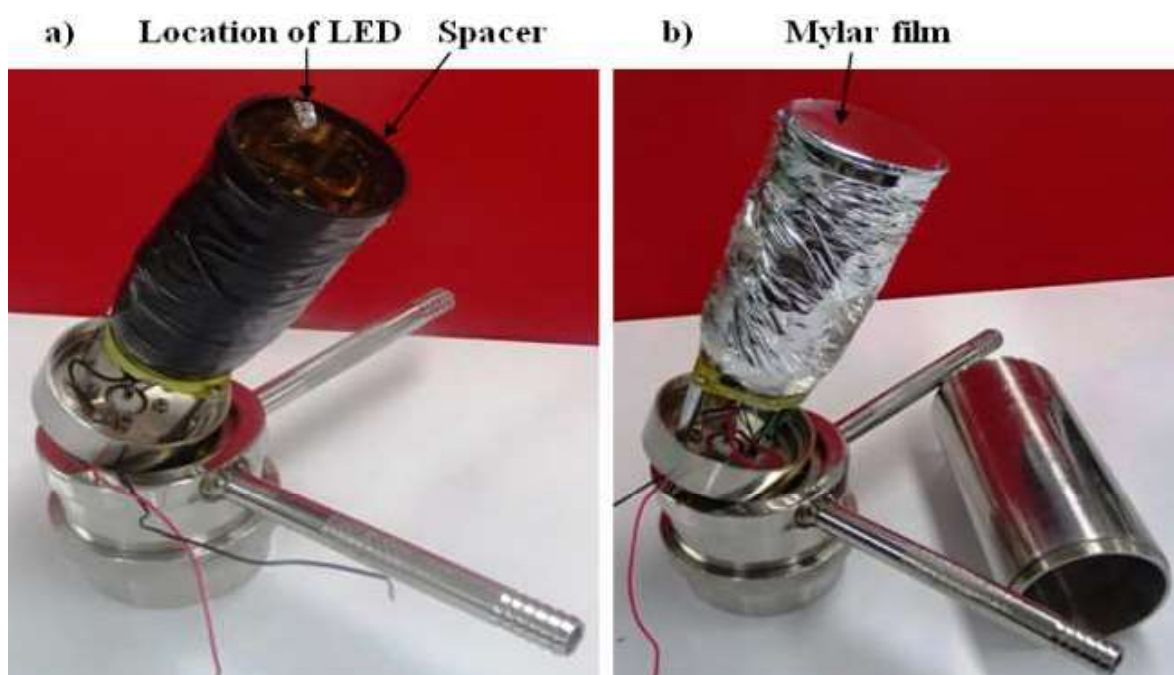


**Figure 4.4.** a) Proposed location of LED on PMT and a ring spacer along with the perimeter of end window are shown. b) The PMT along with LED and dual phosphor scintillator are covered using a single layer of Mylar film.

#### 4.2.4.1 *Pulse amplitude (V) vs counts per minute (CPM) characteristics*

The pulse amplitude of test frequency is varied from 1.0 to 3.6 V with fixed pulse width and frequency. At first, the test carried out to find out the threshold voltage for the each LED that start emitting light photons. Second, the discrimination voltage levels for alpha and beta counts are determined. The experiments are repeated for each LED, the counts of both alpha and beta channels are recorded.

#### 4.2.4.2 *Pulse width ( $\mu$ s) vs CPM characteristics*

The input pulse width of test frequency to the LED is varied from 1  $\mu$ s to 40  $\mu$ s as the pulse amplitude, and test frequency is constant for suitable pulse width. The experiments are repeated for each LED, the counts in both alpha and beta channels are recorded.

#### **4.2.4.3 Selection of suitable LED**

Selection of suitable LED is carried out based on the results of pulse amplitude vs CPM and pulse width vs CPM characteristics. Suitable light wavelength is determined for better alpha-beta pulse discrimination, zero crosstalk and minimum relative intrinsic error. Further, selected LED is tested for a full range of DPCAM in both channels using frequency vs counts characteristics.

#### **4.2.4.4 Frequency (Hz) vs CPM characteristics**

The input frequency to the LED is varied in five-steps at 10 Hz, 200 Hz, 400 Hz, 600 Hz and 800 Hz to cover the full range of DPCAM. The relative error at each step is noted keeping pulse amplitude and pulse width constant.

### **4.3 DESIGN AND DEVELOPMENT OF DPCAM TEST CIRCUIT**

DPCAM test circuit is required to drive the LED with variable test frequency. The pulse amplitude and pulse width of the test frequency shall be variable for selection of required photon counts. Based on the experimental results, the DPCAM test circuit is designed using discrete electronic components as shown in Figure 4.5. The PCB is developed as per IPC-2221A [56] and it is accepted as per IPC-A-610F [57]. Design of additional electronic circuit is provided with proper protection, isolation and fail-safe features. It is also ensured that the failure of the additional circuit does not degrade the performance of DPCAM.

The circuit contains two pole relays, decade counters, timers, oscillator, pulse shaper and a voltage divider network. When this circuit is activated using test button, both relays RL-1 and RL-2 are energised. The power supply to both timers, decade counters, oscillator and pulse shaper is available. Initially, the timer 1 is switched-on for a preset period of 5 minutes, and the timer 2 is switched-on for a preset time of one minute for testing the alpha channel.

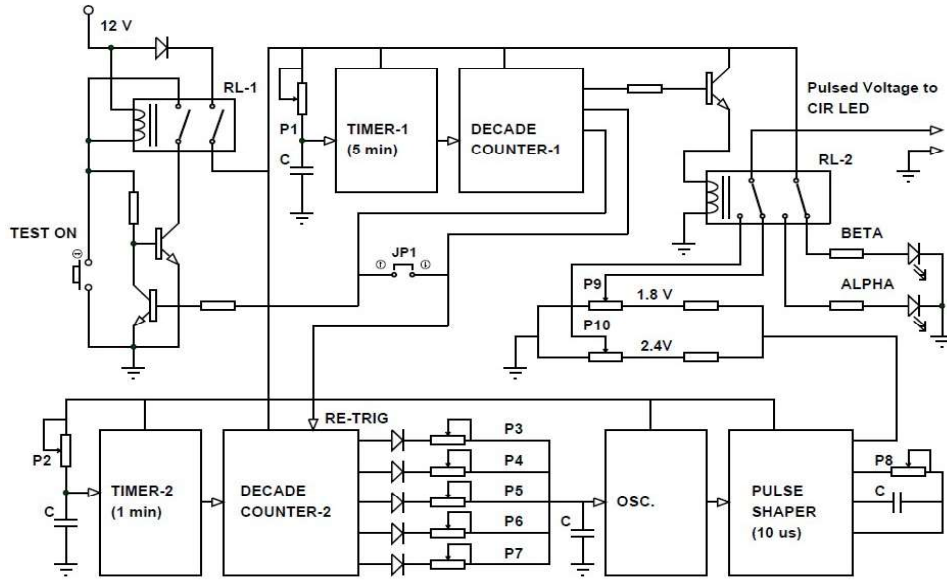


**Figure 4.5.** DPCAM test frequency generation circuit.

The oscillator will generate the test frequency output with pulse amplitude from 1.5 to 4.0 V and the pulse width from 1  $\mu$ s to 40  $\mu$ s using potentiometers. The circuit is designed for five test frequency steps, 10 Hz, 200 Hz, 400 Hz, 600 Hz and 800 Hz automatically for the one-minute duration at each step. At the end of the testing of the alpha channel, automatically the RL-2 is switched-off and retriggers the decade counter 2. The similar test frequency pattern generated for testing of the beta channel on the same output of DPCAM test circuit. The counts in CPM will be updated in both alpha and beta channels (test frequency\*60). The voltage divider network is provided for two different voltage outputs to discriminate alpha-beta counts. At the end of the beta channel test, the circuit is automatically switched-off and isolated from the normal counting electronics. The frequency of oscillation ( $f$ ) is calculated Eqn. (4.6), and the  $f$  value can be varied using potentiometers P2, P3, P4, P5, P6 and P7 shown in Figure 4.5.

$$f = \left[ \frac{1.44}{R_a + 2R_b} * C \right] \text{ Hz} \quad (4.6)$$

The pulse width ( $t_M$ ) of test frequency is calculated Eqn. (4.7), and it can be varied using potentiometer P8.

$$t_M = 2.48 * RC \text{ s} \quad (4.7)$$

The pulse amplitude  $V(t)$  of the test frequency is calculated Eqn. (4.8), at the output voltage using divider network and it can be varied using potentiometers P9 and P10.

$$V(t) = \left[ \frac{R_2}{R_1 + R_2} \right] * V_{in} \quad (4.8)$$

#### 4.4 CONFIGURATION OF DEDICATED RADAS FOR ONLINE PERFORMANCE EVALUATION

##### 4.4.1 Configuration of RADAS and system integration

The configuration of RADAS involved configuration of SCADA, wireless communication modules and system integration. The dedicated RADAS is configured using open platform communications (OPC) server and SCADA software in the server computer. The prototype DPCAM with test circuit is connected to the OPC server using Modbus RTU on RS-485. The serial communication parameters like device ID, port address, data bits, baud rate parity and stop bits are configured in OPC Server for communication with the field DPCAM. Different Modbus RTU tags used in DPCAM are configured in OPC server software to update the engineering values as mentioned in Table 4.1. These values are used to display in real-time and recorded in the database in every 100 ms interval to generate history graphs and reports. The graphical user interface screens are developed against each Modbus tag address in SCADA. The real-time trend graphs are created for counts in the alpha channel, counts in the beta channel, the relative intrinsic error of alpha channel and relative intrinsic error of beta channel in SCADA. The equations for background subtraction, the percentage of relative intrinsic error are written in SCADA for real-time numerical and graphical representation. The DPCAM and server computer are connected to an RS-485 wired network. The communication between these devices is checked in this network. The real-time updates are checked for alpha-beta counts, alarm level, acknowledgement, reset, etc.

**Table 4.1.** Various Modbus Tags used for Online Monitoring and Performance Evaluation of DPCAM

S. No	Tag Description	Modbus Tag Address	Data type	Client Access
1	Alpha counts (CPM)	300007	Word	Read Only
2	Beta counts (CPM)	300009	Word	Read Only
3	Acknowledgment	100002	Boolean	Read/Write
4	Calibration factor	400015	Word	Read/Write
5	Reset	100004	Boolean	Read/Write
6	Alarm level	400030	Word	Read Only
7	Alarm active	100007	Bit	Read Only
8	DPCAM test on	400001	Word	Read/Write
9	Test frequency (Hz)	400008	Word	Read Only

#### **4.4.1.1 Configuration of ZigBee transceiver modules and performance evaluation of wireless link**

For wireless communication, the ZigBee based wireless network is preferred in this work over the other technologies viz., Wi-Fi, Bluetooth, Wibree and Ultrawideband. It is mainly because of its low power consumption, considerable long range and low cost. Commercial available ZigBee Pro modules are used for an indoor application. The ZigBee modules used in the industrial, scientific & medical radio (ISM) band with a frequency of 2.4 GHz, which does not require a license. They employed the IEEE 802.15.4 Standard, a wired antenna, 128-bit advanced encryption and 16 channels in the frequency spectrum. All ZigBee modules are configured for various parameters like 16-bit source, destination address, 19200-baud rate, encryption details, etc. using x-configuration & test utility (X-CTU) software. For wireless communication link, one ZigBee module is connected to DPCAM via RS-485, which works as a field sensor node. Another ZigBee wireless module is connected to RADAS server computer as a base station as shown in Figure 4.6 and Figure 4.7. The experimental setup made for wireless sensor network [58,77] to establish the wireless link between DPCAM located operating area of the plant (ground floor) and RADAS at the control room (first floor). Initially, spectrum analyser of X-CTU software is used for the site survey to identify the interference at 2.4 GHz spectrum range



within the building using the laptop computer, and it is found that the spectrum is fully available without any interference. The experiment is conducted with real-time monitoring of DPCAM in a static environment to find the number of nodes needed to cover non-line of sight (NLOS) distance of 50 m. The wireless path consists of two normal size walls and nine aluminium/glass doors. It is found that three numbers of router nodes along with a sensor node are needed to cover this distance. The nodes are geographically positioned in such a way that they provide multiple routing paths, and hence the fault tolerance is achieved even failure of a single node.

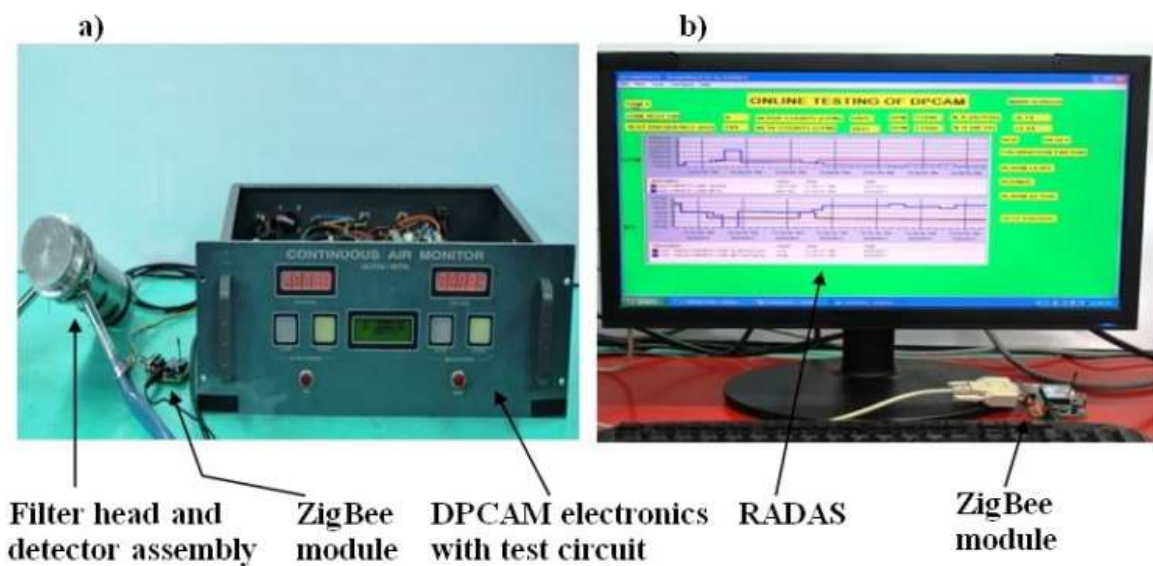


**Figure 4.6.** The experimental setup for online performance evaluation of DPCAM a) Field device b) RADAS in the control room.

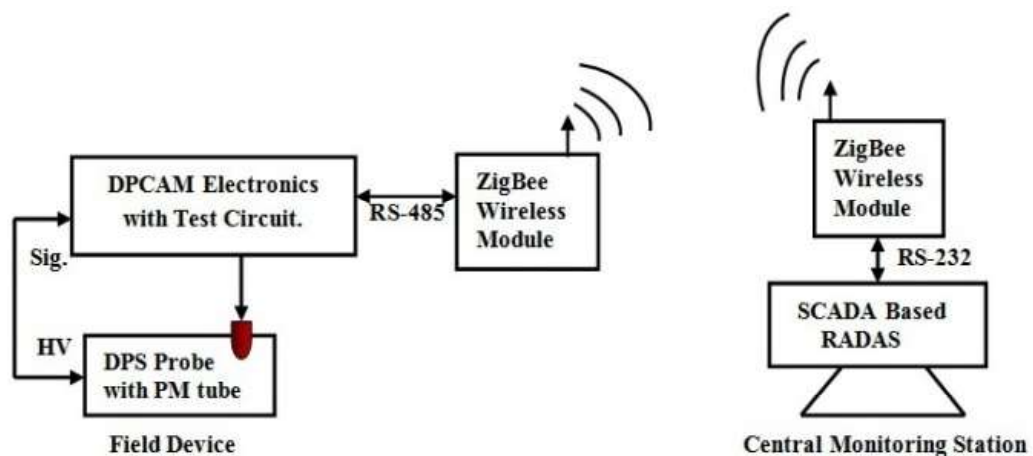


**Figure 4.7.** Block diagram of DPCAM, DPS probe, ZigBee wireless modules and RADAS.

#### 4.4.1.2 Performance evaluation of wireless link

Wireless link performance is tested [59] in terms of the received signal strength indicator (RSSI) and the packet error rate (PER). Wireless link indication studies are carried out between each node as per the Eqn. (4.9).

$$\text{RSSI}_{\text{dBm}} = -(10 * n * \log(d) + A) \quad (4.9)$$

Where  $d$  is the distance between the transmitter and receiver,  $A$  is the received signal strength at one meter (-35 dBm),  $n$  is the propagation exponent. Based on the repeated experiments due to multipath fading and shadowing [78], it is found that the RSSI between each node varied between -50 dBm to -65 dBm. The sensor node is transmitting data continuously to the base station at 1 s interval and the data is collected for a period of seven days. For each day, the data is acquired for a period of one hour at random interval. The acquired data is analysed for packet drop if any. The node transmits 3600 packets per hour. From the database of throughput analysis tool, it is checked that the same 3600 packets are received at the base station. Similarly, for seven days no packet drop was found. Hence, 100% packet delivery is observed, and PER is found to be zero”.

### 4.5 ONLINE TESTING AND PERFORMANCE EVALUATION

#### 4.5.1 Online testing of DPCAM with fresh filter paper

Based on the experimental results, suitable CIR LED is selected and fixed permanently on PMT. The connections are made for online performance evaluation of prototype DPCAM. The DPCAM test circuit is activated remotely using SCADA as shown in Figure 4.7. Various parameters including counts in the alpha channel counts in the beta channel, alarm level, calibration factor, reset and acknowledgement are monitored during the test using fresh filter paper along with the pulsed light source. The real-time trend graphs generated during the test for alpha counts, beta counts, test frequency and relative intrinsic errors are noted.

### 4.5.2 Online performance evaluation of DPCAM

Online performance evaluation of DPCAM is carried out using loaded filter paper in the field and then with different alpha-beta radioactive sources along with the pulsed light source. The alpha channel is evaluated initially with loaded filter paper (240 CPM) in the field. Since the airborne activity in nuclear plant always maintained well below detection limits (BDL), the experiment cannot be continued with loaded filter papers for full range evaluation of DPCAM. The experiments further continued using alpha-beta calibration sources to validate the system during the failure of the exhaust system or leakage of radioactivity. Therefore it is evaluated using  $^{241}\text{Am}$  (121 Bq & 450 Bq) and  $^{239}\text{Pu}$  (975 Bq) radioactive sources. Similarly, the beta channel is evaluated with the same filter paper (550 CPM) and using  $^{90}\text{Sr}$  -  $^{90}\text{Y}$  (190 Bq, 345 Bq & 620 Bq) radioactive sources. The relative intrinsic errors are found in both channels with loaded filter paper and radioactive sources.

## 4.6 RESULTS AND DISCUSSION

### 4.6.1 Pulse amplitude (V) vs CPM characteristics

The pulse amplitude of test frequency applied to each of the LED is varied from 1.0 V to 3.6 V with an optimum pulse width of 10  $\mu\text{s}$  and pulse frequency of 400 Hz (expected counts: 24000 CPM). However, some of the LEDs are barely turning ON at a small voltage with a current in the order of few  $\mu\text{A}$  resulting in detectable photon counts on the PMT. Hence, the voltage range starting from 1.0 V was considered for uniformity and better readability of the graphs. Figure 4.8 shows counts in alpha and beta channels using Red color LED. Counts in the alpha channel are  $23920 \pm 70$  CPM for the pulse amplitude of 1.6 V to 3.6 V and counts in the beta channel for the pulse amplitude of 1.7 V to 3.6 V are  $10000 \pm 20$  CPM. The relative intrinsic errors of alpha and beta channels are + 0.62% and + 58.3% ( $[1-(10020/24000)]*100$ ) respectively. The relative intrinsic errors in beta channel are high since the pulse amplitude of the amplifier output falls below or/and above the ULD. It is due to incoherent and random emission [79] of photons from

Red LEDs. Thus counts are not discriminated in both channels using pulse amplitude method. Figure 4.9 illustrates counts in alpha and beta channels using Green color LED. Counts in the alpha channel are  $23920 \pm 70$  CPM for the pulse amplitude of 2.2 V to 3.6 V and counts in the beta channel are  $24930 \pm 70$  CPM for 1.6 V to 1.9 V. It is able to discriminate the alpha and beta count using pulse amplitude method. Relative intrinsic errors of alpha and beta channels are +0.62% and - 4.2% respectively. In this case, counts in alpha channel are acceptable. Counts in the beta channel are varied by 4.2% due to internal light reflections. Figure 4.10 shows count in alpha and beta channels using Blue color LED. The counts in the alpha channel are  $23920 \pm 70$  CPM for the pulse amplitude 2.1 V to 3.6 V and counts in beta channel are  $10000 \pm 20$  CPM for 1.6 V to 1.9 V. It is able to discriminate the alpha-beta counts using pulse amplitude method. The relative intrinsic errors of alpha and beta channels are varied by 0.62% and 58.3% respectively. The results are similar as that of Red color LED. Figure 4.11 illustrates counts in alpha and beta channels using CIR LED. The counts in the alpha channel are  $23920 \pm 30$  CPM for the pulse amplitude of 2.1 V to 3.6 V and counts in beta channel are  $23920 \pm 30$  CPM for 1.6 V to 1.9 V. It is able to discriminate the alpha and beta counts using pulse amplitude method and relative intrinsic error in both channels are + 0.46%. The errors, in this case, are minimum, and it is due to the uniform light wavelength from CIR LED in the visible region.

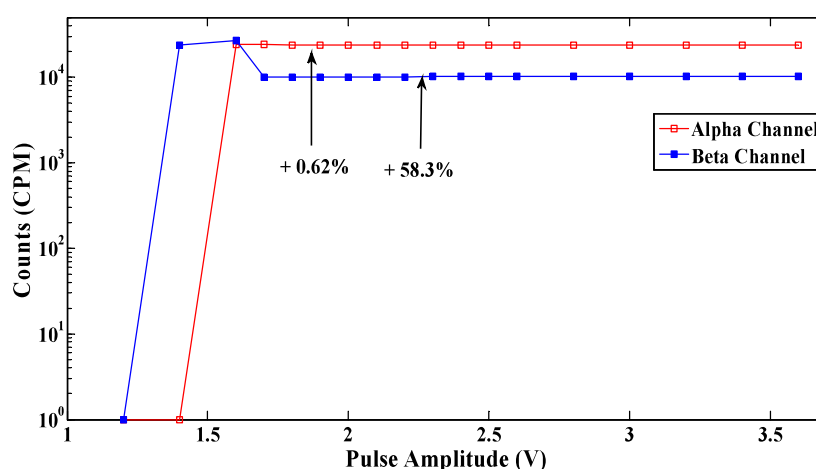


**Figure 4.8.** Counts in the alpha channel using Red color LED are  $23920 \pm 70$  CPM for pulse amplitude of 1.6 V to 3.6 V and counts in the beta channel for the pulse amplitude of 1.7 V to 3.6 V are  $10000 \pm 20$  CPM. The relative intrinsic error in beta channel is high since the pulse amplitude of the amplifier output falls below or above the ULD. It is due to the incoherent and random emission of photons from Red LEDs.

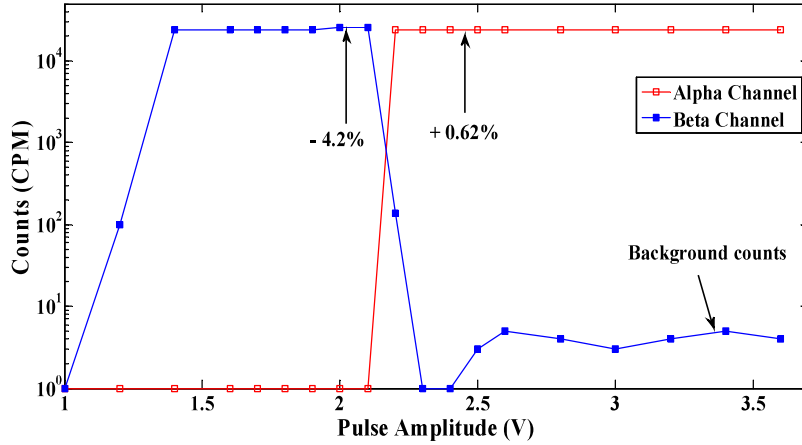


**Figure 4.9.** Counts in the alpha channel using Green color LED are  $23920 \pm 70$  CPM for the pulse amplitude of 2.2 V to 3.6 V and counts in the beta channel are  $24930 \pm 70$  CPM for 1.6 V to 1.9 V. The relative intrinsic errors of alpha and beta channels are  $+0.62\%$  and  $-4.2\%$  respectively. In this case, counts in the beta channel are increased by 4.2%, it is due to the internal light reflections within detector assembly.

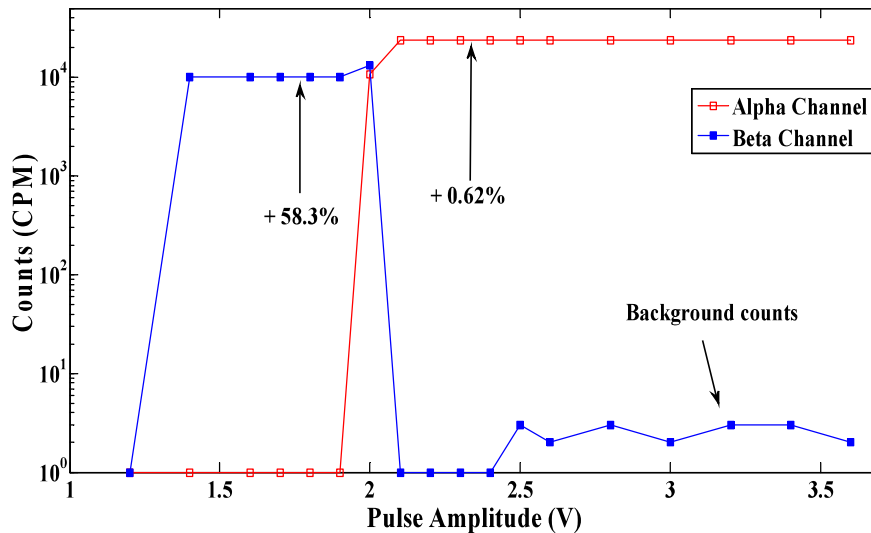


**Figure 4.10.** Counts in the alpha channel using Blue color LED are  $23920 \pm 70$  CPM for the pulse amplitude of 2.1V to 3.6 V and counts in the beta channel are  $10000 \pm 20$  CPM for 1.6 V to 1.9 V. The relative intrinsic errors of alpha-beta channels are shown on the graph. The relative intrinsic error in beta channel is high and it is similar as that of Red color LED.

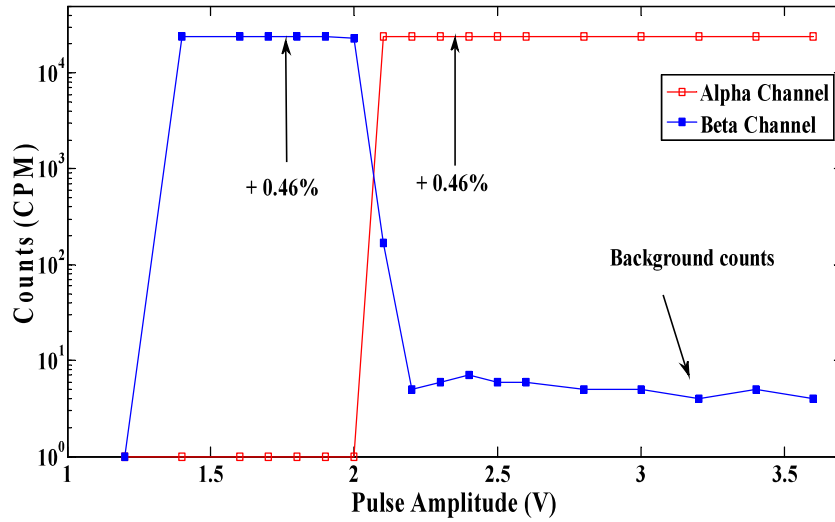


**Figure 4.11.** Counts in the alpha channel using CIR LED are  $23920 \pm 30$  CPM for the pulse amplitude of 2.1 V to 3.6 V and  $23920 \pm 30$  CPM for 1.6 V to 1.9 V in the beta channel. The relative intrinsic errors, in this case, are minimum, and it is due to the uniform light wavelength from CIR LED in the visible region.

#### 4.6.2 Pulse width ( $\mu$ s) vs CPM characteristics

The pulse width to each LED is varied from 1  $\mu$ s to 40  $\mu$ s with the test frequency of 200 Hz. The suitable pulse amplitude is identified as 2.4 V for testing of the alpha channel and 1.8 V for testing of the beta channel. Figure 4.12 illustrates the counts in the alpha channel using Red, Green, Blue and CIR LEDs at pulse amplitude of 2.4 V. These counts are closely overlapping in the range from  $11800 \pm 150$  CPM. Figure 4.13 shows the counts in the beta channel with Red, Green, Blue and CIR LEDs at pulse amplitude of 1.8 V. The counts in beta channel at this voltage using Red and Blue color LEDs are observed as random during repeated experiments as  $9 \pm 1$  or  $6990 \pm 40$  and it is due to the selection of ULD. The counts in both channels using CIR LED for the pulse width from 1  $\mu$ s to 40  $\mu$ s with the test frequency at 200 Hz are equal to the expected counts of  $11960 \pm 20$  CPM. In the present case, the pulse width of 10  $\mu$ s is selected for better counts rates. The random characteristics of the RGB color LEDs as the pulse width varies from 1  $\mu$ s to 5  $\mu$ s are due to the insufficient intensity of photons.

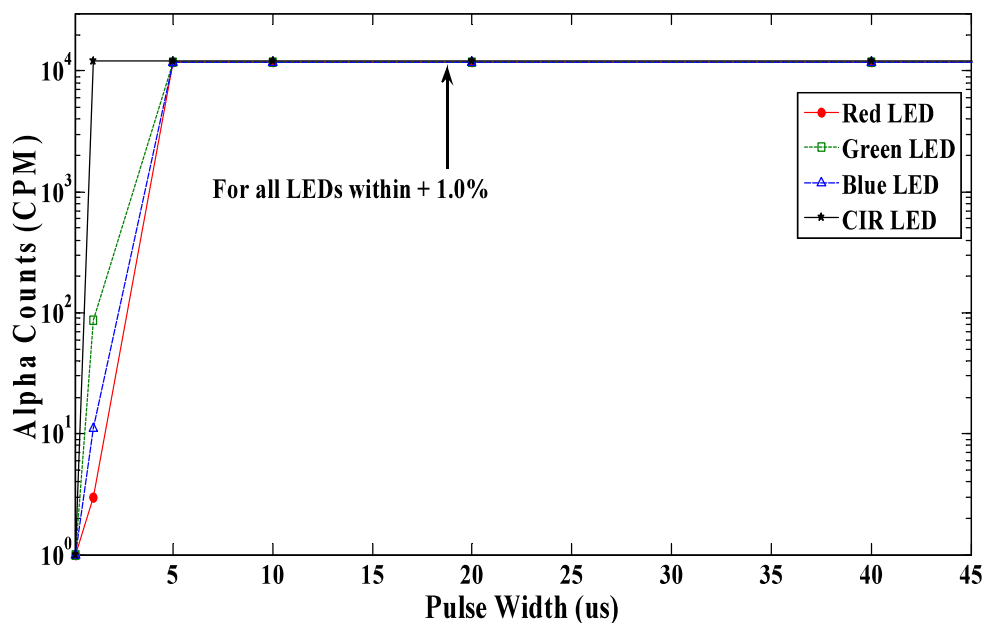


**Figure 4.12.** Alpha channel counts in CPM of RGB and CIR LEDs at pulse amplitude of 2.4 V, a pulse width from 1  $\mu$ s to 40  $\mu$ s and test frequency of 200 Hz. The relative intrinsic errors for all LEDs are within 1%.

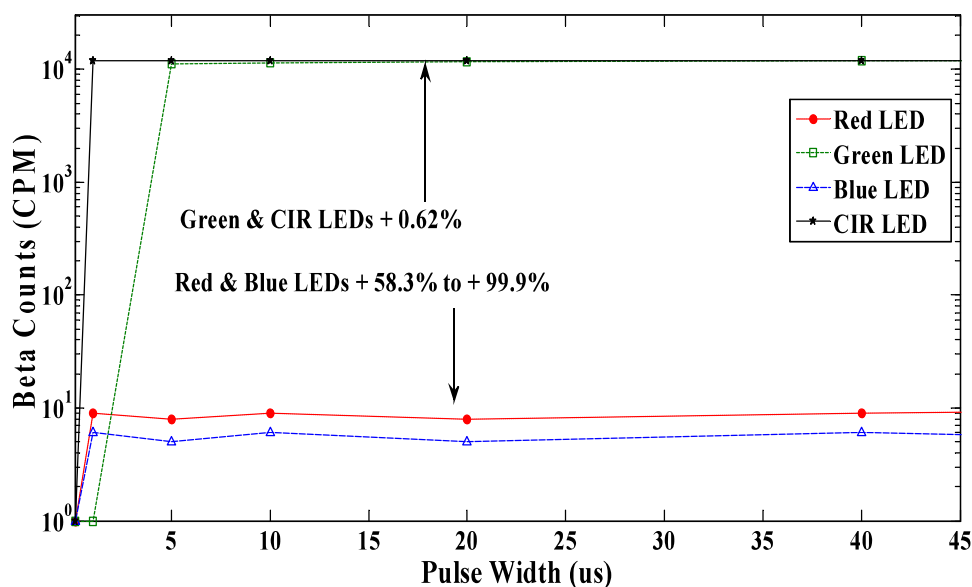


**Figure 4.13.** Beta channel counts in CPM of RGB and CIR LEDs at pulse amplitude of 1.8 V, a pulse width from 1  $\mu$ s to 40  $\mu$ s and test frequency of 200 Hz. The relative intrinsic errors for all LEDs are shown on the graph. The random characteristics of the RGB color LEDs are due to the insufficient intensity of photons.

### 4.6.3 Selection of suitable LED

In case of Red color LED, the alpha & beta channel counts are not discriminated, and the relative intrinsic error in the beta channel is + 58.3%. Similarly, when using Blue color LED, the relative intrinsic error in the beta channel is also calculated as + 58.3%. The Red and Blue LEDs are not be used in this work for the given conditions. Using Green color and CIR LEDs, the maximum relative intrinsic error is - 4.2% and + 0.62% respectively. Among these LEDs, the CIR LED is found to be the most suitable light source, as it is able to discriminate alpha and beta radiation with zero crosstalk and minimum relative intrinsic error. The CIR LED (DST make. Similar LEDs are used in infrared-based cameras) is recommended in this work for remote online performance evaluation of DPCAM. The light wavelength of CIR LED [35] is shown in Figure 4.14 and its peak wavelength is 850 nm. The CIR LED light source prevents the light reflections within DPCAM detector assembly therefore minimum relative intrinsic error recorded during the testing.

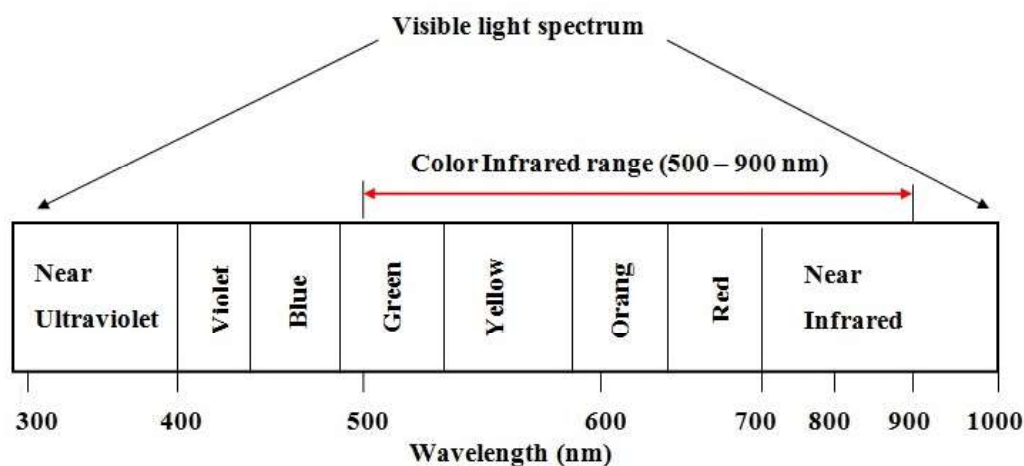


**Figure 4.14.** The light wavelength of CIR LED

### 4.6.4 Frequency (Hz) vs CPM characteristics

Further study is carried out using CIR LED for full counting range of DPCAM. Table 4.2 presented the percentage of relative intrinsic error of CIR LEDs at the pulse width of 10  $\mu$ s with



a pulse amplitude of 2.4 V & 1.8 V when the test frequency varied from 10 Hz, 200 Hz, 400 Hz, 600 Hz and 800 Hz. The relative intrinsic error at 10 Hz is 1% and at all other frequencies is less than 0.5% in both channels. These errors considered as instrumental and zero crosstalk between alpha-beta channels are acceptable.

**Table 4.2.** Percentage of relative intrinsic error of CIR LED at a pulse width of 10  $\mu$ s, a pulse amplitude of 2.4 V, 1.8 V, when the test frequency varied from 10 Hz, 200 Hz, 400 Hz, 600 Hz and 800 Hz.

Test frequency with pulse width of 10 $\mu$ s	Expected counts in CPM	% of Relative Intrinsic Error			
		Pulse amplitude at 2.4 V		Pulse amplitude at 1.8 V	
		Alpha Channel	Beta Channel	Alpha Channel	Beta Channel
10 Hz	600	1.00	100	100	1.00
200 Hz	12000	0.49	100	100	0.48
400 Hz	24000	0.50	100	100	0.45
600 Hz	36000	0.48	100	100	0.44
800 Hz	48000	0.45	100	100	0.44

#### 4.7 FINE TUNING OF DPCAM TEST CIRCUIT FOR CIR LED AND PERFORMANCE EVALUATION

The DPCAM test circuit is installed in a prototype DPCAM unit. The CIR LED is fixed permanently on PMT for online performance evaluation using SCADA. The test frequency output of DPCAM test circuit is connected to the CIR LED. The pulse width of the test frequency is selected as 10  $\mu$ s for testing of both channels. The pulse amplitude of 2.4 V is used for testing alpha channel and 1.8 V for testing of the beta channel. The DPCAM test circuit is fine-tuned for five test frequency steps to cover the full range of DPCAM. The accuracy of test frequency is  $\pm 0.15\%$  of full scale from 1 Hz to 800 Hz at room temperature. Five-step frequencies are selected at 10 Hz, 200 Hz, 400 Hz, 600 Hz and 800 Hz to cover five-point calibration of DPCAM at 600 CPM, 12000 CPM, 24000 CPM, 36000 CPM and 48000 CPM

respectively. The profile of test frequency, time and pulse amplitude applied to the CIR LED during the online performance evaluation of alpha & beta channels are shown in Figure 4.15.

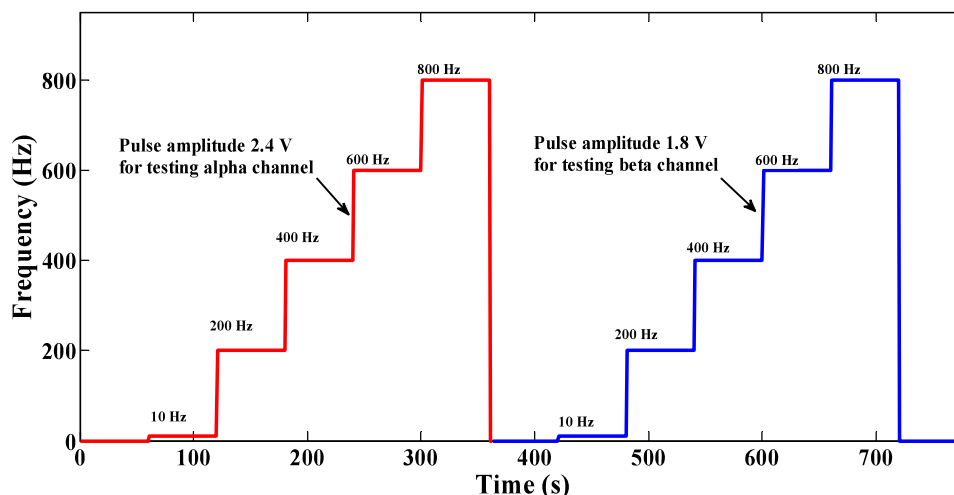


**Figure 4.15.** The profile of test frequency, time and pulse amplitude applied to the LED during the online performance evaluation.

Pulse amplifier output of alpha-beta pulse discrimination logic circuit is captured in the oscilloscope during testing of alpha and beta channels. Figure 4.16 illustrates the signal waveform of input test pulse to CIR LED with pulse amplitude at 2.4 V, pulse width of 10  $\mu$ s and the corresponding output of pulse amplifier. The maximum amplitude of the signal output is -14.0 V. Figure 4.17 shows a signal waveform of test pulse with pulse amplitude at 1.8 V, the pulse width of 10  $\mu$ s and the corresponding output of the DPCAM amplifier. The maximum amplitude of signal output, in this case, is -1.9 V. The LLD and ULD are selected accordingly to achieve maximum efficiency and minimum crosstalk between alpha-beta counts during the test. However, these levels are site condition and instrument-specific values.

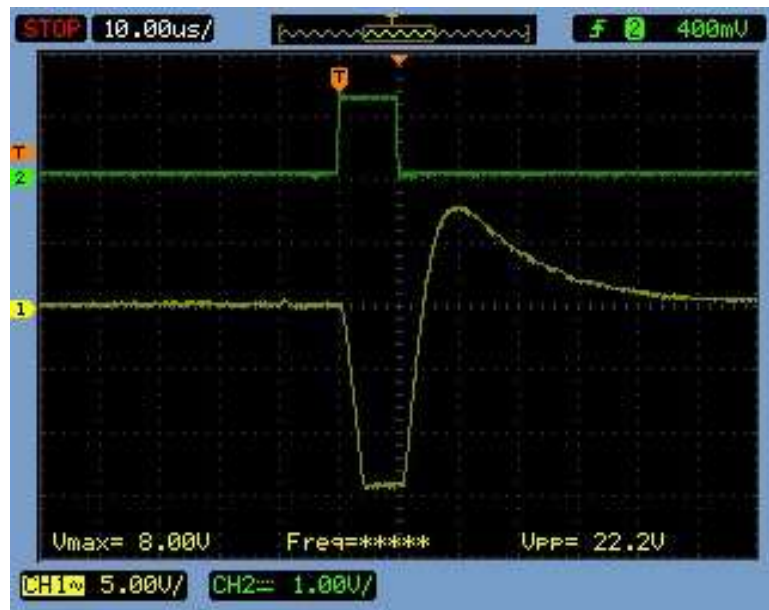


**Figure 4.16.** Signal waveforms 1) Pulse amplifier output of DPCAM electronics. 2) Corresponding input test pulse to CIR LED with pulse amplitude at 2.4 V and a pulse width of 10  $\mu$ s.

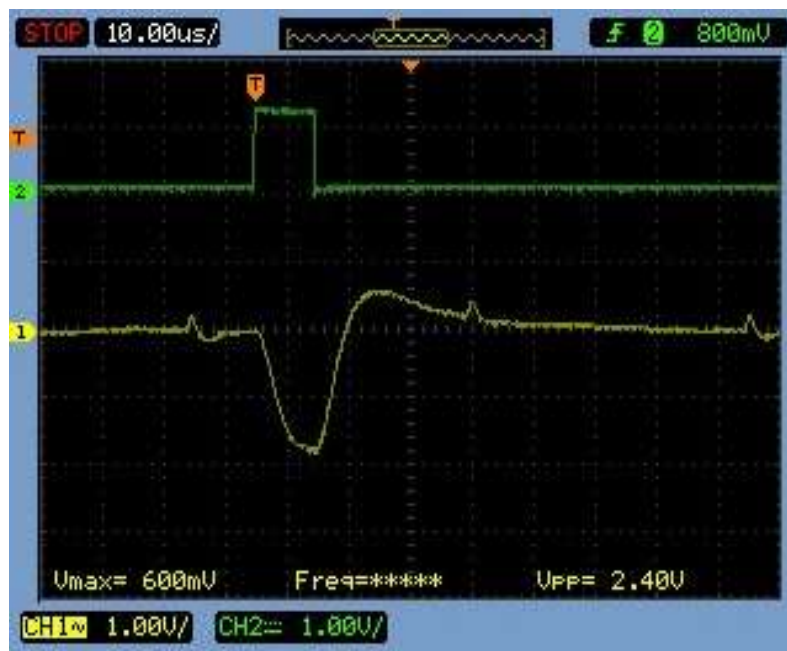


**Figure 4.17.** Signal waveforms 1) Pulse amplifier output of DPCAM electronics. 2) Corresponding input test pulse to CIR LED with pulse amplitude at 1.8 V and a pulse width of 10  $\mu$ s.

#### 4.8 ONLINE TEST RESULTS OF DPCAM

The online test is initiated by pressing DPCAM test button created on the SCADA screen. DPCAM test circuit automatically generates test frequency with a pulse amplitude of 2.4 V for testing alpha channel initially from 10 Hz, 200 Hz, 400 Hz, 600 Hz and 800 Hz at the 60 s duration at each step. At the end of the alpha channel test, the beta channel test is initiated for same frequency patterns with a pulse amplitude of 1.8 V. Figure 4.18 shows real-time trend graphs generated during the online performance evaluation of alpha channel with fresh filter paper. The counts vs time (top graph) for test frequency profile applied and corresponding relative intrinsic error vs time (bottom graph) are shown for both alpha (red) and beta (blue) channels. Figure 4.19 illustrates real-time trend graphs generated during the online performance evaluation of beta channel with fresh filter paper. The counts vs time (top graph) for test frequency profile applied and corresponding relative intrinsic error vs time (bottom graph) are shown for both alpha (red) and beta (blue) channels. The maximum relative intrinsic error, in this case, is less than + 1%. Real-time graphs show that the error reached the maximum value to a minimum value after a corresponding change in counts due to change in the test frequency.

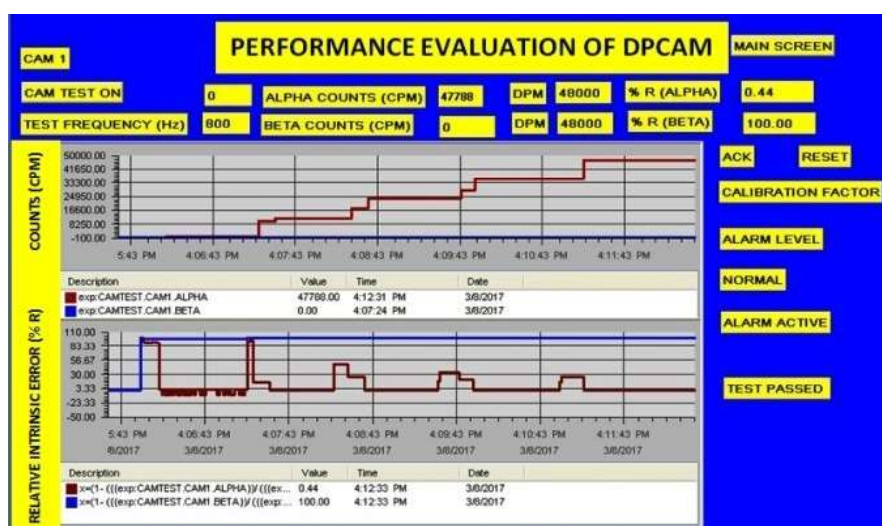


**Figure 4.18.** Real-time trend graphs generated during the online performance evaluation of alpha channel with fresh filter paper. The counts vs time (top graph) for test frequency profile applied and corresponding relative intrinsic error vs time (bottom graph) are shown for both alpha (red) and beta (blue) channels.

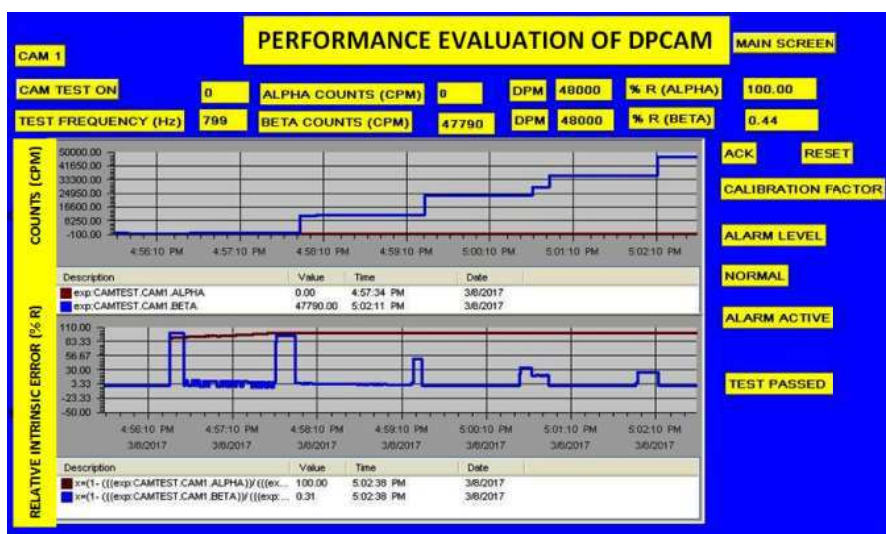


**Figure 4.19.** Real-time trend graphs generated during the online performance evaluation of beta channel with fresh filter paper. The counts vs time (top graph) for test frequency profile applied and corresponding relative intrinsic error vs time (bottom graph) are shown for both alpha (red) and beta (blue) channels.

#### 4.8.1 Periodical online performance evaluation

Periodical online performance evaluation methods [61,62,63] enable trend analysis of DPCAM electronics along with PMT towards its early failure detection. Many different techniques available for trend analysis such as anomaly detection, qualitative trend analysis and shape based on a linear piece-wise time-invariant model to estimate the downtime of the system.

#### 4.9 ONLINE PERFORMANCE EVALUATION AND VALIDATION OF THE SYSTEM IN RADIATION FIELD

Initially, the alpha-beta counts of loaded filter paper and test frequency alone are noted separately. The expected counts are calculated by addition of counts due to loaded filter paper and counts of test frequency. The observed counts are noted by an online test performed with loaded filter paper, and test frequency applied simultaneously. Similarly, the performance evaluation carried out using radioactive sources. The relative intrinsic error is calculated at each step of the test frequency. Figure 4.20 shows the relative intrinsic error in the alpha channel using test frequency alone, loaded filter paper in the field and three different alpha sources

including counts of test frequency. It is found considering background subtraction the maximum relative intrinsic error is + 3.1%. Figure 4.21 illustrates the relative intrinsic error in the beta channel using test frequency alone, loaded filter paper in the field and three different beta sources including counts of test frequency. The maximum relative intrinsic error, in this case, is + 6.9%. The relative intrinsic errors of both channels are within acceptable limits [72] ( $\pm 10\%$ , as per OEM) and compatible with the intended application. These errors are mainly due to instrumental, statistical fluctuations of radioactive sources and coincidence loss due to overlapping of photons from LED & scintillation photons. In the beta channel, the error is more due to the selection of ULD. Thus, the system is validated for full-scale range, so remote online performance evaluation efficiently brings out any deviation in the performance of PMT and electronics of DPCAM in terms of efficiency, verification of relative intrinsic error and crosstalk between alpha-beta channels.

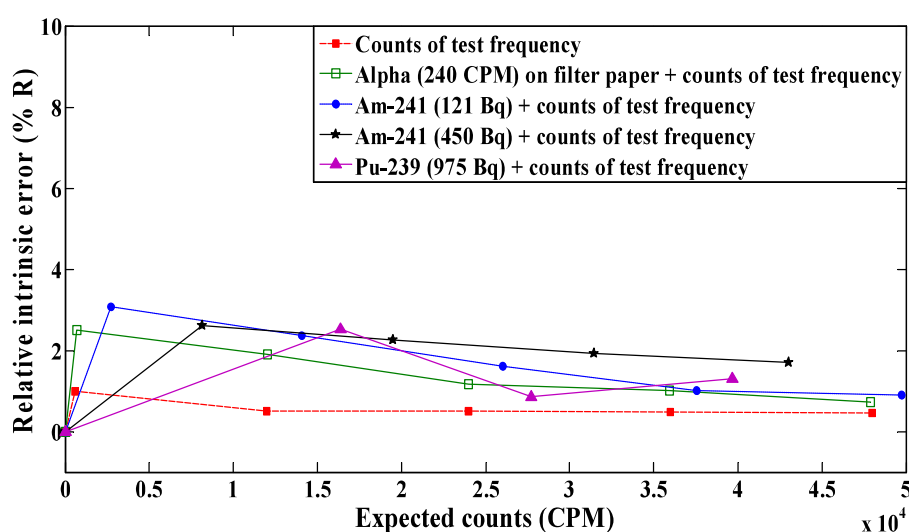


**Figure 4.20.** Relative intrinsic errors in the alpha channel using test frequency alone, loaded filter paper and three different alpha sources including counts of test frequency.

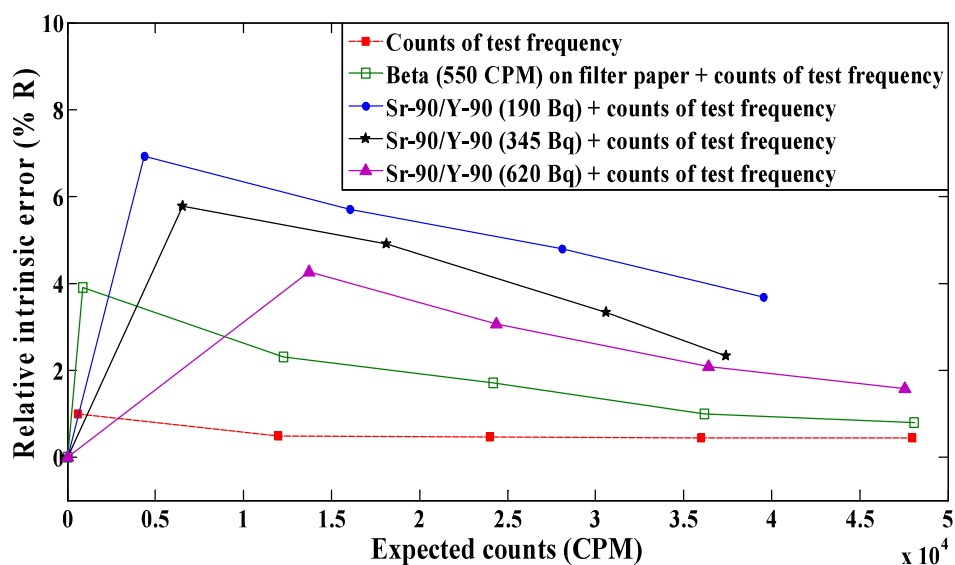


**Figure 4.21.** Relative intrinsic errors in the beta channel using test frequency alone, loaded filter paper and three different beta sources including counts of test frequency.

#### 4.10 COMPARISON BETWEEN CONVENTIONAL AND ONLINE SURVEILLANCE METHODS

The periodical surveillance of DPCAM is carried out as per the typical technical specification of the plant. Detailed person-hours requirement analysis of conventional and online surveillance methods of DPCAM are shown in Table 4. 3. The radioactive source calibration is performed using conventional surveillance method. Hence there is no change in the requirement of Person-hours per year. The person-hours per unit per year saved [64] using online surveillance method are 65.8% even after radioactive source calibration considered as mandatory.

**Table 4.3.** Person-hours comparison between conventional and online surveillance methods of DPCAM.

S. No	Surveillance plan as per the technical specification of the plant	Surveillance type	Conventional surveillance			Remote online surveillance		
			Average time (h) per year	No. of persons	Person -hours	Average time (h) per year	No. of persons	Person -hours
1	Continuous monitoring	RADAS readings checking	(No change)			(No change)		
2	Monthly	Checking	0.33x12	2	7.92	0.17x12	1	2.04
3	Quarterly	Radioactive source testing	0.42x4	2	3.36	0.17x4	1	0.68
4	Half year	Radioactive source calibration	0.5x2	2	2.00	0.5x2	2	2.00
5	Yearly	Electronic calibration	0.5x1	2	1.00	0.17x1	1	0.17
Total no. of person-hours per unit per year			14.28			4.89		
Total no. of person-hours per 50 units per year in a nuclear plant			714			244.5		
Person-hours per unit per year saved using online surveillance method.			65.8% (Including radioactive source calibration)					

#### 4.11 CONCLUSION

In this chapter, a newly developed remote online performance evaluation method for PMT and electronics of DPCAM from the control room using wireless network is presented. Based on the experimental results, colour infrared LED is found to be the most suitable light source. It is able to discriminate alpha and beta radiation using pulse amplitude discrimination technique with zero crosstalk. The optimal pulse width of 10  $\mu$ s and pulse amplitudes of 2.4 V & 1.8 V (for



alpha and beta respectively) are selected for performance evaluation. The relative intrinsic error for this LED is less than + 1% in both channels with fresh filter paper. The performance evaluation is carried out in the radiation field with loaded filter paper and different alpha-beta radioactive sources along with the pulsed light source. The maximum relative intrinsic error obtained in alpha and beta channels are + 3.1% and + 6.9% respectively. The errors are within the acceptable limits ( $\pm 10\%$ , as per OEM) and compatible with the intended application. The real-time trend and historical trend graphs generated in RADAS effectively bring out any deviation in the performance of PMT and electronics of DPCAM. The time required for online performance evaluation of both alpha and beta channels of DPCAM is 10 minutes. The person-hours per unit per year saved using online surveillance method are 65.8% as compared with conventional methods. Wireless communication link performance is tested in terms of received signal strength indicator (RSSI) and the packet error rate (PER), the RSSI between each node varied between  $-50$  and  $-65$  dBm and 100% packet delivery is observed hence, the PER is found to be zero. The proposed method is applicable for all other scintillation based radiation monitors. The feasibility of surface-mount color infrared LED is to be investigated further for a compact test setup. Advanced electronics like FPGAs are to be used for generation of test frequency in place of discrete electronic components for better stability and reliability.

## 5

## DEVELOPMENT OF ONLINE FAULT DIAGNOSTICS, ONLINE TESTING AND DESIGN ENHANCEMENT OF CRITICALITY ALARM SYSTEM

---

*The present chapter explains the failure mode and effect analysis of each element of criticality alarm system (CAS) to detect inherent dangerous faults and development of early fault detection circuits for alarm annunciation in control room. In addition, two different novel methods explained to ensure the reliable functionality of CAS, one method for online channel loop functionality test and another method to dose alarm test using transient electronic pulse. The design enhancement of external systems that are integrated into CAS such as the power supply, criticality evacuation hooter circuit, radiation data acquisition system are elaborated. Reliability analysis of additional components used in the CAS, person-hours requirement analysis of conventional and online surveillance methods of CAS are also described.*

---

### 5.1 INTRODUCTION

Significant quantities of strategic nuclear fissile materials such as  $^{233}\text{U}$ ,  $^{235}\text{U}$ , and  $^{239}\text{Pu}$  are handled in nuclear plants. These plants adopt ever-safe geometry, safe mass, safe concentration, and administrative controls. Still, there exists an extremely small probability of occurrence of criticality. Nevertheless, in view of the radiological consequences of such events in terms of large exposures to radiation personnel, a criticality alarm system (CAS) [37,38,39,40,80,81,82] is employed for prompt detection and alarm against such criticality events. The event could be a single excursion ( $10^{14}$  -  $10^{19}$  fissions) or could be multiple events followed by self-sustaining chain reactions of various amplitudes in duration from 1 s to several hours [83]. The gamma and

neutron doses from such events are significantly higher, necessitating the immediate evacuation of the area by the occupants. Design of CAS is meant for continuous operation such that it neither failed to detect even a single criticality event nor triggered a false criticality alarm due to system failure. However, failures associated with low voltage power supply, high voltage, system on battery, battery charging/isolation diode, and single channel alarm are found as the primary cause of system unavailability that can generate false criticality alarms. False criticality alarms not only create panic among radiation personnel but also erode the credibility of the system, resulting in failure to prompt action in response to criticality alarms. CAS suffers design deficiencies on the diagnosis of dangerous detectable and undetectable failures. This work aims to enhance CAS design at each stage by means of early fault alarm announcement in the control room, in and ex-situ surveillance techniques for maximum availability, and prevention of false criticality alarms.

Presently, failure mode and effect analysis (FMEA) [41] is carried out on each element of CAS to detect inherent dangerous faults and to develop early fault detection circuits for alarm announcement in the control room. In addition, the detailed developments for design enhancement of CAS are also presented. Two different novel methods are developed to ensure the functionality, one method for channel loop functionality test and another method for dose alarm test using transient electronic pulse. The design enhancements of the external systems that are integrated in the CAS include the power supply, criticality evacuation hooter circuit, radiation data acquisition system (RADAS) along with a selection of different soft alarm set-points, and centralised online electronic test facility. The soft alarm is a user-defined level or a condition specified in RADAS for visual indication without audio. Reliability analysis of additional components used in the CAS, Person-hours requirement analysis of conventional and online surveillance methods of CAS is also presented.

## 5.2 CONVENTIONAL CAS DESIGN

The CAS consists of three independent channels. Each channel contains an ionization chamber, preamplifier, and an electronic module. The ionization chamber is a gamma-based detector, qualified for radiation tolerance of  $10^3$  Gy/h; it has a sensitivity of  $3 \times 10^{-8}$  A/Gy/h [82] for an operating voltage of 200 to 1000 V. The current signal from the detector is connected to the RC network for the equivalent output voltage. The output voltage is applied to the preamplifier for further amplification from 1 to 5 V for the dose rate display of 0.01 to 100 mGy/h. The preamplifier is an integrated FET based amplifier, and its output is connected to the electronic module. The electronic module consists of low and high voltage power supplies, processing electronics, display, and channel alarm relay contacts. Each channel is provided with class I (battery) power supply in case of mains failure. During the normal operation, the channel works on the low voltage power supply and provides a float charge on battery through a battery charging/isolation diode. The front panel of each electronic module provides LED indications for normal operation, channel alarm with a beep sound, mains, and high voltage. An electronic test/reset facility is provided within each electronic module. A test voltage of 1 V is applied to the input stage of the preamplifier during the test. This displays an equivalent dose rate of 40 mGy/h as well as a testing of the channel alarm. Figure 5.1 is a block diagram of the CAS in which the alarm relay contacts from three electronic modules are connected to the alarm module. The alarm module generates a criticality alarm based on 2 out of 3 (2-o-o-3) voting logic using a relay that operates in a fail-safe mode [41], i.e., the alarm relay de-energises on criticality alarm condition. Maintaining this system with maximum availability and minimum false criticality alarm probability is a challenging task. CAS design is capable of detecting a minimum accident of concern of the accident mechanism. This is the one that results in a dose of 0.2 Gy in the first minute at a distance of 2 m from the reacting material assuming only nominal shielding [84,85,86,87]. CAS initiates a channel alarm if the steady dose rate exceeds 40 mGy/h or if the integrated dose is delivered at 30  $\mu$ Gy due to criticality spike of duration within 500 ms.

Fail-safe behaviour is the capability of any system or component to proceed to a predefined safe state in the event of a malfunction. In CAS, triple modular redundancy with 2-o-o-3 voting logic is used. It offers a balance between safety and reliability actions. To reduce the probability of failure on demand [88] of CAS, there is a scope to reduce the failure rates associated with dangerous detected and undetected failures. The dangerous detected component is improved by selection of an appropriate configuration (fail-safe design) and by providing fault diagnostics of the system in case of a dangerous failure. The dangerous undetected component is reduced by improving the diagnostic coverage, periodic surveillance, and testability of the system.

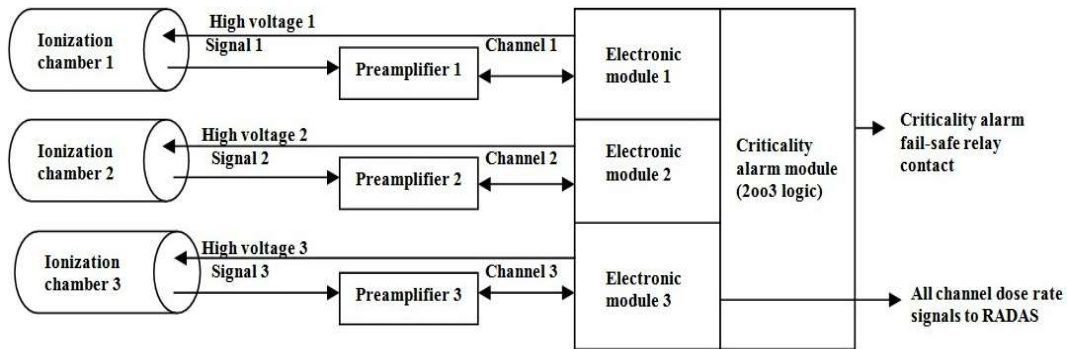


**Figure 5.1.** Block diagram of the CAS.

### 5.3 DESIGN ENHANCEMENTS IN CAS

#### 5.3.1 FMEA of CAS

The failure mode and effect analysis of existing CAS carried out as per the standard MIL-STD-1629A [89] for potential failures of components/modules that may cause channel alarm at the system level considered. Based on FMEA, the elements that cause system unreliability and generate false criticality alarms are identified. Table 5.1 shows the failure mode and effects analysis of crucial elements in CAS. The failures associated with the low voltage power supply in both electronic and alarm modules are dangerous but detectable. In case of low power supply failure to these modules, due to the failure of the DC regulator, the battery charging/isolation diode opens. If this is not noticed within 40 h, the battery of the electronic module drained

completely; the fail-safe channel relay, de-energised, triggers the false channel alarm and the channel will not be available.

Similarly, if high voltage power supply to the ionization chamber fails, and if it is not noticed immediately, the channel will subsequently not be available. If the channel battery fails, then channel availability depends on the uninterruptible power system (UPS) back up. Failures in either ionization chamber or preamplifier is caused by unavailability of the channel. Channel loop functionality failure occurs due to loss of integrity between the preamplifier, high voltage, detector, cables, and connectors. These dangerous undetectable failures cause channel unavailability. Failures of criticality evacuation hooter circuit detect immediately as this circuit is operated in a fail-safe condition. The communication bus, along with RADAS, is used for data acquisition and logging. Failures of such systems will not affect the prime functionality of the system for triggering the criticality alarm. Based on the FMEA, two additional hardware circuits are developed, one for early detection of failures and another circuit for channel loop functionality test.

**Table 5.1.** Failure mode and effects analysis of crucial elements in CAS

S. NO	FMEA Component	Potential failure mode	Potential cause(s) / mechanism	Effects of failure	(P) Probability (estimate)	(S) Severity	Detection (Indications to Operator, Maintainer)	(D) Detection Dormancy Period	Risk Level (P*S)+D	Mitigation/ Requirement
1. Detector	Ionization chamber	Detector fail	Gas leak/guard ring/electrode fault	Channel fails to detect criticality	Remote (B)	Minor (III)	Detectable in quarterly surveillance	Quarterly surveillance	Low	The failures of low voltage, high voltage, system on battery, battery charging/isolation
2. Pre-amplifier	Integrated FET amplifier	FET/ Transistor/ Zener diode fail	FET/Transistor/ Zener diode Open/short	Channel fails to detect criticality/Channel alarm	Remote (B)	Minor (III)	No response in channel during test	Weekly (surveillance)/ alarm in CR immediately	Low	diode, and single channel alarm shall be provided with an alarm
3. Electronic module	Low voltage power supply	DC regulator fail/battery charging/ isolation diode open	Overheating/comp onent fail	No immediate effect, after class I battery drain (40 hr), higher chance for channel not available and false channel alarm	Remote (B)	Minor (III)	After class I battery drain, higher chance of channel not available and false channel alarm	Within a shift/weekly (surveillance)	Low	annunciation in control room for immediate attention and action to prevent false criticality alarm.
	Class I	Battery failure	Battery open/ no charging/fails to drive load	No immediate effect, after class II fails higher chance for channel not available and false channel alarm	Remote (B)	Moderate (IV)	After class II fails higher chance for channel not available and false channel alarm	Weekly (surveillance)	Low	&
	High voltage	High voltage failure	High voltage transformer/oscillator fail	CAS channel is not available to detect criticality event	Extremely unlikely (A)	Moderate (IV)	Indication in CAS	Within a shift (surveillance)	Low	A method is to be developed to test the channel loop functionality test for each channel.
	Channel loop	Detector/Pre amplifier/ electronic module/ cables and connectors	Loose contact/wrong connections/comp onent failures	CAS channel is not available to detect criticality event	Extremely unlikely (A)	Moderate (IV)	Indication in CAS	Weekly (surveillance) or during maintenance	Low	

## Chapter 5

S. NO	FMEA Component	Potential failure mode	Potential cause(s) / mechanism	Effects of failure	(P) Probability (estimate)	(S) Severity	Detection (Indications to Operator, Maintainer)	(D) Detection Dormancy Period	Risk Level (P*S)+D	Mitigation/ Requirement
4. Alarm module	Low voltage power supply	DC regulator fail/battery charging/isolation diode open	Overheating/component fail	No immediate effect, after class I battery drain, higher chance for false criticality alarm	Remote (B)	Moderate (IV)	After class I battery drain, higher chance for false criticality alarm	Within a shift/weekly (surveillance)	Low	The failures of low voltage, high voltage, system on battery, battery charging/isolation diode, and single channel alarm shall be provided with an alarm annunciation in control room for immediate attention and action to prevent false criticality alarm.  & A method is to be developed to test the channel loop functionality test for each channel.
		Battery failure	Battery open/no charging/fails to drive load	No immediate effect, after class II fails chance for false criticality alarm	Remote (B)	Moderate (IV)	After class II fails chance for false criticality alarm	Weekly (surveillance)	Low	
		Driving transistor open/relay failure	Overheating, output transistor open/relay coil open	False criticality alarm	Remote (B)	Minor (III)	Indication in CAS	Immediately	Low	
5. RADAS	Communication bus	CAS channel connectivity fail	Cable fault/loose contact/digital I/O module	Alarm indication in RADAS	Occasional (C)	Very Minor (II)	Alarm in RADAS	Immediately	Low	The failures of low voltage, high voltage, system on battery, battery charging/isolation diode, and single channel alarm shall be provided with an alarm annunciation in control room for immediate attention and action to prevent false criticality alarm.  & A method is to be developed to test the channel loop functionality test for each channel.
		RADAS Server/ connectivity fault	Server/cable/software problem	RADAS display is not available	Occasional (C)	Very Minor (II)	RADAS Display is not available/ hanging	Immediately	Low	
6. Criticality evacuation hooter circuit	External hooters	Redundant hooter power supply	One power supply fail	No immediate effect	Remote (B)	Moderate (IV)	Indication on alarm annunciation	Immediately	Low	The failures of low voltage, high voltage, system on battery, battery charging/isolation diode, and single channel alarm shall be provided with an alarm annunciation in control room for immediate attention and action to prevent false criticality alarm.  & A method is to be developed to test the channel loop functionality test for each channel.
		Individual hooter fail	Fuse fail/hooter fail	No immediate effect	Remote (B)	Minor (III)	Faulty hooter detected in weekly test; hooter LED fails to glow	Weekly (surveillance)	Low	
		Hooter relay failure	Relay coil open	False criticality alarm	Remote (B)	Minor (III)	Immediately	Immediately	Low	
7. Centralized electronic test facility	Electronic test	Channel failed to test/ reset	Mechanical problem/human error	Channel test not possible/channel alarm	Remote (B)	Minor (III)	Immediately	Immediately	Low	The failures of low voltage, high voltage, system on battery, battery charging/isolation diode, and single channel alarm shall be provided with an alarm annunciation in control room for immediate attention and action to prevent false criticality alarm.  & A method is to be developed to test the channel loop functionality test for each channel.
		CAS Hooter bypass switch on	Mechanical problem/human error	Hooters are not available during particular criticality alarm	Remote (B)	Minor (III)	Alarm in CR	Immediately	Low	



### 5.3.1.1 Development of early fault detection circuit

Based on the FMEA, an early fault detection circuit is developed for failures associated with low voltage, high voltage, system on battery, battery charging/isolation diode, and single channel alarm to alarm annunciation. The circuit contains two comparators, two driving transistors, and a two-pole relay. A channel PCB is designed as per IPC-2221A [56], as any inherent faults generate an announcement based on fail-safe condition. The sampled high voltage is compared with the respective battery reference voltage using a level comparator (U1), as shown in Figure 5.2. Similarly, the battery voltage is compared to the low voltage supply reference using a level comparator (U2). The output of each comparator drives two independent transistors, and the circuit requires fine-tuning of reference voltages for the intended function. The output of the transistors is connected to the AND gate logic to drive a two pole relay in fail-safe mode. This circuit is installed in each electronic module. A similar PCB is used in the alarm module to detect failures of the low voltage power supply, the system on the battery, and the battery charging/isolation diode. Normally open (NO) contacts of each relay in all the electronic modules are connected in series and the series combination of such modules routed for early fault detection circuit for alarm annunciation.

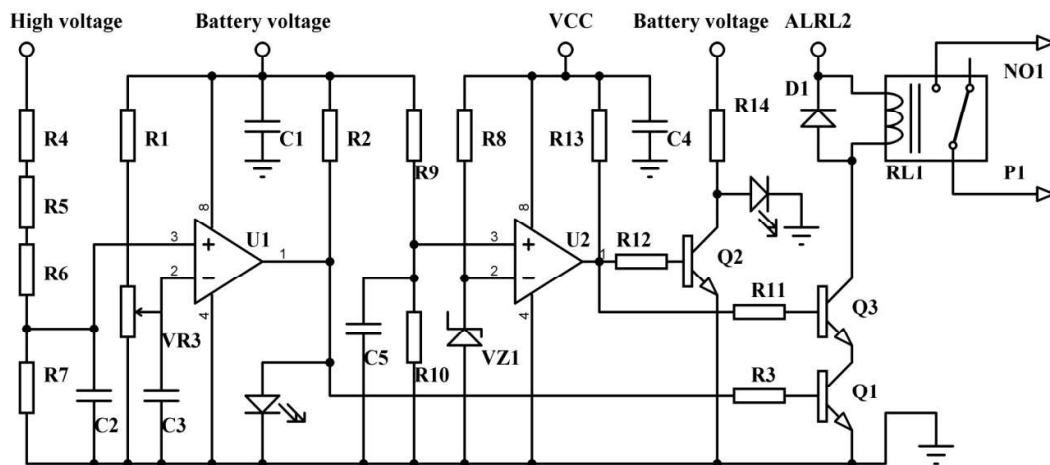


**Figure 5.2.** Early fault detection circuit.

Both electronic PCBs are accepted as per IPC-A-610F [57]. Design of all electronic circuits is provided with proper protection, isolation and fail-safe features. It is also ensured that the failures of additional circuits does not degrade the performance of CAS.

#### **5.4 METHOD DEVELOPED FOR CHANNEL LOOP FUNCTIONALITY TEST**

The ionization chamber [90], preamplifier, and high voltage/electronic module of the CAS channel are located geometrically at different places in the plant. The channel loop functionality of the CAS channel is to be tested at periodic intervals to ensure its availability. The channel loop functional test method is developed based on creating a known perturbation in the high voltage applied to the ionization chamber during the test. The dose rate response is compared with the predefined response of each channel. Based on the equivalent circuit of the ionization chamber, as shown in Figure 5.3, it offers a current source  $I_1$  in series with a capacitance ( $C_i$ ) at zero background radiation. As soon as the high voltage is applied to the ionization chamber, voltage across the capacitance of the chamber gradually increases and fully charges within 5 time constants. Similarly, the charging current through  $C_i$  is at its maximum and gradually decreases to zero within 5 time constants. The current from the ionization chamber contributes a maximum dose rate of 100 mGy/h in the channel display for a period of 5 to 6 s. The current from the ionization chamber depends on the amplitude of the high voltage applied. This concept is used to test the channel loop functionality of the ionization chamber, the high voltage, the electronic module, the cables, and the connectors in each channel. The experiments are conducted for optimum test perturbation in the high voltage supply.

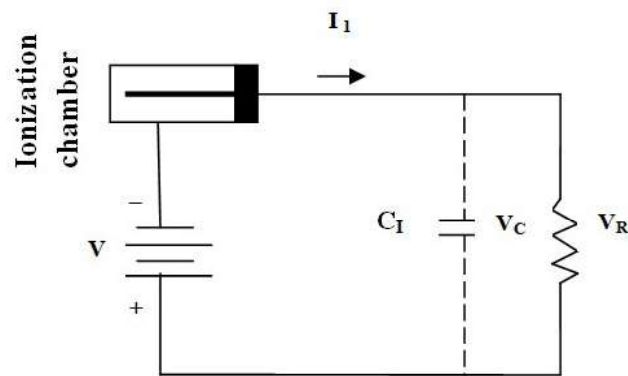


**Figure 5.3.** Equivalent circuit for ionization chamber.

#### 5.4.1 Development of channel loop and functional test circuit

Based on the experiments, channel loop and functional test circuits are developed. The circuit, containing a monostable multivibrator, two-pole relay, and driving transistor, is shown in Figure 5.4. The output of the monostable multivibrator is a single shot pulse with pulse width of 6 s; it is connected through a driving transistor to a two pole relay. The relay pulls the primary winding of the high voltage blocking oscillator to lower the voltage from its normal value. The high voltage (typical 700 V) is instantly reduced to 620 V, subsequently reducing the electric field in the ionization chamber, which causes a reduction in output current due to the internal capacitance. As a result, the preamplifier output voltage is reduced from its normal value. The high voltage output automatically increases to its typical value up to 6 s. The charging current in the ionization chamber is increased instantly. The preamplifier output voltage increases greater than the normal value and is restored after 10 s. The Figure 5.5 shows test profile of high voltage applied to the ionization chamber during the channel loop functional test. The channel loop functional test can be triggered manually using a spring-loaded key operated switch mounted on the three electronic modules of the CAS. The test is a more comprehensive system test to ensure the reliability of CAS.

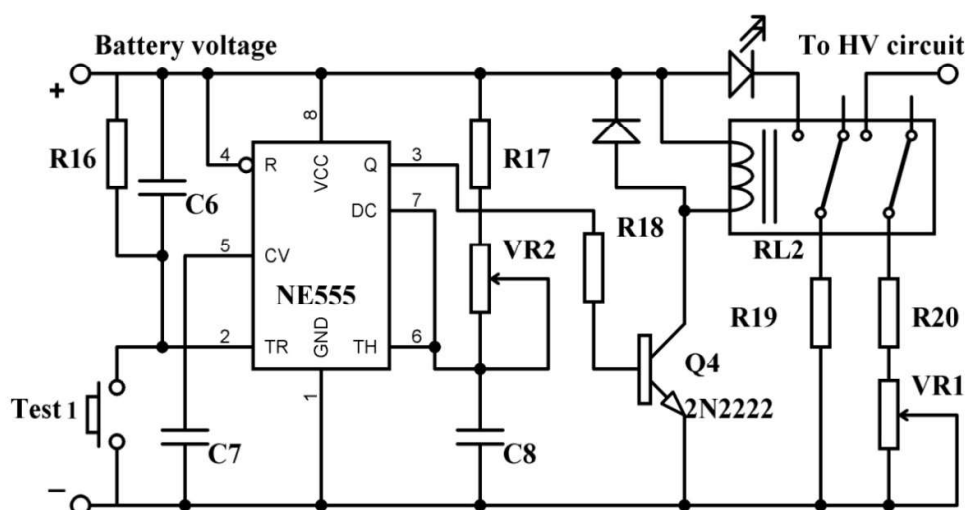


**Figure 5.4.** Channel loop functional test circuit.

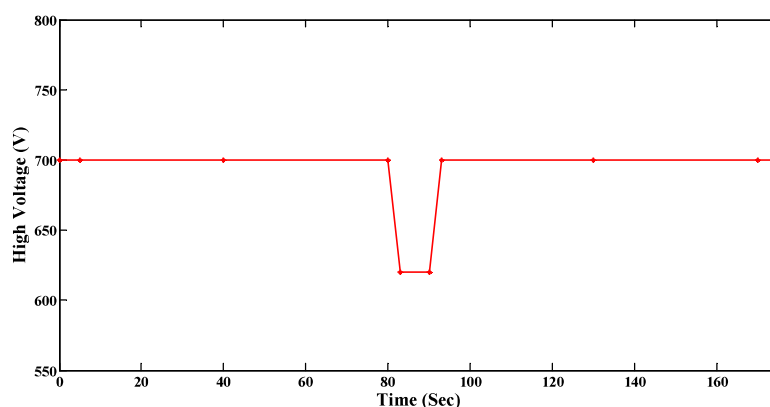


**Figure 5.5.** The test profile of the high voltage applied to the ionization chamber during the channel loop functional test.

## 5.5 METHOD DEVELOPED FOR DOSE ALARM TEST

CAS initiates a channel alarm if dose rate exceeds 40 mGy/h or if the dose exceeds 30  $\mu$ Gy within 500 ms. Dose rate alarm is tested using the standard  $^{137}\text{Cs}$  or  $^{60}\text{Co}$  radioactive source at the installed location of the ionization chamber. However, the dose alarm is tested using X-ray dose or similar radioactive source motion setup, which is practically difficult for installed detectors. The dose alarm test method is developed using an electronic transient pulse. The sensitivity of the ionization chamber, the dose rate alarm set-point, and the input one-Giga ohm resistance are considered. Location of test input applied during the electronic and transient test as shown in Figure 5.6.

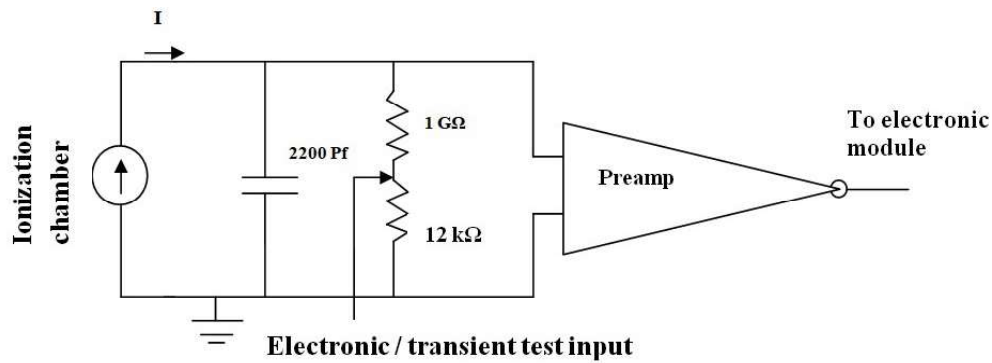


**Figure 5.6.** Ionization chamber, RC network and preamplifier circuit. Location of test input applied during the electronic and transient test.

The voltage developed across the one-Giga ohm resistance due to the sensitivity of the ionization chamber is 0.3 V per 10 mGy/h. The corresponding voltage at dose rate alarm (40 mGy/h) is 1.2 V. The dose alarm set point is 30  $\mu$ Gy/500 ms and the equivalent dose rate is 216 mGy/h. The voltage for the dose alarm at 216 mGy/h is 6.48 V. The time (t) required to trigger the dose rate alarm at 1.2 V is calculated based on the transient response of the RC network, having a time constant ( $\tau$ ) of 2.2 s during charging.

$$t = -\tau * \ln\left[1 - \frac{V_{in}(t)}{V_0(t)}\right] \quad (5.1)$$

Based on Eqn. (5.1), the value of t is calculated and it is found to be 450 ms. Using a programmed pulse generator, the dose alarm of each channel is practically tested with the transient pulse of pulse amplitude 6.48 V and with pulse width varied from 300 ms to 600 ms. Status of the channel alarm corresponding to the preamplifier output voltage is captured in the oscilloscope. Similarly, the response of the dose rate at different pulse widths is also recorded in RADAS.

## 5.6 DESIGN ENHANCEMENT OF EXTERNAL SYSTEMS FOR CAS

### 5.6.1 Reliable power supply to CAS

Four different classes of power supplies are connected such that one acts as the backup to another power supply. To ensure reliable power supply to CAS, each electronic module is provided with a

class I (battery) power supply, which is connected from sealed maintenance free type lead-acid batteries. Class II (UPS) backs up the class I power supply. Similarly, Class III (diesel generator) backs up Class II, and Class III is backed up by the Class IV (off-site) power supply. Each electronic module operates on DC power obtained from AC 230V, 50Hz through an AC transformer, rectifier, DC filter, and DC regulator output voltage. A dedicated double conversion based online UPS is recommended for CAS loads; this device provides electrical isolation against surges. The DC voltage at the filter capacitor output is used to provide the float charge on class I batteries. This voltage is connected to class I batteries through a battery charging/isolation diode; at this point, both power supplies are connected in parallel. Class I power supply is provided to three electronic modules and the alarm module using independent batteries. For immediate attention, the fail-safe based relay contacts are provided for both UPS input and output AC mains failure alarm announcement on the control panel.

## **5.7 DESIGN OF CRITICALITY EVACUATION HOOTER CIRCUIT**

The criticality alarm fail-safe relay contacts from each alarm module of CAS (considering five CAS in the plant, CAS1, CAS2...and CAS5) are multiplied using interposing relays. One pair of relay contacts are used to connect the alarm annunciation in the control room, and another set of relay contacts is used to activate the criticality evacuation hooter circuit in case of criticality alarm. This circuit is provided with redundant 24V DC power supply. The inputs to the power supplies are connected from two different AC sources (UPS). The healthy status relay contacts (NO) of both 24V DC power supplies are connected in series and routed to the alarm announcement in the control room in case of any fault in the 24 V DC power supplies. Figure 5.7 shows that the output of the evacuation hooter circuit is connected to the distributed low powered high sound DC piezoelectric hooters with individual fuses for failure indication. Each piezoelectric hooter provides 120 dB audio at a one-meter distance. The advantage of distributed piezoelectric hooters is low power consumption and the provision of audio redundancy.

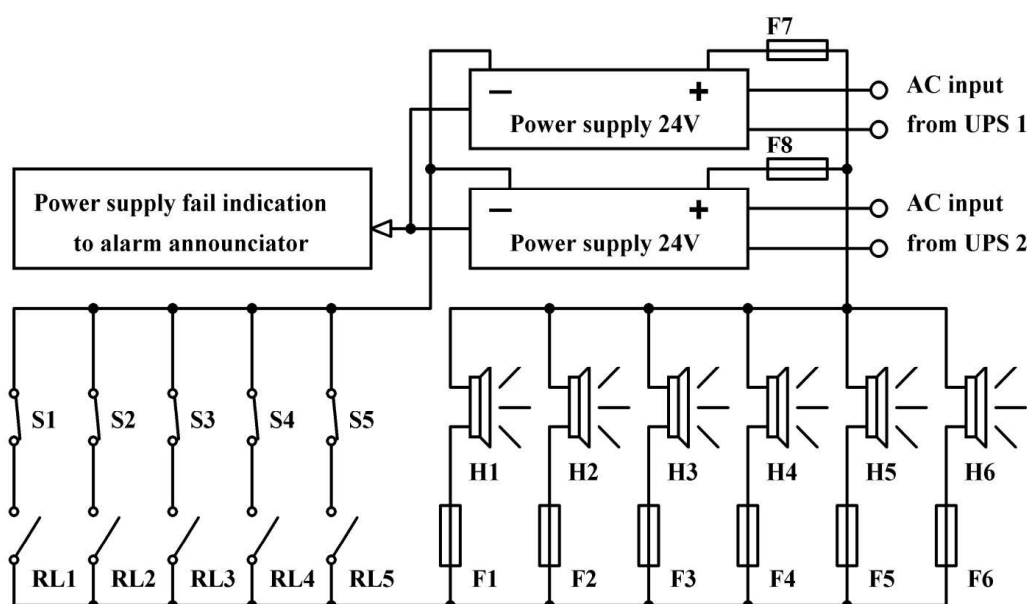


**Figure 5.7.** Criticality evacuation hooter circuit consists of CAS hooter bypass switches S1 to S5, CAS alarm relays RL1 to RL5 and electronic hooters H1 to H6.

The series combinations of the fail-safe criticality alarm relay contact and the criticality evacuation hooter bypass switch of each CAS are connected in parallel with similar series combinations of other CAS. Similarly, the series combination of electronic hooter along with fuse failure indication is connected in parallel. These combinations are connected in series with redundant power supply. In case of a criticality alarm from any of the CAS, the criticality alarm relay de-energises, NO contact becomes normally closed contact, and the criticality evacuation hooter circuit is triggered. In this design, it is ensured that the current rating of the criticality alarm relay contact provides sufficient current for a number of electronic hooters in the loop. The criticality alarm relays in CAS, the piezoelectric hooters, the criticality evacuation hooter bypass switch, the 24 V DC power supplies/fuse failure indications, and the alarm announcement are placed geometrically at different locations in the nuclear plant. The internal cabling between these components becomes very complicated. The cable route will be diverse and must be properly labelled for easy identification.

### 5.7.1 Criticality evacuation hooter bypass facility

The criticality evacuation hooter circuit provides a bypass facility for any one of the CAS using criticality hooter bypass switch (S1 to S5) during preventive maintenance; other CAS will continue to be operated normally. Each hooter bypass switch is a two pole key-operated switch installed on the control panel. One set of NC contacts are used to bypass the CAS from the evacuation alarm circuit, as shown in Figure 5.7. Another set of NC contacts are connected in series and routed for alarm annunciation on the control panel. This is done to ensure that the bypass is restored after preventive maintenance in CAS.

## 5.8 CONFIGURATION OF CAS FOR ONLINE MONITORING AND TESTING

Figure 5.8 shows the architecture of RADAS along with one CAS. The voltage output signal (1 – 5 V) from each CAS, the preamplifier output is connected to a digital I/O module 1 to display the dose rate in RADAS. The digital I/O module is provided with galvanic isolation and no loading effect on the input signal. The digital I/O module converts analog voltage signals (dose rate) to corresponding digital RS-485 signals. Similarly, digital I/O module 2 is provided for testing of online loop functionality in each channel and digital I/O module 3 is provided for online electronic test/reset of each channel. The RS-485 signals are converted to TCP/IP signals using an RS-485 to TCP/IP converter. The RADAS server communicates with the field devices through the Modbus protocol in TCP/IP. Table 5.2 shows the different Modbus tags used for data communication and online testing of CAS. An open platform communication (OPC) server and supervisory control and data acquisition (SCADA) software are installed in the RADAS server. The graphical user interface (GUI) screens are developed in SCADA for each CAS channel dose rate, as well as in the bar graph, soft alarms for each channel alarm, real-time graphs, historical trend graphs and soft alert alarms for each channel. The channel soft alert alarms enable blue indication in RADAS without audio. A soft criticality alarm indication is developed for each CAS



in SCADA. All the CAS information is available on GUI screens in real-time and these data are logged in the RADAS server for historical trend graphs.

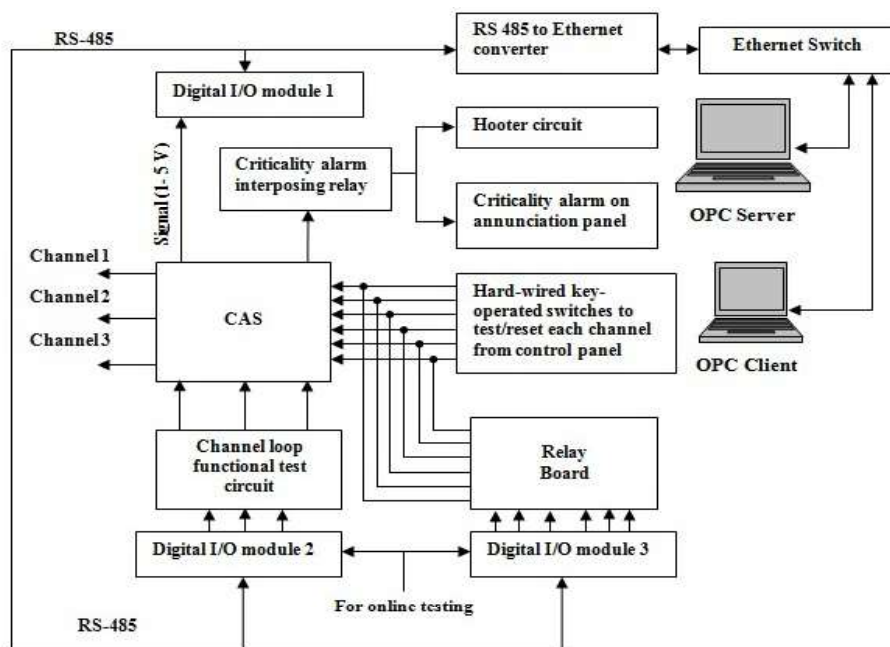


**Figure 5.8.** The centralized online electronic test facility, alarm annunciation and RADAS architecture of CAS.

**Table 5.2.** Different Modbus tags for data communication and online testing of CAS.

S. No	Digital I/O module & ID	Tag description in CAS	Modbus tag address	Data type	Client access
1	1 & 6	Channel 1 Dose rate	400001	Word	Read Only
2		Channel 2 Dose rate	400002	Word	Read Only
3		Channel 3 Dose rate	400003	Word	Read Only
4		Criticality Alarm	400004	Word	Read Only
5	3 & 8	Channel 1 test	400001	Boolean	Read/Write
6		Channel 1 reset	400002	Boolean	Read/Write
7		Channel 2 test	400003	Boolean	Read/Write
8		Channel 2 reset	400004	Boolean	Read/Write
9		Channel 3 test	400005	Boolean	Read/Write
10		Channel 3 reset	400006	Boolean	Read/Write
11	2 & 9	Channel 1 loop functionality test	400001	Boolean	Read/Write
12		Channel 2 loop functionality test	400002	Boolean	Read/Write
13		Channel 3 loop functionality test	400003	Boolean	Read/Write

### 5.8.1 Validation of RADAS for dose alarm

The practical scan time of RADAS is 0.5 to 1.5 s; in this case, some of the dose alarms are not recorded during the electronic transient test due to high scan time if the dose rate of the soft alarm has its set-point at 40 mGy/h for each channel in RADAS. RADAS must detect each criticality event without failure. An experiment is conducted with a transient pulse of 6.48 V amplitude and pulse width of 500 ms using a programmed pulse generator, which is applied to the preamplifier input as well as to the digital storage oscilloscope.

$$V_o = e^{\frac{-t}{RC}} \quad (5.2)$$

Based on the discharging characteristics of the RC network, as per Eqn. (5.2), the total time taken to discharge the capacitor up to the equivalent voltage from the preamplifier output (1.5 V) of 10 mGy/h is found suitable for the dose alarm set-point in RADAS. The preamplifier output during capacitor discharge and channel alarm are reordered in the oscilloscope.

## 5.9 CENTRALIZED ELECTRONIC TEST AND ALARM ANNUNCIATION

Using key operated switches from the control panel, three channels of each CAS are provided with independent hard-wired remote electronic test/reset for online testing of the dose rate and the channel alarm, as shown in Figure 5.8. During the test, 1 V test voltage is applied to the input of the preamplifier and the corresponding channel dose rate is shown on the electronic module and OPC client computer in RADAS. This test ensures the functionality of the preamplifier, electronic module, visual and audio alarms in each channel, real-time trend graph, and all soft alarms in RADAS. Electronic test is also carried out periodically to test the 1 out of 3 (1-o-o-3), 2-o-o-3, and 3 out of 3 (3-o-o-3) logics, the audiovisual criticality alarm, and the corresponding dose rate values recorded in RADAS.

## 5.10 RELIABILITY ASSESSMENT OF ADDITIONAL PCBS USED IN THE CAS

Reliability is defined as the probability that a system will continue to perform its intended function under stated operating conditions over a specified period. The most common method is

to calculate the probability of failure rate ( $\lambda$ ). The values used for calculating the level of reliability are failures in time (FIT) and mean time between failures (MTBF) depending on type of component or system being evaluated. The failure rate is calculated by dividing the total number of failures or rejects by the cumulative time of operation. In the high temperature operating life (HTOL) model [91], the cumulative time of operation is referred to as equivalent device hours (EDH).

$$EDH = D * H * Af \quad (5.3)$$

Here: D = Number of devices tested, H = Test hours per device and Af = Acceleration factor derived from the Arrhenius equation. The failure rate ( $\lambda$ ) per hour is given by

$$\lambda_{\text{hour}} = \frac{r}{E * D * H} \quad (5.4)$$

Here: r = number of failures or rejects.

$$Af = e^{\frac{E_a}{k} \left( \frac{1}{T_{\text{use}}} - \frac{1}{T_{\text{test}}} \right)} \quad (5.5)$$

Here: Ea = Activation energy (eV) of the failure mode, k (Boltzmann's constant) =  $8.617 \times 10^{-5}$  eV/°K,  $T_{\text{use}}$  = Use temperature in °K and  $T_{\text{test}}$  = test temperature in °K.

$$r \sim \frac{\chi^2(\alpha, v)}{2} \quad (5.6)$$

Here:  $\chi^2/2$  (Chi-squared/2) is the probability estimation for the number of failures or rejects,  $\alpha$  (alpha) is confidence level (CL), and v (nu) is degrees of freedom (DF). The equation for failure rate ( $\lambda$ ) per hour then becomes,

$$\lambda_{\text{hour}} = \text{FIT} = \frac{\chi^2(\alpha, v)}{2 * E * D * H} \quad (5.7)$$

The FIT is a standard industry value defined as the failure rate ( $\lambda$ ) per billion hours.

$$\text{MTBF}_{\text{hour}} = \frac{\text{FIT}}{10^9 \text{ h}} \quad (5.8)$$

Early fault detection PCB of CAS processes different signals that need to generate an alarm annunciation in the control room as shown in Figure 5.9. It receives status signals of high voltage, low voltage, system on battery, battery charging/isolation diode and single channel alarm from the

CAS electronic module. It performs a comparison of signals, logical operations and de-energises the relay for early fault detection in CAS modules. The channel loop functional test circuit is also embedded in the same PCB as it is also required for each CAS channel. Another PCB is designed for early fault detection for alarm module. It receives status signals from low voltage, system on battery and battery charging/isolation diode for alarm annunciation in the control room.



**Figure 5.9.** Developed PCBs a) Early fault detection with channel loop functional test PCB for each channel and b) early fault detection PCB for alarm module.

#### 5.10.1 MTBF estimation methodology

The MTBF estimation methodology is based on the MIL-HDBK-217-F notice-2 [92] Handbook. This can be used to assess the ability of the system to perform under given conditions within an acceptable safe probability. For MTBF estimation, parts stress method is used. The parts stress method involves the multiplication of various stress factors like voltage, current, temperature, etc. stresses to the base failure rate. The failure rate model differs from component to component. Applicable stresses for each component should be known to determine the system failure rate, and it is performed after the completion of the circuit design. This prediction method can be used to identify and improve the weak links in the system.

#### 5.10.2 MTBF estimation of PCBs

CAS early fault detection system consists two different hardware PCBs. One PCB is required for early fault detection with channel loop functional test for each channel of CAS (three PCBs per CAS). Another PCB is used for early fault detection for alarm module (one PCB per CAS). The failure rates of various components on each PCB are calculated, and these failure rates are arrived

by adding the individual components failure rate. These failure rates are estimated using MTBF calculator tool by M/s ALD for reliability prediction based on the assumptions as follows.

### 5.10.3 Assumptions made during the assessment

1. All the PCBs are used in a temperature controlled environment and maintained at  $24 \pm 3$  °C. For calculations, the 40°C ambient temperature is considered.
2. It is assumed that the systems are kept in Ground Benign condition. The description of Ground Benign environment according to MIL-217-F notice-2 is,  
*“Ground Benign: Non-mobile, temperature and humidity controlled environments readily accessible to maintenance.”*
3. All components of the hardware nature are assumed in series connection for the MTBF calculation.
4. Source of failure data of each component is used in both PCBs as per the manufacturer data or/and M/s ALD database values as it is built as per MIL-217FN-2.

## 5.11 RESULTS AND DISCUSSION

### 5.11.1 FMEA of CAS

Based on failure mode and effect analysis, the critical elements that cause system unreliability and trigger false CAS alarms are identified. Failures associated with low and high voltage power supplies, system on battery, battery charging/isolation diode, and single channel alarm are considered to develop on printed circuit boards (PCB). These PCBs are tested, validated, and installed in the CAS for a common alert alarm annunciation in control room for immediate attention to prevent false criticality alarm.

### 5.11.2 Channel loop functional test circuit output

Figure 5.10 shows the RADAS historical trend graph during the online channel loop functional test for three channels of CAS. The responses of channels 1 & 2 show high voltage test profiles applied to the ionization chamber. As the high voltage is changed from 700 V to 620 V, reduced

current flows from the ionization chamber due to its internal capacitance. The preamplifier output voltage becomes less than its normal voltage. Subsequently, the dose rate reaches a negative peak and then returns to zero. After 6 s, the high voltage is increased back to 700 V, the current from the ionization chamber is increased, and then the preamplifier output voltage becomes greater than normal voltage. The dose rate output generates a positive peak and then returns to zero. Similarly, the response of channel 3 is improper in shape concerning the pulse amplitude, pulse width, and timing. This is due to the inappropriate sensitivity and high voltage adjustments. The proper shapes of channels 1 & 2 indicate that the integrity of the ionization chamber, high voltage, preamplifier, cables, and connectors is intact and that the functionality of the channels is healthy. The soft alarm in each channel is also observed at 10mGy/h. The channel loop functional test is in-situ and is recommended as a final test during maintenance works in CAS because, to avoid human-related errors, it consists of three sets of similar cables and connectors.

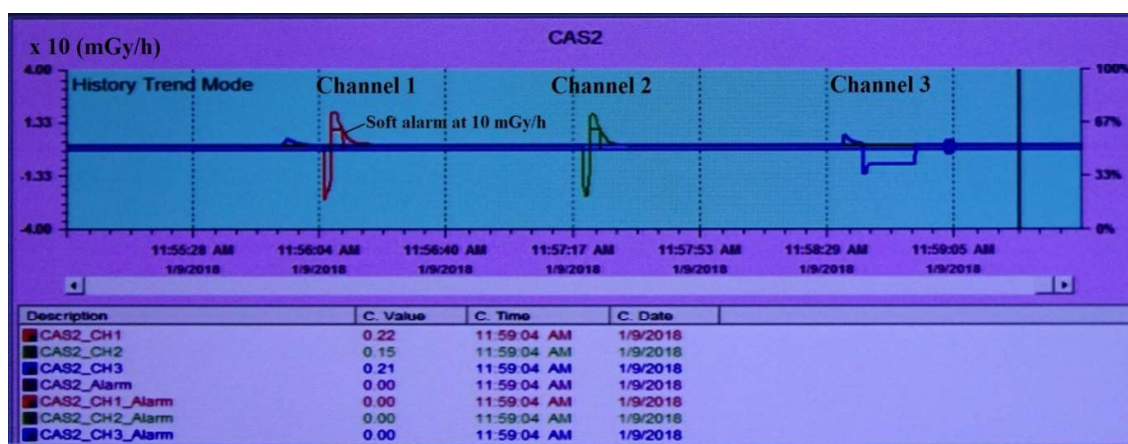


**Figure 5.10.** The RADAS historical trend graph during the online channel loop functional test for three channels of CAS. The responses of the channel 1 & 2 show high voltage test profiles applied to the ionization chamber. As the high voltage is changed as 700 V - 620 V - 700 V, the dose rate reaches a negative peak and then returns to zero, a positive peak and then returns to zero. Similarly, the response of channel 3 is improper in shape due to the inappropriate sensitivity and high voltage adjustments.

### 5.11.3 Dose alarm test using electronic transient pulse

The transient pulse amplitude of 6.48 V with pulse width 500 ms is applied to the input of the preamplifier and the channel alarm status along with the dose rate are noted. Figure 5.11 shows dose alarm test results obtained using transient pulse captured in the oscilloscope. The yellow color represents transient input test pulse with pulse amplitude of 6.48 V and pulse width of 500 ms. The green color shows the equivalent voltage level of channel alarm at 40 mSv/h. The pink color represents the corresponding preamplifier output due to transient test pulse and the blue color shows the channel alarm generation within 500 ms from the high logic level to the low logic level. As soon as preamplifier output voltage reaches the alarm set-point, the channel alarm is triggered within 450 ms; this is also equal to the theoretically calculated value as per Eqn. (5.2). Figure 5.12 shows the historical trend graph generated in RADAS during the dose alarm test using a transient pulse. The pulse width of the test pulse varied from 300 ms to 600 ms and, as a result, there is a gradual increase in the dose rate. The dose rate alarm is initiated at 40 mGy/h in CAS channel for pulse widths of 500 ms and above.

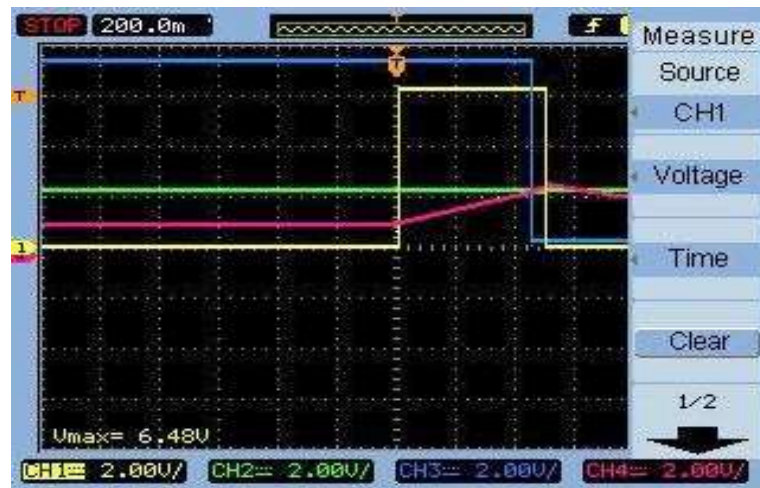


**Figure 5.11.** Dose alarm test using transient pulse captured in the oscilloscope. The yellow color represents transient input test pulse with a pulse amplitude of 6.48 V and pulse width of 500 ms. The green color shows the equivalent voltage level of channel alarm at 40 mSv/h. The pink color represents the corresponding preamplifier output due to transient test pulse, and the blue color shows the channel alarm generation within 500 ms from the high logic level to the low logic level.



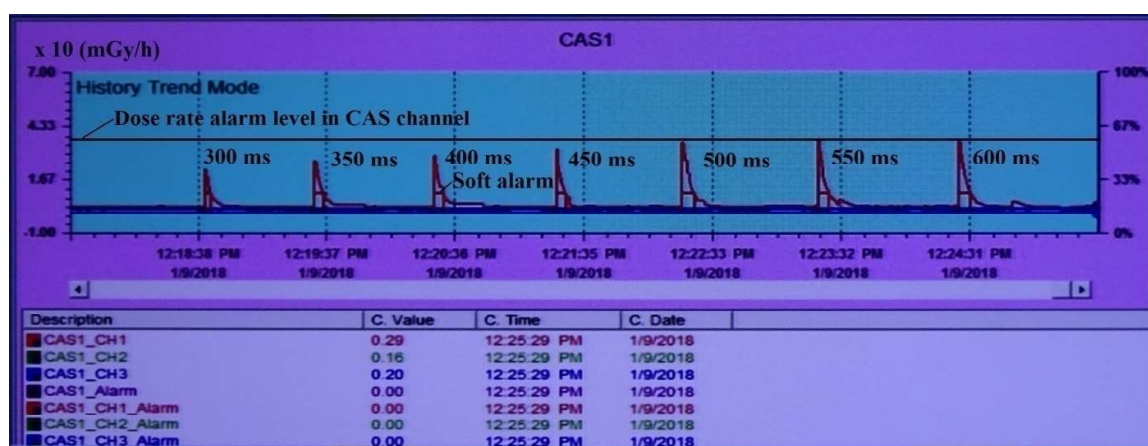


**Figure 5. 12.** The historical trend graph generated in RADAS during the dose alarm test using a transient pulse. The pulse width of the test pulse varied from 300 ms to 600 ms and, as a result, there is a gradual increase in the dose rate. The dose rate alarm is initiated at 40 mGy/h in the CAS channel for pulse widths of 500 ms and above.

#### 5.11.4 Centralized online electronic test and alarm annunciation facility

The electronic test is enabled on each channel of the CAS using the key-operated switch as well as the online test from the control panel. Figure 5.13 shows the historical trend graph generated during the electronic test for the three channels as red, green, and blue colors. The test voltage of 1 V is applied to the input stage of the preamplifier to the three 1-o-o-3 logic, independently, to test each channel dose rate and channel alarm. Similarly, testing is performed of all the combinations, including three 2-o-o-3 and one 3-o-o-3 logics, to generate the criticality alarm in CAS and RADAS. The soft alarm in RADAS for each channel is also observed at 10 mGy/h.

#### 5.11.5 Selection of dose alarm in RADAS

Dose alarm is initiated using transient input test pulse with an amplitude of 6.48 V and pulse width of 500 ms. Figure 5.14 shows the discharge characteristics of the RC network captured in the oscilloscope to select the dose alarm setpoint in RADAS. CH2 (blue) shows that the preamplifier output voltage during the discharge cycle up to 3.04 s is 0.5 V. This is equal to 10 mGy/h, which is selected as the dose alarm set-point in RADAS. CH3 (pink) shows channel alarm generation from high logic level to low logic level. In this case, no dose alarm is missed in RADAS.



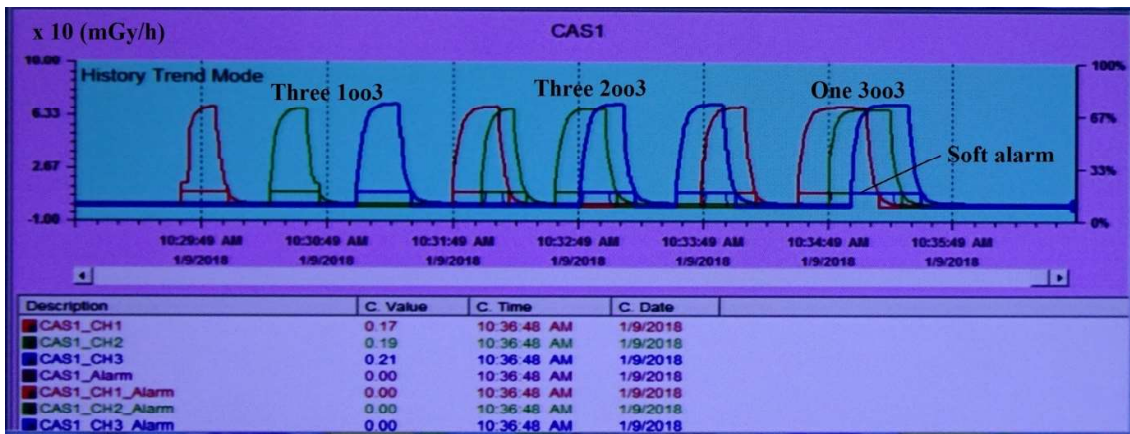


**Figure 5.13.** The historical trend graph generated during the electronic test for the three channels as red, green, and blue colors. The test voltage of 1 V is applied to the input stage of the preamplifier to the three 1-o-o-3 logic, independently, to test each channel dose rate and channel alarm. Similarly, testing is performed of all the combinations, including three 2-o-o-3 and one 3-o-o-3 logics, to generate the criticality alarm in CAS and RADAS. The soft alarm in RADAS for each channel is also observed at 10 mGy/h.

A soft alert alarm set-point is also provided at +4 mGy/h for each channel. These additional alarms alert the operator for any fluctuations in dose rate beyond this level due to background radiation or drift associated with low voltage power supply, high voltage, etc.

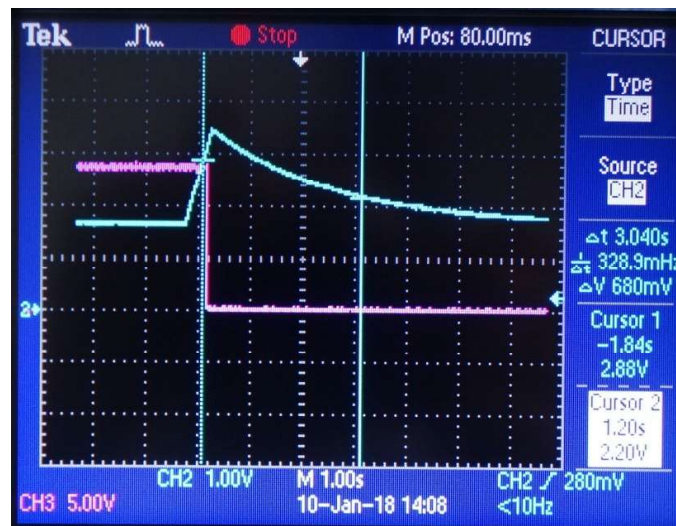


**Figure 5.14.** Discharge characteristics of the RC network captured in the oscilloscope to select dose alarm set-point in RADAS. CH2 (blue) shows that the preamplifier output voltage during the discharge cycle up to 3.04 s is 0.5 V. This is equal to 10 mGy/h, which is selected as the dose alarm set-point in RADAS. CH3 (pink) shows channel alarm generation from high logic level to low logic level.

### 5.11.6 Enhanced CAS design along with periodic surveillance procedures

The CAS incorporated with all improvements are assembled, installed, tested online, and validated in a nuclear plant for a period of 22000 h. Rigorous periodic surveillance procedures are carried out on each channel of CAS and the class I batteries, class II power, RADAS, and other developed circuits, daily, weekly, quarterly, and yearly for maximum availability. Thus, the system is found to operate reliably with no false criticality alarm. The design enhancements are compatible with the intended application.

### 5.11.7 Failure rate and MTBF of PCBs

The failure rate of each component is calculated using M/s ALD MTBF calculator software as shown in Figure 5.15 for a transistor at 40°C. The FIT data is added 7 different categories of the electronic components as mentioned in the tables. Table 5.3 gives the component failure rate, and quantity used in the CAS channel PCB and Table 5.4 gives the component failure rate and quantity used in the CAS alarm module PCB. Table 5.5 shows the failure rate and MTBF values of both PCBs. The MTBF of CAS channel PCB and alarm module PCBs are calculated as  $3.46 \times 10^6$  h and  $9.32 \times 10^6$  h respectively.

MTBF Calculator by ALD

Perform reliability prediction and MTBF/FR calculation for electronic and mechanical components in 5 simple steps:

- 1. Select Component Family and Type**  
 Family: ELECTRONIC  
 Item Code: IC-Memory, IC-Analog, IC-Digital, Bubble Memory, Resistor, Potentiometer, Capacitor, Switch, Relay, Connector, LF Diode, HF Transistor
- 2. Select Reliability Prediction Method**  
 MIL-217E-1 Part stress, MIL-217F-1 Part count, MIL-217F-1 Part stress, MIL-217F-2 Part count, MIL-217F-2 Part stress, ANS/MITA 51.1, ALCATEL, BELLCORE Issue 5, BELLCORE Issue 6, BRITISH TELECOM HRD4, BRITISH TELECOM HRD5
- 3. Select Environment and Temperature**  
 Environment: GB Ground, Benign  
 Temperature: 40 degrees Centigrade
- 4. Enter Component Parameters**  
 Calculate
- 5. Get MTBF and FR**  
 MTBF: 12452586982.31 hours  
 Failure Rate: 0.0001 failures per million hours  
 Failure Rate: 0.0803 FIT

**Figure 5.15.** MTBF and FIT values of an NPN Si transistor are shown at 40°C in a ground benign environment as per MIL-217F-2 using part stress reliability prediction method.

**Table 5.3.** PCB level component failure rate and quantity of CAS channel PCB.

S. No	Name of the component	Quantity	FITs/unit	FITs
1	Resistances (potentiometer replaced with fixed resistances)	23	2.73	62.80
2	Capacitors	8	8.72	69.83
3	Relays	2	5.37	10.74
4	ICs	3	20.96	62.90
5	Diodes	3	0.50	1.51
6	Transistor	3	0.08	0.24
7	Connectors	2	75.10	80.93
Total FITs per billion hours				288.97

**Table 5.4.** PCB level component failure rate and quantity of CAS alarm PCB.

S. No	Name of the component	Quantity	FITs/unit	FITs
1	Resistances (potentiometer replaced with fixed resistances)	8	2.73	21.84
2	Capacitors	2	8.72	17.45
3	Relays	1	5.37	5.37
4	ICs	1	20.96	20.96
5	Diodes	2	0.50	1.00
6	Transistor	2	0.08	0.16
7	Connectors	1	40.46	40.46
Total FITs per billion hours				107.27

**Table 5.5.** Failure rate and MTBF values of additional PCBs used in CAS.

Sl. No	Name of the PCB	Failure rate per hour = FITs*10 <sup>-9</sup>	MTBF in hours
1	Early fault detection and channel loop functional test PCB for CAS channel	0.2889743 x 10 <sup>-6</sup>	3.46 x 10 <sup>6</sup>
2	Early fault detection circuit for alarm module	0.1072788 x 10 <sup>-6</sup>	9.32 x 10 <sup>6</sup>

## 5.12 COMPARISON BETWEEN CONVENTIONAL AND ONLINE SURVEILLANCE METHODS OF CAS

The periodical surveillance of CAS is carried out as per the typical technical specification of the plant. Detailed person-hours requirement analysis of conventional and online surveillance methods of CAS are shown in Table 5.6. The radioactive source calibration is performed using conventional surveillance method. Hence there is no change in the requirement of Person-hours per year. Person-hours per unit per year saved [64] using online surveillance method are 78.6% even after radioactive source calibration considered as mandatory.

**Table 5.6.** Person-hours comparison between conventional and online surveillance methods of CAS.

S. No	Surveillance plan as per the technical specification of the plant	Surveillance type	Conventional surveillance			Remote online surveillance		
			Average time (h) per year	No. of persons	Person -hours	Average time (h) per year	No. of persons	Person -hours
1	Continuous monitoring	RADAS reading checking	(No change)			(No change)		
2	Weekly	Electronic test	0.25x52	3	39	0.17x52	1	8.84
3	Quarterly	Channel integrity test	0.67x4	2	5.36	0.1x4	1	0.40
4	Half year	Dose alarm test	1x2	3	12.00	0.17x2	2	0.68
5	Yearly	Radioactive source calibration	0.67x1	4	2.68	0.67x1	4	2.68
Total no. of person-hours per unit per year			59.04			12.6		
Total no. of person-hours per 15 units per year in a nuclear plant			885.6			189		
Person-hours per unit per year saved using online surveillance method.			78.6% (Including radioactive source calibration)					

### 5.13 CONCLUSION

In this work, a novel development of online fault diagnostics, online testing and design enhancement of criticality alarm system for maximum availability and prevention of false criticality alarms is presented. The early fault detection circuits developed for immediate attention to prevent false criticality alarm. Methods for online channel loop functional test and dose alarm using transient electronic pulse are developed to ensure the functional availability of CAS. Design enhancement is also performed for the external systems that are integrated with CAS. Based on experimental studies on the discharging characteristics of the RC network, the total time taken to discharge the capacitor up to 10 mGy/h is found to be 3.04 s. The voltage equivalent of 10 mGy/h dose rate output is selected for the dose alarm set-point in RADAS. A soft alert alarm set-point is also provided at + 4 mGy/h for detection of fluctuations in each channel. Rigorous periodic surveillance procedures are carried out for maximum availability of the system. The CAS incorporated with all improvements are assembled, installed, tested, and validated in the operating nuclear plant for a period of 22000 h. The system is found to operate reliably with no false criticality alarms. The enhanced CAS designs are compatible with the intended application and the person-hours per unit per year saved using online surveillance method is 78.6% as compared with conventional methods. For higher reliability and stability, advanced electronics like FPGAs are to be used in place of discrete electronic components.

# 6

## DEVELOPMENT OF FPGA BASED ELECTRONICS FOR REMOTE ONLINE PERFORMANCE EVALUATION OF AGRM AND DPCAM

---

*This chapter elucidates the development of FPGA based electronics along with in-house made interfacing card for remote online performance evaluation of GM tube, photomultiplier tube along with its electronics using ZigBee based RADAS. A robust two-process coding method is utilised to provide uniform algorithm encoding with increased abstraction level, and improved readability. In FPGA, the global clock, de-bounce, glue logic, timing controller and test frequency generation modules are designed in hardware description language for five-point electronic calibration and verification of accuracy.*

---

### 6.1 INTRODUCTION

The different radiation monitors employed [1,2] in nuclear plants and their nature are dictated by the complexity of the process operation of the plant. The Geiger Muller (GM) tube based area gamma radiation monitors (AGRM) [9] are used for continuous monitoring of gamma radiation levels. Similarly, dual phosphor scintillator based continuous air monitors (DPCAM) [10] are meant for measurement of air-borne alpha - beta radioactivity. During the lifetime of the plant, the functional availability of these instruments is ensured through periodic surveillance, routine calibration and rigorous quality assurance programs. As the number of radiation monitors is large, the online performance evaluation methods using conventional discrete electronics are mandatory for easy surveillance on the healthiness of these instruments. The design and development of conventional discrete electronics are time-consuming, labour intensive, low product life cycle and

testability. Development of remote online performance evaluation of GM tube, photomultiplier tube (PMT) along with its electronics using advanced high speed, stable, accurate and reliable electronics is mandatory. In nuclear domain, the field programmable gate array (FPGA) is the recent electronic device that replaces the software-based systems in nuclear power plants because of its advantages such as simplicity, testability, long-term support, and easy qualification [42,43,44,93]. Similarly, the wireless networks are a novel technology with a potential to perform distributed sensor tasks, especially online monitoring and control. The ZigBee based wireless communication [36,78] is preferred in this work mainly because of its low power consumption, considerable long range coverage and low cost.

Development of FPGA based electronics along with in-house developed interfacing card for remote online performance evaluation of GM tube, PMT along with its electronics using ZigBee based radiation data acquisition system (RADAS) is demonstrated. A robust two-process, VHDL (very high-speed integrated circuit hardware description language) coding method is utilised to provide uniform algorithm with encoding, increased abstraction level, and improved readability. In FPGA, the global clock, de-bounce, glue logic, timing controller and test frequency generation modules are designed in VHDL for five-point electronic calibration and verification of accuracy. The performance evaluation of AGRM is carried out in terms of GM threshold voltage, plateau slope and relative intrinsic error. Similarly, the performance evaluation of DPCAM is carried out for verification of relative intrinsic error in alpha-beta channels and crosstalk between alpha-beta channels. The real-time trend graphs generated during the performance evaluation of prototype AGRM and DPCAM have identified the functionality of these devices accurately than conventional technologies.

## 6.2 MATERIALS AND METHODS

### 6.2.1 AGRM and performance evaluation techniques

The performance evaluation of AGRM [9] is to be carried out for GM tube and its electronics independently. The online AGRM electronic test detects the faults associated with the pulse processing and counting electronics of the AGRM. The five-point electronic calibration provides checking of the accuracy of the AGRM. The percentage of relative intrinsic error is calculated at these points to verify the accuracy. The online GM tube test is designed based on count-rate versus applied high voltage characteristics of the GM tube. The values of GM threshold voltage, plateau length, and plateau slope are considered as per the technical specification. The online testing of GM tube is nothing but verification of the GM threshold voltage and plateau slope in the limits.

#### 6.2.1.1 Test profiles for AGRM

##### 6.2.1.1.1 AGRM electronic test

A known test frequency of constant pulse width is applied at the input stage of AGRM counting electronics during the AGRM electronic test. The test frequency is selected based on the sensitivity (180 CPS/ $\mu$ Sv/h) of the GM tube. Five dose rate points are selected to verify the accuracy at 5  $\mu$ Sv/h, 25  $\mu$ Sv/h, 50  $\mu$ Sv/h, 75  $\mu$ Sv/h and 90  $\mu$ Sv/h for equal test frequencies at these points are 90 Hz, 450 Hz, 900Hz, 1350Hz and 1620Hz. The time interval is approximately 30 s at each step for stable dose rate readings on AGRM display. During the performance evaluation, a two-pole relay energises simultaneously to latch the test frequency to the counting electronics and disconnect the GM tube temporarily. This is to avoid the background dose rate during the calibration for better accuracy. At the end of the test, the GM tube is automatically (fail-safe design) connected for normal operation. Figure 6.1 shows the timing diagram of events take place during AGRM electronic test. During the test, LED indication and GM tube isolation relay is activated to connect constant pulse width test frequency to AGRM electronics.



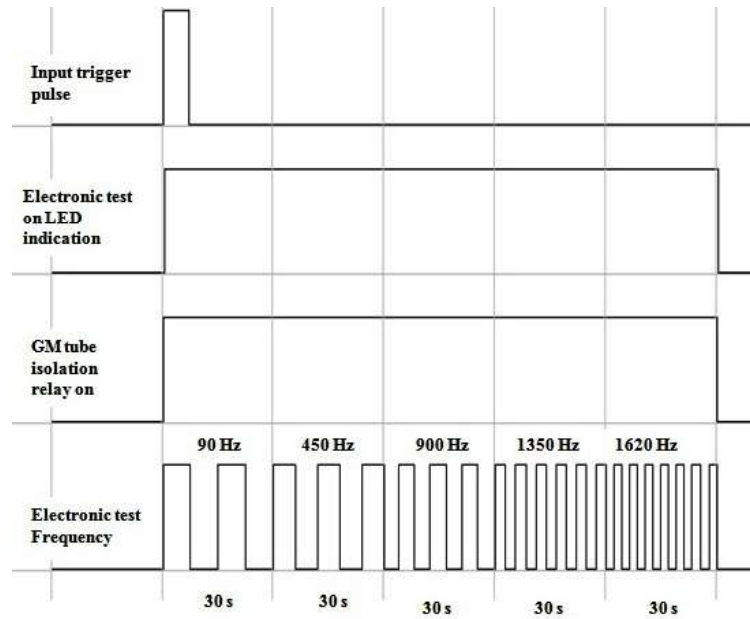


**Figure 6.1.** The timing diagram of AGRM electronic test, during the test, LED indication and GM tube isolation relay is activated to connect constant pulse width test frequency to AGRM electronics.

#### 6.2.1.1.2 AGRM GM tube test

During the remote online AGRM GM tube test, a control signal is given to high voltage circuit obtain the different output voltage from its nominal voltage of 500 V to 320 V, 450 V, and 650 V for the time interval of 40 s at each step. The high voltage at 320V is just below the GM threshold voltage (325V), where ideally no counts are expected for a working GM tube. The high voltage at 450V is the minimum operating voltage, and 650V is the maximum operating voltage. At the end of the test, the control signal automatically connects 500V, which is the standard operating voltage of the GM tube. The average dose rate value of AGRM at each step is used to calculate the percentage of plateau slope of GM tube in RADAS. Figure 6.2 shows the high voltage test profile applied to GM tube.

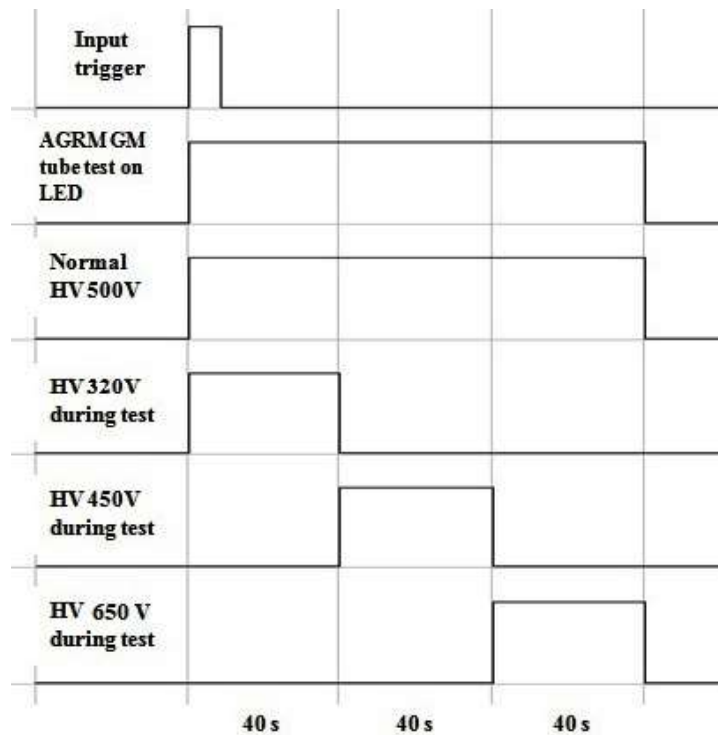


**Figure 6.2.** High voltage test patterns applied during the AGRM GM tube test. The high voltage from a nominal operating voltage (500 V) to 320 V for 40 s, 450 V for 40 s, 650 V for 40 s and back to 500 V.

## 6.2.2 DPCAM and performance evaluation techniques

The performance evaluation of PMT along with its electronics is carried out using the light source from the CIR LED [10], that is found to be the most suitable light source as it is able to discriminate alpha and beta radiation with zero crosstalk and minimum relative intrinsic error.

### 6.2.2.1 Test profiles of alpha and beta channels

Based on the experiments, the pulse width of the test frequency is selected as 10  $\mu$ s for testing of both alpha-beta channels. The pulse amplitude of 2.4 V is used for testing alpha channel and 1.8 V for testing of the beta channel. Five-step frequencies are selected at 10 Hz, 200 Hz, 400 Hz, 600 Hz and 800 Hz to cover five-point calibration of DPCAM at 600 CPM, 12000 CPM, 24000 CPM, 36000 CPM and 48000 CPM respectively. The timing diagram of test frequency applied to the CIR LED during the online performance evaluation of alpha & beta channels with LED indication are shown in Figure 6.3.

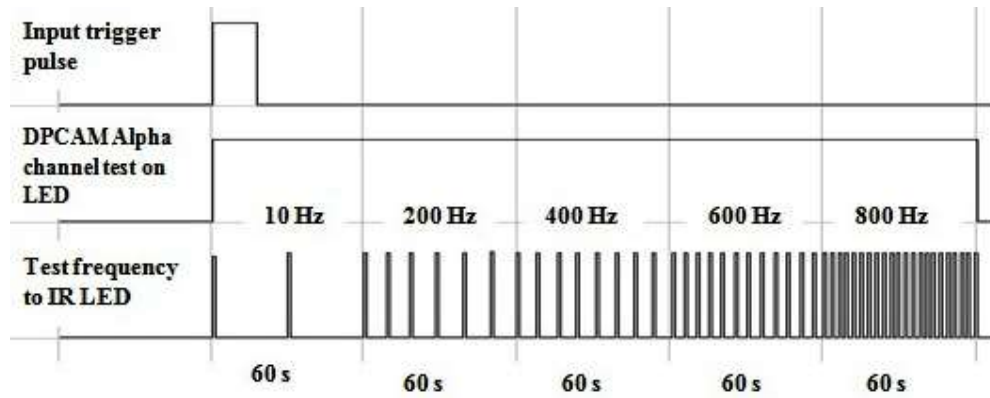


**Figure 6.3.** The timing diagram of test frequency of constant pulse width applied to the CIR LED during the online performance evaluation of alpha & beta channels with the LED indication.

### 6.3 FPGA ARCHITECTURE

#### 6.3.1 Two-process design method

The design of the FPGA architecture is carried out using a robust two-process VHDL coding [45] in such a way to overcome the limitations in the data flow design style. This method applies to any synchronous single-clock design, which represents the majority of all designs. The goal of the two-process method is used to provide uniform algorithm encoding with increased abstraction level, improved readability, identify sequential logic, simplify debugging, improved simulation speed, provide one model for both synthesis and simulation. Figure 6.4 shows a block diagram of a two-process design. I/p denoted inputs to the entity and connected to the combinational process.

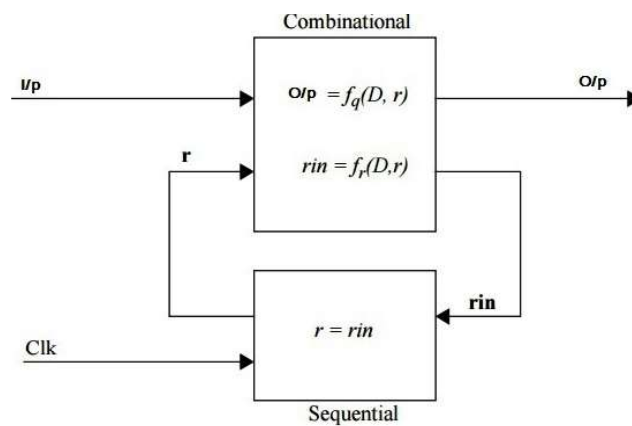


**Figure 6.4.** Two-process design in VHDL

The input to the sequential process is denoted by rin and drive by the combinational process. In the sequential process, the input (rin) is copied to the o/p (r) on the clock edge. The functionality of the combinational process is described using two equations as shown in the Figure 6.4. The syntax for a two-process design along with port definition, signal description and variable descriptions is as follows.

```
entity entity_name is
port (
// Port Definitions
);
end;
architecture twoproc of entity_name is
// Signal Description
begin
combinational : process(*Sensitivity List*)
// Variable Description
begin
//Combinational logic
end process;
sequential : process(*Sensitivity List*)
begin
// Sequential Logic
end process;
end;
```

## 6.4 DESIGN AND DEVELOPMENT OF FPGA BASED ELECTRONICS

The design of FPGA based electronics is divided into three modules, it includes the input module for generation of test frequency, a processing module for generation of test patterns and the output module for driving the outputs. Four different test frequency patterns are used for performance evaluation of AGRM and DPCAM. The test frequency patterns are AGRM electronic test, AGRM detector test, DPCAM alpha channel test and DPCAM beta channel test. A Digilent Atlys Xilinx

Spartan 6 LX45 FPGA development board [94,95] is used in this work. The Spartan-6 FPGA has 324-pin BGA package, 128 Mbyte DDR2 with 16-bit wide data; its high-performance logic offers 6,822 slices, each containing four 6 - input LUTs and 100MHz CMOS oscillator. The Digilent Atlys Xilinx Spartan 6 LX45 FPGA board is also provided with 48 I/O's routed to expansion connector, eight LEDs, six buttons, eight tactile switches and serial peripheral interface (SPI) flash memory. Xilinx devices need configuration data to be stored in flash memory. It is a low pin count configuration program memory using SPI. On power-up, configuration data is automatically written into Spartan 6 LX45 FPGA. Tactile switches are used for local testing where the operator is provided access to the FPGA board. Soft switches are also configured in supervisory control and data acquisition (SCADA) system software in RADAS for online testing from the control room. Online test can be initiated in two ways either using tactile switches present on the FPGA board or soft switches from SCADA through digital I/O module as shown in Figure 6.5.

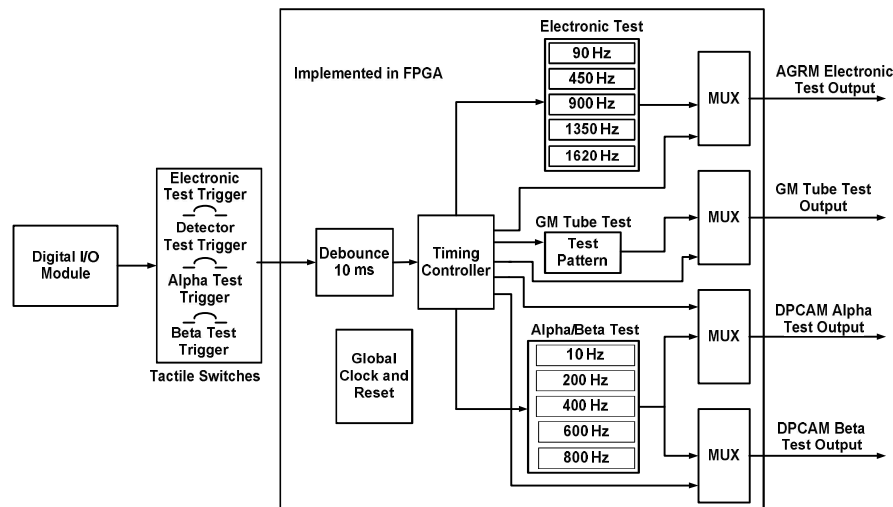


**Figure 6.5.** Design architecture of FPGA based electronics, interface with digital I/O module and output signals to interface card for online testing of AGRM and DPCAM.

The output of digital I/O module is enabled using RADAS via RS-485 network to activate the FPGA for the four different test frequency patterns mentioned earlier. The test frequency, control and LED indication signals from the FPGA are connected to AGRM and DPCAM through an in-house developed interface card for sufficient current driving capability. VHDL code is developed

for each module in the design and integrated using structural style VHDL coding. The integrated VHDL code for FPGA based electronics (Integrated) is provided in the Appendices – A. The operation of each block in FPGA is mentioned as follows.

#### **6.4.1 Global clock and reset**

Global clock and reset module is an internal resource of FPGA that routes 100 MHz clock and reset signal to the entire logical circuit. To achieve synchronous behaviour, the reset of the global design resources are utilised [96]. Nowadays it is common for all FPGAs to have an internal global clock, reset and portability is ensured in choosing FPGA based designs [97] for critical applications. The design only consists of a single clock domain 100 MHz where all logic is clocked with rising edge and single reset domain where all logic is reset with active low reset.

#### **6.4.2 De-bounce block**

The output command from tactile switches consists of glitches. A de-bounce circuitry is used to avoid these glitches. It provides 10 ms de-bounce during the manual testing using tactile switches.

#### **6.4.3 Timing controller**

The valid commands used during the performance evaluation are AGRM electronic test, AGRM GM tube test, DPCAM alpha channel test and DPCAM beta channel test. The timing controller is the central part of the FPGA design. It receives inputs from the tactile switches through de-bounce logic or digital I/O module to generate required test frequency. Timing controller also generates select signals for multiplexers to route the required waveform to the output. Each frequency generation module has input clock of 100 MHz, global active low reset and enables signal from the timing controller. Required frequency is generated using synchronous clock division. In this logic module, the 100 MHz clock is divided, and the required clock frequency signal is generated. Conceptual circuit diagram for clock division module is shown in Figure 6.6. This scheme is used for generating both 500 Hz and 0.33 Hz clocks. Figure 6.7 shows the timing diagram of clock division.

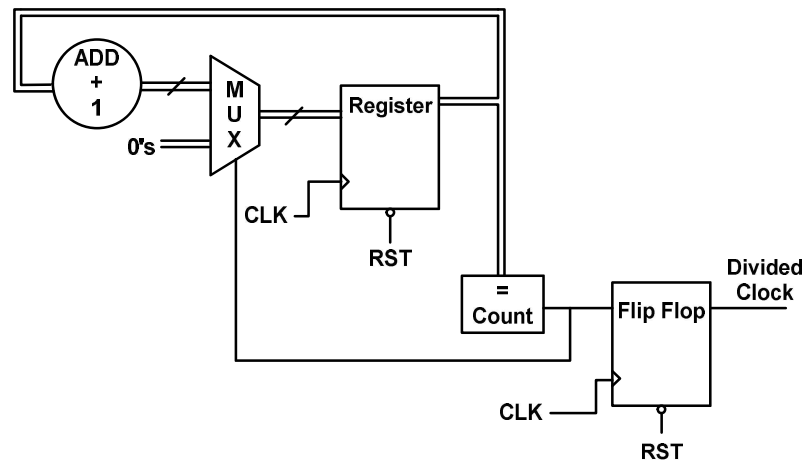


**Figure 6.6.** Conceptual diagram for clock division

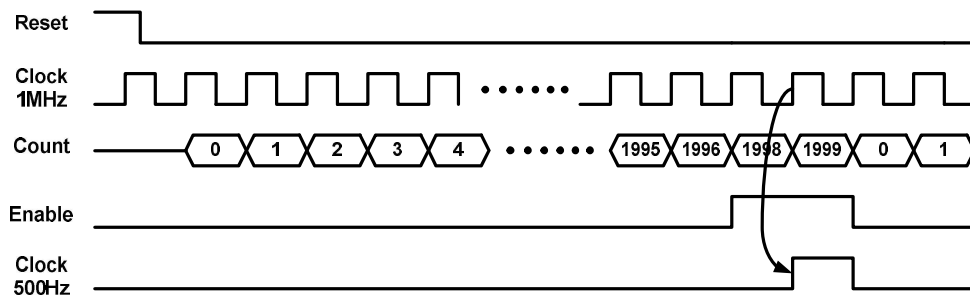


**Figure 6.7.** A timing diagram for clock division module

## 6.5 DIFFERENT OUTPUTS OF FPGA DESIGN

### 6.5.1 AGRM electronic test and frequency generation

During the AGRM electronic test, the frequency patterns of 90 Hz, 450 Hz, 900 Hz, 1350 Hz and 1620 Hz with 30 s duration are used. The generated test frequency accuracy and timing is better than  $\pm 0.01\%$  of full scale from 0.1 Hz to 2000 Hz at room temperature. Required pulse amplitude of 0.3 V is obtained by adjusting the potentiometers in the interface card and it also provides sufficient current driving capability using a high current Darlington transistor array (IC: ULN2003A).

### 6.5.2 AGRM detector test and voltage output

In case of AGRM GM tube test, three different square pulses of pulse duration of 40 s are used to trigger high voltage circuit for required output. Required pulse amplitudes such as 1.5 V, 1.8 V, 2.1 V and 2.4 V are obtained using potentiometers in the interface card. These voltage outputs in turn are used to generate high voltages of 320 V, 450 V and 650 V with 40 s in each step. At the end of the test, the GM tube is automatically connected to 500 V, which is the normal operating voltage of GM tube.

### 6.5.3 DPCAM alpha and beta channels test and frequency generation

The test frequencies of 10 Hz, 200 Hz, 400 Hz, 600 Hz and 800 Hz with a pulse amplitude of 5 V are used for full range testing of the alpha channel. All waveforms are pulsed in nature where  $T_{ON}$  of the pulse is 10  $\mu$ s. The generated test frequency accuracy and timing is better than  $\pm 0.01\%$  of full scale from 0.1 Hz to 2000 Hz at room temperature. Each frequency generation module has input clock of 100 MHz, global active low reset and enables signal from the timing controller. Required test frequency is generated using synchronous clock division. The pulse amplitude required for testing of alpha channel is 2.4 V, and that of beta channel is 1.8 V. Required pulse amplitudes are to be adjusted using potentiometers in the interface card.

## 6.6 DEVELOPMENT OF FPGA INTERFACE CARD

In-house developed interface card provides a proper signal interface between I/Os of Digilent Atlys Xilinx Spartan 6 LX45 FPGA board with AGRM and DPCAM. The I/Os of Spartan 6 LX45 FPGA board is connected to the external device via 68-pin VHDCI high-speed connector. A ULN2003A (buffer) IC is used for suitable current driving using Darlington transistor arrays. Figure 6.8 shows the schematic diagram of the interface card including different blocks, 68-pin VHDCI connector, LED indication and relays. Interface card consists of four different blocks namely AGRM electronic test, AGRM GM tube test, DPCAM alpha channel test and DPCAM beta channel test. The AGRM electronic test block is provided with a buffer IC, six LEDs, and



AGRM GM tube relay (RL 3) located in GM tube probe. Among six LEDs, one LED is provided to indicate AGRM electronic test operation, and other five LEDs are provided for indication of corresponding test frequency feeding to the AGRM. The RL 3 is used to isolate the GM tube, and buffered test frequency is applied to the input stage of AGRM counting electronics during the AGRM electronic test. The AGRM GM tube test block is provided with a buffer IC, four LEDs for indication of corresponding operation and high voltage output. The potentiometers are provided for selection of required high voltage steps. A single pole relay (RL 1) is used to latch different high voltage output during the AGRM GM tube test. Similarly, the DPCAM alpha channel and beta channel test blocks are provided with separate buffer ICs, six LEDs for indication of channel operation and corresponding frequency outputs. A single pole relay (RL 2) is provided to select 2.4 V or 1.8 V during testing of alpha channel or beta channel respectively.

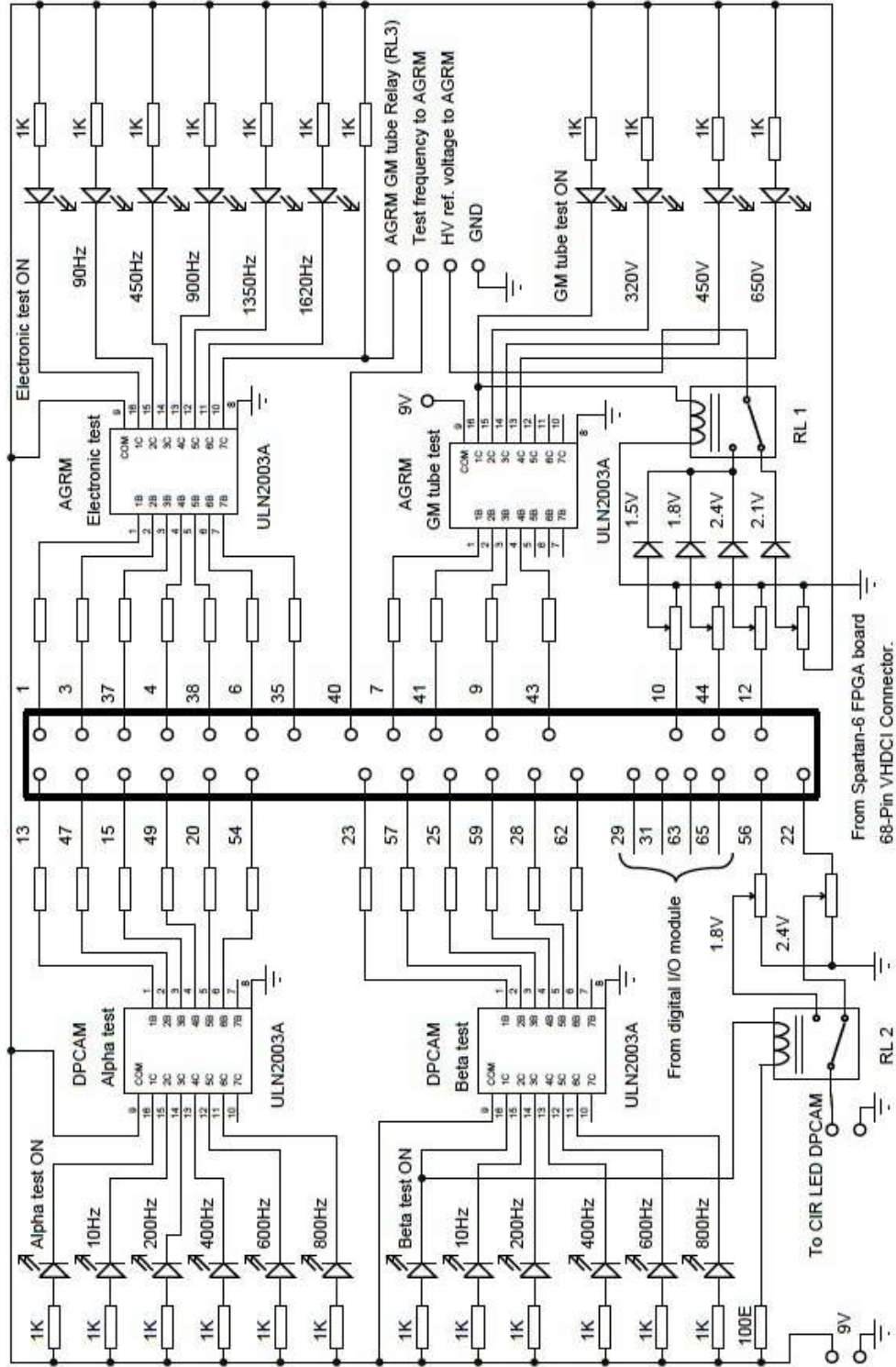


**Figure 6.8.** Interface card design for signal integration from Digilent Alys Xilinx Spartan 6 LX45 FPGA board with AGRM and DPCAM and digital I/O module for remote online testing.

## 6.7 CONFIGURATION OF RADAS AND SYSTEM INTEGRATION

The configuration of RADAS includes configuration of SCADA, wireless communication-based ZigBee modules and system integration. Dedicated RADAS is configured using open platform communications (OPC) server and SCADA software in the server computer. The prototype field devices AGRM, DPCAM and a Modbus protocol, supported digital I/O module are connected to the OPC server using Modbus RTU on RS-485. Serial communication parameters like device ID, port address, data bits, baud rate parity and stop bits are configured in OPC Server for communication with the field device. Different Modbus RTU tags of AGRM, DPCAM and digital I/O module are configured in OPC server software to update the engineering values as mentioned in Table 6.1. These values are used to display in real-time and recorded in the database in every 100 ms interval to generate history graphs and reports. Graphical user interface screens are developed against each Modbus tag address in SCADA. Real-time trend graphs are created for high voltage, dose rate, plateau slope and relative intrinsic error of AGRM in SCADA. Similarly, counts in the alpha channel, counts in the beta channel, the relative intrinsic error of alpha and beta channels in SCADA. The test buttons created for AGRM electronic test, AGRM GM tube test, DPCAM alpha channel test and DPCAM beta channel test. The mathematical equations for plateau slope, background subtraction, the percentage of relative intrinsic error are written in SCADA for real-time numerical and graphical representation. AGRM, DPCAM, Digilent Atlys Xilinx Spartan 6 LX45 FPGA development board along with digital I/O module and the server computer are connected to the RS-485 wired network. The communication between these devices is checked in this network.

**Table 6.1** Various Modbus tags used for online monitoring, fault diagnostics and performance evaluation of AGRM and DPCAM.

S. No	Device name & ID	Tag Description	Modbus Tag Address	Data type	Client Access
1	AGRM & 4	Low voltage	300030	word	Read Only
2		High voltage	300031	Word	Read Only
3		Dose rate	300032	Word	Read Only
4		Reset	100003	Boolean	Read/Write
5		Acknowledgement	100002	Boolean	Read/Write
6		Calibration factor	400015	Word	Read/Write
7		Alarm level	400030	Word	Read/Write
8		Alarm active	100007	Bit	Read Only
9	DPCAM & 11	Alpha counts	300007	Word	Read Only
10		Beta counts	300009	Word	Read Only
11		Acknowledgement	100002	Boolean	Read/Write
12		Calibration factor	400015	Word	Read/Write
13		Reset	100004	Boolean	Read/Write
14		Alarm level	400030	Word	Read/Write
15		Alarm active	100007	Bit	Read Only
16	Digital I/O module & 15	AGRM electronic test	400001	Word	Read/Write
17		AGRM GM tube test	400002	Word	Read/Write
18		DPCAM alpha channel test	400003	Word	Read/Write
19		DPCAM beta channel test	400004	Word	Read/Write

### 6.7.1 Configuration of ZigBee wireless modules and performance evaluation of wireless link

For wireless communication link, one ZigBee module is connected to AGRM, DPCAM and digital I/O module via RS-485, which works as a field sensor node. Another ZigBee wireless module is connected to RADAS server computer as a base station as shown in Figure 6.9. The experimental setup is developed for wireless sensor network to establish the wireless link between AGRM, DPCAM and Digilent Atlys Xilinx Spartan 6 LX45 FPGA development board located in operating area of the plant and RADAS at the control room.

The performance evaluation of wireless link is tested for 100% packet delivery in terms of the received signal strength indicator (RSSI) and the packet error rate (PER) is zero.

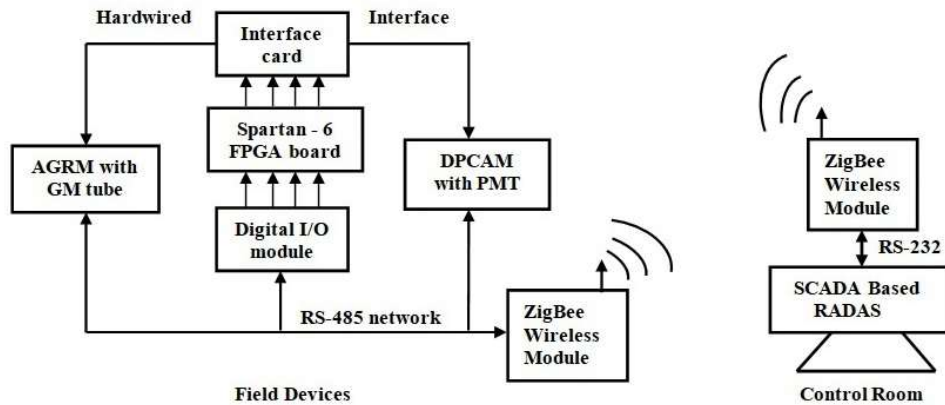


**Figure 6.9.** Block diagram of FPGA based performance evaluation system for AGRM and DPCAM.

## 6.8 RESULTS AND DISCUSSION

### 6.8.1 FPGA simulation results

#### 6.8.1.1 AGRM electronic and GM tube tests

All the features of the FPGA based electronics are verified using directed test benches in VHDL through simulations in iSim tool from XilinxTM. ISim is full-featured VHDL simulator integrated with design environment for Xilinx FPGAs. Integrated FPGA is initiated in the top-level test bench (TB), and all the interfaces of the FPGA are tested. Figure 6.10 shows simulation output of iSim during AGRM electronic test with a frequency of 1 GHz. Functional simulations are run at a higher frequency (1 GHz) to span the waveforms in the single window and to reduce simulation time. The design signals, test trigger input, LED indication, GM tube isolation relay activation and test frequency output are shown in the Figure 6.10.



**Figure 6.10.** Simulation output of iSim during AGRM electronic test with a frequency of 1 GHz. The design signals, test trigger input, LED indication, GM tube isolation relay activation and test frequency output are shown.

## 6.8.2 FPGA synthesis report

### 6.8.2.1 Schematic and technology view

The schematic representation of FPGA is verified after the VHDL synthesis phase [96]. It is basically to verify whether the VHDL modules codes are adequately synthesized or omitted by optimisation of the synthesis tool, RTL schematic view and technology view are checked. The design issues found in schematic and technology views are addressed early in the design process. Figure 6.11 shows the RTL schematic view generated during the synthesis of top FPGA module. The interconnections are shown with red color and various modules in green color.

### 6.8.2.2 Timing report and device utilisation report

As per static timing analysis, though the design supports maximum frequency up to 208.420 MHz, it is de-rated to 100 MHz for proper operation. The design is ensured that it is well within the storage capacity of Xilinx Spartan 6 LX45 FPGA. The optimum device utilisation is shown in Table 6.2.

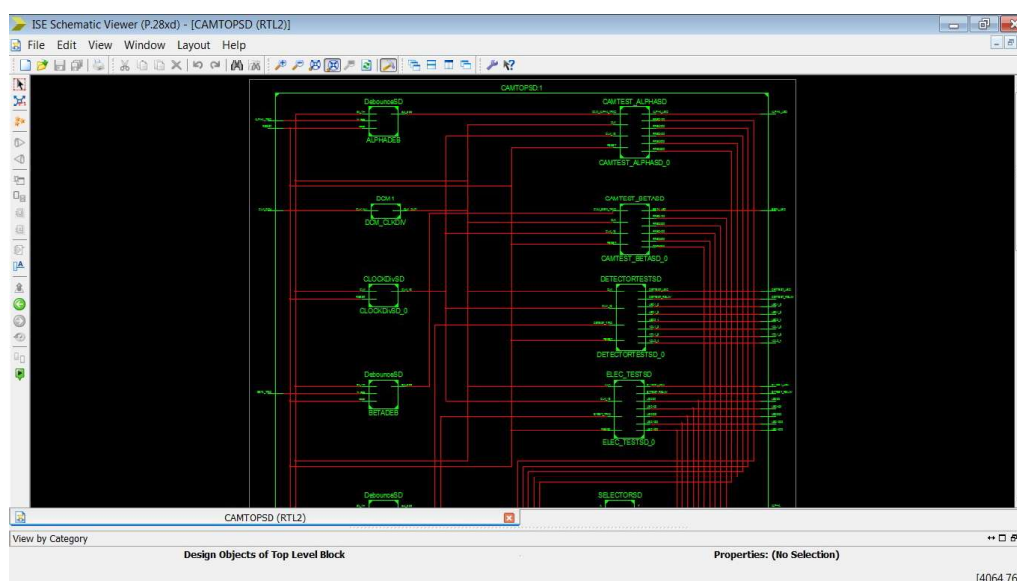


**Figure 6.11.** RTL schematic view generated during the synthesis of top FPGA based electronics. The interconnections are shown with red color and various modules in green color.

**Table 6.2.** Device utilization summary of Spartan 6 FPGA

Device utilization summary	
Selected device	6slx45csg324-2
<b>Slice logic utilisation</b>	
Number of slice registers	426
Number of slice LUTs	668
<b>Slice logic distribution</b>	
Number of LUT flip-flop pairs used	676
<b>IO utilisation</b>	
Number of IOs	26
<b>Specific feature utilisation for clock and reset</b>	
Number of BUFG/BUFGCTRLs	2

The detailed VHDL synthesis report of macro statistics, final register, primitive & black box usage, device utilization summary, timing and clock information is provided in the Appendices – B.

### 6.8.3 Remote online performance evaluation results of AGRM

The AGRM, DPCAM and digital I/O module are connected to an RS-485 network. The digital outputs of I/O module for AGRM electronic test and AGRM GM tube test are connected to Digilent Atlys Xilinx Spartan 6 LX45 FPGA board through the interface card. Communication between these devices to the server computer is checked using ZigBee wireless network. Both

AGRM electronic and AGRM GM tube test are carried out using wired / wireless network. The experimental setup for online performance valuation of AGRM is shown in Figure 6.12.

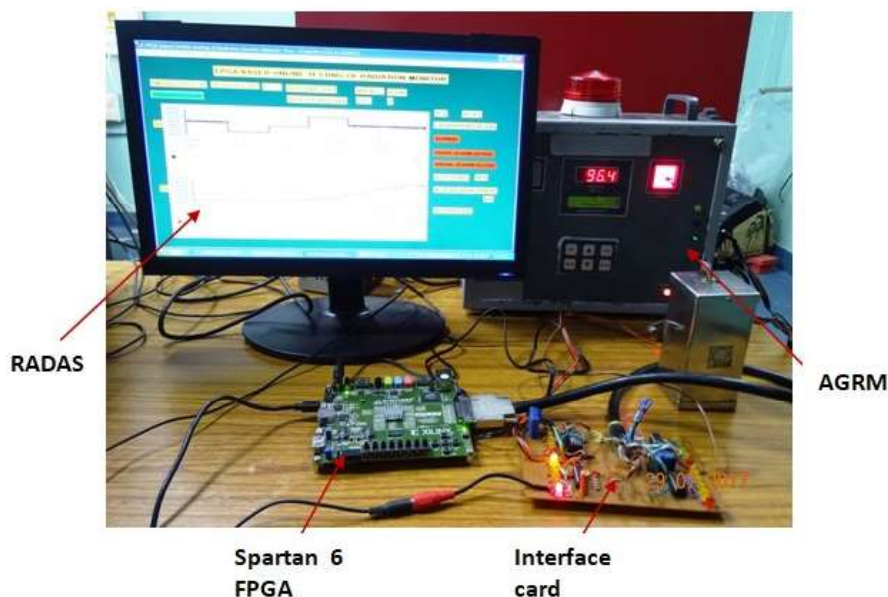


**Figure 6.12.** Experimental setup for online performance evaluation of AGRM; the AGRM, Spartan 6 FPGA board, interface card and RADAS are connected with the RS-485 network.

#### 6.8.3.1 AGRM electronic test

The online AGRM electronic test is conducted on prototype AGRM. A real-time trend graph is generated in SCADA during AGRM electronic test using FPGA based electronics under the dose rate of  $15 \mu\text{Sv/h}$  is shown in Figure 6.13. The test frequency (TF, top graph) is applied for online testing and corresponding the dose rate varied (bottom graph) from  $5 \mu\text{Sv/h}$ ,  $25 \mu\text{Sv/h}$ ,  $50 \mu\text{Sv/h}$ ,  $75 \mu\text{Sv/h}$  and  $90 \mu\text{Sv}$  in the span of 30 s. The percentage of relative intrinsic error (%R) is calculated at each dose rate. The maximum percentage of relative intrinsic error among five expected dose rates is displayed as 3.2 in SCADA.



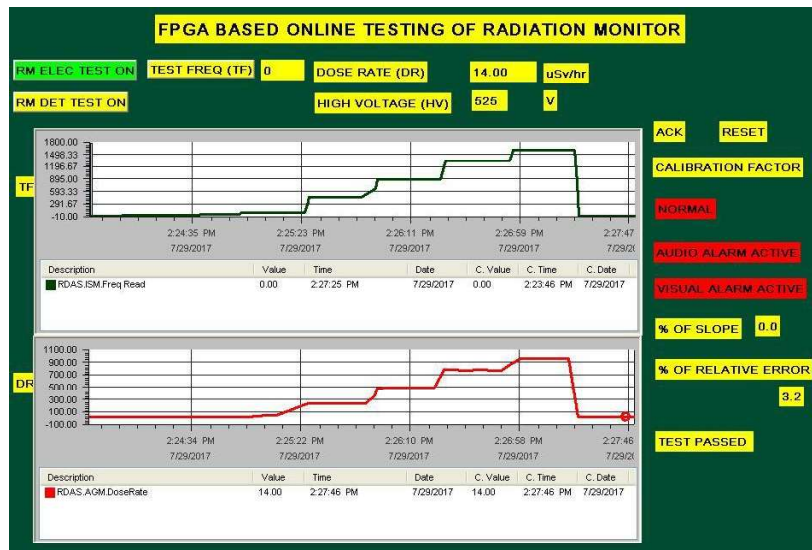


**Figure 6.13.** Real-time trend graph is generated in SCADA during AGRM electronic testing using FPGA based electronics under the dose rate of 15  $\mu\text{Sv/h}$ . The test frequency (TF, top graph) is applied for online testing and corresponding the dose rate varied (bottom graph) from 5  $\mu\text{Sv/h}$ , 25  $\mu\text{Sv/h}$ , 50  $\mu\text{Sv/h}$ , 75  $\mu\text{Sv/h}$  and 90  $\mu\text{Sv}$  in the span of 30 s.

#### 6.8.3.2 AGRM GM tube test

The online AGRM detector test is conducted under the dose rate of 500  $\mu\text{Sv/h}$  on LND 7121 GM tube. Figure 6.14 shows Real-time trend graph generated during AGRM detector test under dose rate of 500  $\mu\text{Sv/h}$  of working GM tubes using FPGA. When the high voltage (top graph) is changed to 320V (below GM threshold voltage), the dose rate (bottom graph) is zero. The high voltage is increased further to 450 V, 650 V and then 500 V, the dose rate is constant at 500  $\mu\text{Sv/h}$ . It is the ideal characteristics of a working GM tube. At the end of the test, the numerical value of plateau slope displayed on SCADA is 4.5%. The dose rate at 500 V (high voltage) is approximately 500  $\mu\text{Sv/h}$ . Figure 6.15 shows when high voltage is changed to 320 V and up to 450 V, the dose rate is constant at zero  $\mu\text{Sv/h}$  (whereas dose rate is expected to be zero for working GM tube). When the high voltage is changed from 320 V to 450 V, the dose rate is also shown as zero  $\mu\text{Sv/h}$  (it shall be approximately 500  $\mu\text{Sv/h}$  for a working GM tube). When high voltage is changed from 450 V to 650 V suddenly, the dose rate raised to 900  $\mu\text{Sv/h}$  and shown erratic behaviour in this region. When the high voltage decreased from 650 V to 500 V, dose rate

has fallen to 500  $\mu\text{Sv/h}$  with random variation. The dose rate patterns indicate as a faulty GM tube. The plateau slope displayed in RADAS is 95.4%.

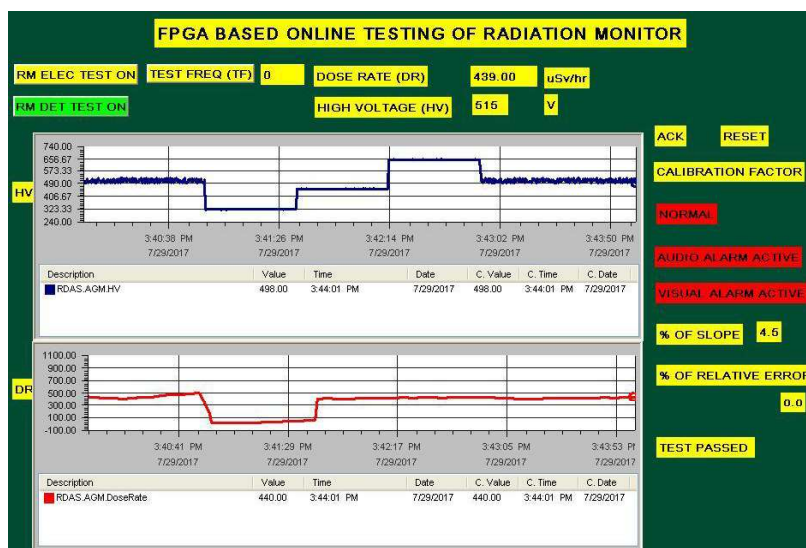


**Figure 6.14.** Real-time trend graph generated during AGRM detector test under dose rate of 500  $\mu\text{Sv/h}$  of working GM tubes. When high voltage (top graph) is changed to 320V (below GM threshold voltage), the dose rate (bottom graph) is zero. The high voltage is increased further to 450 V, 650 V and then 500 V, the dose rate is constant at 500  $\mu\text{Sv/h}$ . It is the ideal characteristics of a working GM tube.

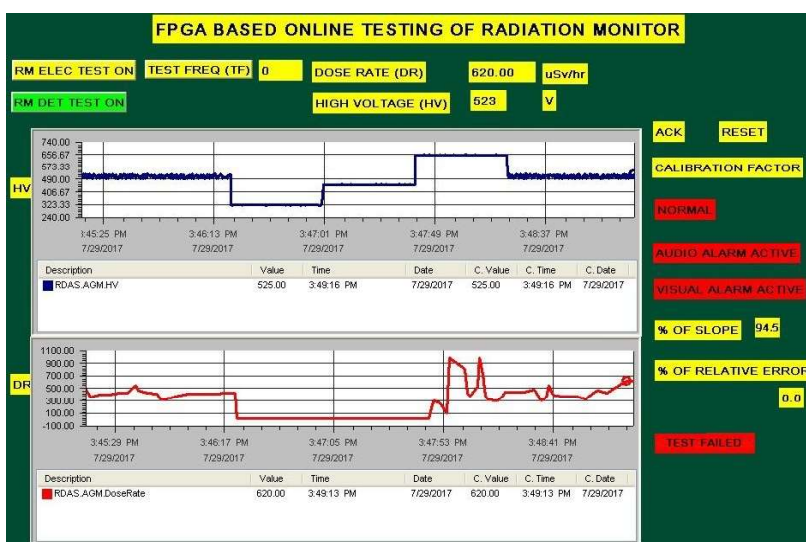


**Figure 6.15.** Real-time trend graph generated during AGRM detector test under dose rate of 500  $\mu\text{Sv/h}$  of a faulty GM tube. When high voltage (top graph) is changed to 320V and up to 450 V, the dose rate (bottom graph) is zero  $\mu\text{Sv/h}$ . high voltage is changed from 450 V to 650 V, the dose rate suddenly raised up to 900  $\mu\text{Sv/h}$  with fluctuations. As high voltage decreased from 650 V to 500 V, the dose rate is fallen to 500  $\mu\text{Sv/h}$ . The dose rate patterns indicate as a faulty GM tube.

#### 6.8.4 Remote online performance evaluation results of DPCAM

DPCAM and digital I/O module are connected to the RS-485 network. Digital outputs of I/O module for DPCAM alpha channel test and beta channel test are connected to Digilent Atlys Xilinx Spartan 6 LX45 FPGA board through the interface card. Communication between these devices to the server computer is checked using ZigBee wireless network. Both alpha and beta channel tests are carried out using the wireless network. Figure 6.16 shows the experimental setup for online performance evaluation of DPCAM; The DPCAM, Spartan 6 FPGA board, interface card and RADAS are connected using ZigBee based wireless network.

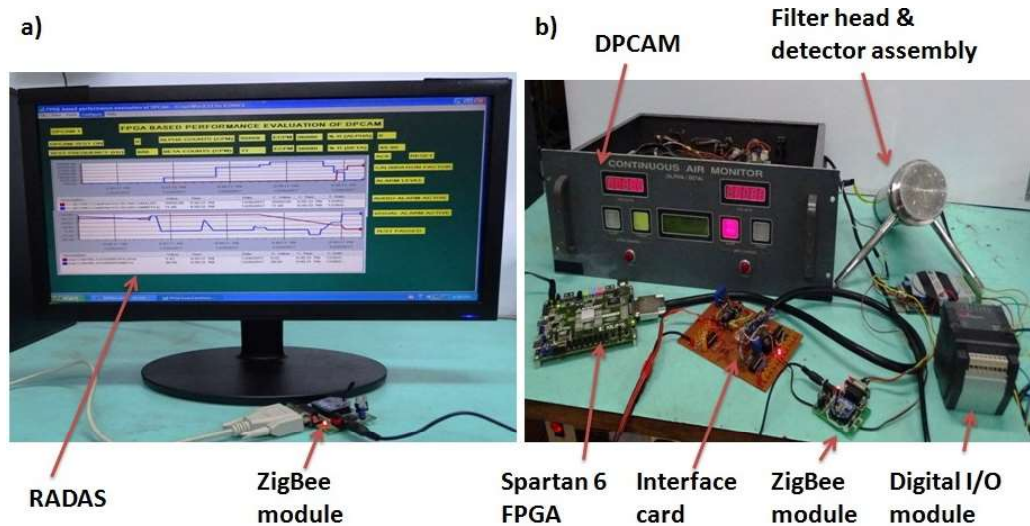


**Figure 6.16.** Experimental setup for online performance evaluation of DPCAM; The DPCAM, Spartan 6 FPGA board, interface card and RADAS are connected using ZigBee based wireless network.

##### 6.8.4.1 DPCAM Alpha channel test & Beta channel test

The online test is initiated by pressing DPCAM test button created on the SCADA screen. DPCAM test circuit automatically generates test frequency with a pulse amplitude of 2.4 V for testing alpha channel initially from 10, 200, 400, 600, and 800 Hz at the 60 s duration at each step. Figure 6.17 shows Real-time trend graphs are generated during the online performance evaluation of an alpha channel with low background counts. The counts vs time (top graph) for test frequency profile applied and corresponding relative intrinsic error vs time (bottom graph) are shown for both alpha (red) and beta (blue) channels. Real-time graphs show that the error reached

the maximum value to a minimum value after a corresponding change in counts due to change in the test frequency. At the end of the alpha channel test, similarly, the beta channel test is initiated for same frequency patterns with a pulse amplitude of 1.8 V. The maximum relative intrinsic error in both cases is less than +1%.

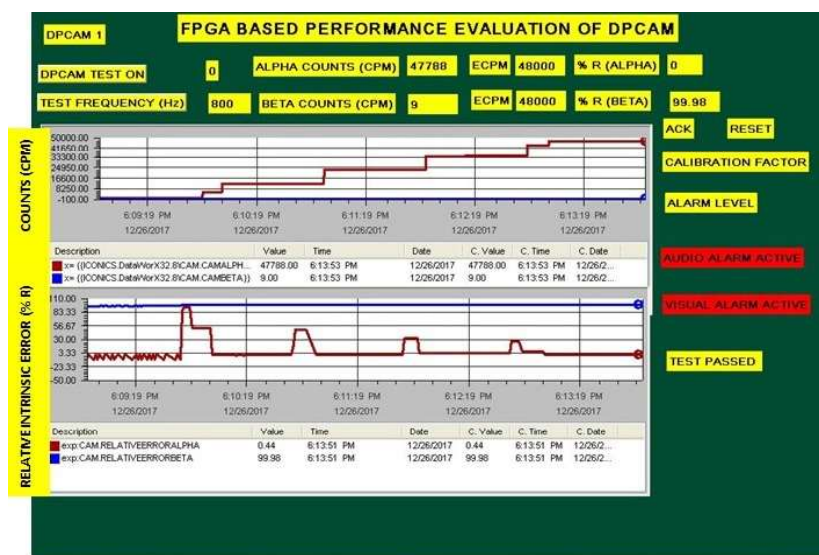


**Figure 6.17.** Real-time trend graphs are generated during the online performance evaluation of alpha channel with low background counts. The counts vs time (top graph) for test frequency profile applied and corresponding relative intrinsic error vs time (bottom graph) are shown for both alpha (red) and beta (blue) channels.

## 6.9 CONCLUSION

In this chapter, a newly developed FPGA based electronics for remote online performance evaluation of area gamma radiation monitor and dual phosphor scintillator based continuous air monitor is described. A robust two-process VHDL coding method is utilised to provide uniform algorithm encoding with increased abstraction level, and improved readability. A Digilent Atlys Xilinx Spartan 6 LX45 FPGA board along with in-house developed interface card is used in this work. Remote online performance evaluation of GM tube, PMT along with its electronics is carried out. Relative intrinsic error and crosstalk of FPGA based system are found to be within  $\pm 10\%$  and  $\pm 1\%$  respectively. Test frequency accuracy and timing of the FPGA is better than  $\pm 0.01\%$  of full scale from 0.1 Hz to 2000 Hz at room temperature. The techniques adopted for remote online performance evaluation are meeting the system requirements.

## CONCLUSION AND FUTURE DIRECTIONS

---

*The present chapter summarises the results of online performance evaluation of AGRM, DPCAM and CAS in nuclear plants. Directions for further work that needs to be carried out for research in this area are also discussed in this chapter. Further research needs to be carried out for performance evaluation of radiation monitors that use two different GM tubes. Similarly, boron coated counter (BCC), Helium-3 ( $^3\text{He}$ ) and solid-state detector-based radiation monitors are discussed in this context. Further studies need to be carried out for a comprehensive evaluation of wireless sensor networks (WSN) for online performance evaluation of large number of radiation monitors for future deployment in nuclear plants. Feasibility of criticality alarm systems (CAS) to be carried out using FPGA based electronics along with WSN are also mentioned in this chapter.*

---

### 7.1 CONCLUSION

The present thesis aims at the fault diagnostics, online testing and online performance evaluation of radiation monitors including GM tube based AGRM, PMT based DPCAM and ionization chamber based CAS through RADAS using upcoming technologies like wireless networks & FPGAs.

- A new development is proposed for online testing of AGRM electronics and GM tube from the control room using wireless network. The real-time trend and history graphs generated in RADAS help to identify the performance of AGRM electronics and GM tube in-situ. The online AGRM electronic test helps to calculate the percentage of relative intrinsic error to verify the AGRM accuracy. The accuracy of a working

system is expected to be within  $\pm 10\%$ . Online AGRM detector test is used to check the response of GM tube below GM threshold voltage (320 V) and verification of plateau slope (%/100 V). Ideally, no dose rate is expected for a working GM tube below GM threshold voltage. The plateau slope (%/100 V) of GM is expected to be within 10 (as per OEM). The time required for the proposed online testing method of AGRM electronics along with GM tube is less than 6 minutes. Based on the person-hours requirement analysis, the person-hours per unit per year saved using online surveillance method are 78.9% as compared with conventional methods. The proposed method is applicable for testing of all GM tube based radiation monitors in the nuclear plants.

- A novel development is made for remote online performance evaluation for PMT and electronics of DPCAM from the control room using a wireless network. Based on the experimental results, the colour infrared LED is found to be the most suitable light source in this work, as it discriminates alpha and beta radiation using pulse amplitude discrimination technique with zero crosstalk. The optimal pulse width of 10  $\mu$ s and pulse amplitudes of 2.4 V & 1.8 V (for alpha and beta respectively) are selected for performance evaluation. The relative intrinsic error for this LED is less than + 1% in both channels with fresh filter paper. Robustness of the wireless communication link is tested in terms of RSSI and PER. The RSSI between each node varied between  $-50$  and  $-65$  dBm and the PER is found to be zero. The real-time trend and historical trend graphs generated in RADAS effectively bring out any deviation in the performance of PMT and electronics of DPCAM. The time required for proposed online performance evaluation of both alpha and beta channels of DPCAM is 10 minutes. Based on the person-hours requirement analysis, the person-hours per unit per year saved using online surveillance method are 65.8% as compared with conventional methods. The

proposed method of evaluation is applicable for all other scintillation based radiation monitors.

- Several new developments have been made for online fault diagnostics, online testing and design enhancement of criticality alarm system (CAS) for maximum availability and prevention of false criticality alarms. The early fault detection circuits are developed for diagnostics with alarm annunciation. Two novel methods are developed, one method for channel loop functionality test and another method for dose alarm test using electronic transient pulse to ensure the functional reliability of CAS. Design enhancement is also made for the external systems that are integrated with CAS. Based on experimental investigations on the discharging characteristics of the RC network, the total time taken to discharge the capacitor up to 10 mGy/h is found to be 3.04 s. The voltage equivalent of 10 mGy/h dose rate output is selected for the dose alarm set-point in RADAS. A soft alert alarm set-point is also provided at + 4 mGy/h for detection of fluctuations in each channel. MTBF values of additional PCBs used in the CAS are found to be  $3.46 \times 10^6$  h for channel PCB and  $9.32 \times 10^6$  h for alarm module PCB. The CAS incorporated with all improvements is validated in the operating nuclear plant for a period of 22000 h. The enhanced CAS designs are compatible with the intended application. Based on the person-hours requirement analysis, the person-hours per unit per year saved using online surveillance method are 78.6% as compared with conventional methods.
- An FPGA based electronics for remote online performance evaluation of AGRM and DPCAM has been developed. A robust two-process VHDL coding method is utilised to provide uniform algorithm encoding with increased abstraction level, and improved readability. A Spartan 6 LX45 FPGA board along with in-house developed interface

card is used in this work. Relative intrinsic error and crosstalk of FPGA based electronics are found to be within  $\pm 10\%$  and  $\pm 1\%$  respectively. Test frequency accuracy and timing of the FPGA is better than  $\pm 0.01\%$  of full scale from 0.1 Hz to 2000 Hz at room temperature. The techniques adopted for remote online performance evaluation are meeting system requirements.

The remote online performance evaluation techniques for nuclear radiation monitors provide accurate and easy surveillance during all the states of the plant, minimum human intervention and minimum human errors, simultaneous data collection, storage and presentation in a single step from a single point. In addition, the methodology provides significant person-days per unit per year saved by 3 to 5 times as compared with conventional surveillance methods. In case of AGRM, the periodical conventional radioactive source calibration test can be reduced as online AGRM electronic test is provided with complete information of dose rate, relative intrinsic error at each step of test frequency and electronic calibration. The online GM tube test provides the information on GM threshold voltage, plateau slope and status of GM tube in the existing background conditions. Similarly, in case of DPCAM, the dual phosphor scintillator detector being a passive element, it is well protected in filter head cum detector assembly. As the detector performance is not degraded in the standard operating environment, accordingly there is a scope to reduce the number of periodical radioactive source calibrations per unit per year. Thus, person-days per unit per year can also be saved up to 7 times by minimising the radioactive source calibrations.



## 7.2 FUTURE DIRECTIONS

Based on the successful development of novel online performance evaluation techniques for the essential radiation detectors, the future directions of research in this area are outlined as follows.

- Wide range gamma area radiation monitors (WGRM) are required to measure gamma dose rate range from 0.1 to 1 Sv/h with an accuracy of  $\pm 10\%$ . Two different GM tubes are used to cover this range, one GM tube is used for low range, and another GM tube is required for high range operation. The fault diagnostics, online testing, calibration and performance evaluation of WGRM are to be studied for both the GM tubes.
- Boron coated counters (BCC) and Helium-3 ( $^3\text{He}$ ) detectors are used for assay and accounting of  $^{239}\text{Pu}$  by detecting neutron radiation. They are also used for neutron flux measurement in reactors. The fault diagnostics, online testing, calibration and performance evaluation of instruments based on these radiation detectors are to be investigated.
- Solid-state radiation detectors including passivated ion-implanted planar silicon (PIPS) detector and high pure germanium (HPGe) detectors that are used for spectroscopic analysis. The fault diagnostics, online testing, calibration and performance evaluation of these radiation detectors based systems are also to be investigated.
- Wireless sensor networks (WSN) are needed to integrate with existing SCADA systems for remote online performance evaluation of a large number of radiation monitors. The comprehensive evaluation of the WSN is to be carried out for signal processing capabilities, communication constraints, robustness of communication link, energy consumption and scalability for future deployment in the nuclear plants.

- Dedicated PCBs are to be designed, fabricated and validated using FPGA along with interface components for remote online performance evaluation of different radiation monitors in nuclear plants.
- The feasibility of FPGA based electronics and WSN are to be tested for online performance evaluation of CAS for higher reliability, stability and diagnostics for prevention of false criticality alarms.

## REFERENCES

- [1] IAEA safety standards series, occupational radiation protection, safety guide no. RS-G-1.1, jointly sponsored by the IAEA and ILO, IAEA, Vienna, pp. 1-28, 2009.
- [2] IAEA-tecdoc, work place workplace monitoring, airborne contamination, volume 2, IAEA, Vienna, pp. 1-19, 2013.
- [3] G.F. Knoll, Radiation detection and measurement, 3rd Edition, John Wiley and Sons, New York, pp. 103-284, 1999.
- [4] James E. Martin, Physics for radiation protection, a handbook, second edition, completely revised, Wiley-VCH, pp. 557-574, 2006.
- [5] ANSI N42.3, 1999, IEEE Standard Test procedures and basis for Geiger-Mueller counters, [Online]. available at <http://ieeexplore.ieee.org/stamp/stamp.jsp?Arnumber=768235>.
- [6] Broadway, Sweetwater, 2017, TX, USA. Alpha/Beta Detection, EJ-444; ELJEN Technology, [Online]. Available: [http://www.eljentechnology.com/images/products/data\\_sheets/EJ-444.pdf](http://www.eljentechnology.com/images/products/data_sheets/EJ-444.pdf)
- [7] K. Yasuda, S. Usuda, and H. Gunji, "Simultaneous alpha, beta/gamma, and neutron counting with phoswich detectors by using a dual-parameter technique," IEEE Trans. Nucl. Sci., vol. 48, no. 4, pp. 1162-1164, 2001.
- [8] B. K. Seo et al., "Development of the dual phosphor detector for simultaneous alpha- and beta-ray counting in a Pipe," in Proc. Korean Nucl. Soci. Autumn Meet., Gyeongju, South Korea, 2006.
- [9] Padi Srinivas Reddy, R. Amudhu Ramesh Kumar, M. Geo Mathews and G. Amarendra, Online fault diagnostics and testing of area gamma radiation monitor using a wireless network, Nuclear Instruments and Methods in Physics Research A, vol. 859, pp. 23-30, 2017.
- [10] Padi Srinivas Reddy, R. Amudhu Ramesh Kumar, M. Geo Mathews and G. Amarendra, Remote online performance evaluation of photomultiplier tube and electronics of DPCAM, IEEE Transactions on Nuclear Science, vol. 64, 11, pp. 2843-2853, 2017.
- [11] Padi Srinivas Reddy, R. Amudhu Ramesh Kumar, M. Geo Mathews and G. Amarendra, Design and development of enhanced criticality alarm system for nuclear applications, Nuclear Engineering and Technology, vol. 50, pp. 690-697, 2018.
- [12] IAEA, Safety Reports Series 16, "Calibration of radiation protection monitoring instruments", 2000, pp. 1-45 [online]. Available: [www-ub.iaea.org/MTCDD/Publications/PDF/P074\\_scr.pdf](http://www-ub.iaea.org/MTCDD/Publications/PDF/P074_scr.pdf)

- [13] Jianping Ma and Jin Jiang, Applications of fault detection and diagnosis methods in nuclear power plants: A review, *Progress in Nuclear Energy*, 53, pp. 255-266, 2011
- [14] Rao Kalapatapu, SCADA protocols and communication trends, 2004 [Online]. Available: <http://citeseerx.ist.psu.edu/viewdoc/download?doi=10.1.1.401.6666&rep=rep1&type=pdf>
- [15] Claudio Urrea, Claudio Morales, Rodrigo Muñoz, Design and implementation of an error detection and correction method compatible with MODBUS-RTU by means of systematic codes, *Measurement*, 91, pp. 266-275, 2016.
- [16] Niv Goldenberg and Avishai Wool, Accurate modeling of Modbus/TCP for intrusion detection in SCADA systems, *international journal of critical infrastructure protection*, 6, pp. 63-75, 2013.
- [17] Rania Ibrahim Gomaa, Ihab Adly Shohdy, Karam Amin Sharshar, Ahmed Safwat Al-Kabbani, and Hani Fikry Ragai, "Real-time radiological monitoring of nuclear facilities using ZigBee technology," *IEEE Sensors*, Vol. 14, no. 11, pp. 4007-4013, Nov. 2014.
- [18] S.A.V. Satya Murty, Wireless sensor networks for nuclear reactor applications, Ph. D Thesis, pp. 1-144, 2014, [Online]. Available: By [http://www.hbni.ac.in/students/dsp\\_ths.html?nm=engg/ENGG02200704009.pdf](http://www.hbni.ac.in/students/dsp_ths.html?nm=engg/ENGG02200704009.pdf)
- [19] IAEA Nuclear Energy Series No. NP-T-3.17, Application of field programmable gate arrays in instrumentation and control systems of nuclear power plants, pp. 1-29, 2016, [Online]. available at [http://www-pub.iaea.org/MTCD/Publications/PDF/Pub1701\\_web.pdf](http://www-pub.iaea.org/MTCD/Publications/PDF/Pub1701_web.pdf)
- [20] Tadashi Miyazaki, Naotaka Oda, Yasushi Goto, and Toshifumi Hayashi, Qualification of FPGA-based safety-related PRM system, IAEA-CN-164-7S02, pp. 1-8, 2009.
- [21] A. Aloisio, P. Branchin, F. Ceveninil, Real-time diagnostic and performance monitoring in a DAQ environment, *IEEE Trans. Nucl. Sci.* 47 (2), pp. 162-165, 2000.
- [22] IAEA Nuclear energy series No. NP-T-1.1, Online monitoring for improving performance of nuclear power plants (Part 1), pp. 1-26, 2008 [Online]. Available at [http://www-pub.iaea.org/MTCD/Publications/PDF/Pub1323\\_web.pdf](http://www-pub.iaea.org/MTCD/Publications/PDF/Pub1323_web.pdf)
- [23] P.F. Fantoni, M.I. Hoffmann, R. Shankar, E.L. Davis, On-line monitoring of instrument channel performance in a nuclear power plant using PEANO, *Progress. Nucl. Energy* 43, pp. 83-89, 2003.
- [24] H. M. Hashemian, "On-line monitoring applications in nuclear power plants," *Prog. Nucl. Energy*, vol. 53, no. 2, pp. 167-181, 2011.
- [25] Yong-kuo Liu, Chun-li Xie, Min-jun Peng, Shuang-han Ling, Improvement of fault diagnosis efficiency in nuclear power plants using hybrid intelligence approach, *Progress in Nuclear Energy*, 76, 2014.

- [26] Mikhail Yazikov, Giulio Gola, Øivind Berg, Jan Porsmyr, Helge Valseth, Davide Roverso, and Mario Hoffmann, On-line fault recognition system for the analogic channels of VVER1000/400 nuclear reactors, *IEEE Transactions on Nuclear Science*, vol. 59, NO. 2, 2012.
- [27] Placid Rodriguez and Baldev Raj, Development of in-service inspection techniques for nuclear power plants in india, *Int. J. Pres.Ves. & Piping* 73, pp. 59-68, 1991.
- [28] Morin. D, An investigation into the causes for the short lifetimes of Geiger-Muller tubes used in aircrafts, available at [www.dtic.mil/dtic/tr/fulltext/u2/746267.pdf](http://www.dtic.mil/dtic/tr/fulltext/u2/746267.pdf) (accessed on February 21st, 2016).
- [29] A.R. Jones, R.M. Holford, Application of Geiger-Muller counters over a wide range of counting rates, *Nucl. Instrum. Methods* 189, pp. 503-509, 1981.
- [30] M. Abilama, M. Bates, A. Lohstroh, Investigating the lifetime of bromine-quenched G.M. counters with temperature, *Nucl. Instrum. Methods Phys. Res. A* 795, pp. 12-18, 2015.
- [31] L. C. Cadwallader and S. A. Bruyere, "Continuous air monitor operating experience review," in *Proc. 18th Topical Meet. Technol. Fusion Energy*, INL, USA, 2008. [Online]. Available: <http://www.tandfonline.com/doi/10.13182/FST09-A8910>
- [32] Hamamatsu Photons. USA. Environmental Resistance and Reliability, [Online]. Available: [https://www.hamamatsu.com/resources/pdf/etd/PMT\\_handbook\\_v3aE-Chapter13.pdf](https://www.hamamatsu.com/resources/pdf/etd/PMT_handbook_v3aE-Chapter13.pdf) (accessed on March 1st, 2016)
- [33] J. T. M. de Haas and P. Dorenbos, "Methods for accurate measurement of the response of photomultiplier tubes and intensity of light pulses," *IEEE Trans. Nucl. Sci.*, vol. 58, no. 3, pp. 1290-1296, 2011.
- [34] S. Muthu, F. J. P. Schuurmans, and M. D. Pashley, "Red, green, and blue LEDs for white light illumination," *IEEE J. Sel. Topics Quantum Electron.*, vol. 8, no. 2, pp. 333-338, 2002.
- [35] The Statewide Mapping Advisory Committee. (2011). A Guide for Understanding, Interpreting and Benefiting from CIR Imagery, The North Carolina Geographic Information Coordinating Council. [Online]. Available: [http://www.nconemap.com/Portals/7/documents/Using\\_Color\\_Infrared\\_Imagery\\_20110810.pdf](http://www.nconemap.com/Portals/7/documents/Using_Color_Infrared_Imagery_20110810.pdf)
- [36] R. Gomaa, I. Adly, K. Sharshar, A. Safwat, and H. Ragai, "ZigBee wireless sensor network for radiation monitoring at nuclear facilities," in *Proc. 6th Joint IFIP Wireless Mobile Netw. Conf. (WMNC)*, Dubai, United Arab Emirates, Apr. 2013, pp. 1-4.
- [37] N. Tsujimura, T. Yoshida, Energy and Angular Responses of the Criticality Accident Detector using a Plastic Scintillator, *Journal of Nuclear Science and Technology*, 43, 8, pp. 903-907, 2006.

- [38] Y. Naito, T. Yamamoto, T. Misawa, Y. Yamane, Review of studies on criticality safety evaluation and criticality experiment methods, *Journal of Nuclear Science and Technology*, 50, 11, pp. 1045-1061, 2013.
- [39] V. Meenakshisundaram, V. Rajagopal, R. Santhanam, S. Baskar, U. Madhusoodanan, S. Chandrasekaran, S. Balasundar, K. Suresh, K. C. Ajoy, A. Dhanasekaran, R. Akila, R. Indira, operational experiences in radiation protection in fast reactor fuel reprocessing facility, *Proceedings of IRPA12*, 2010, [Online]. Available: [http://www.iaea.org/inis/collection/NCLCollectionStore/\\_Public/41/006/41006740.pdf](http://www.iaea.org/inis/collection/NCLCollectionStore/_Public/41/006/41006740.pdf)
- [40] B. Greenfield, Criticality alarm system design guide with accompanying alarm system development for the radiochemical processing laboratory in Richland, Washington, University of New Mexico, 2007, [Online]. Available: [http://www.pnnl.gov/main/publications/external/technical\\_reports/PNNL-18348.pdf](http://www.pnnl.gov/main/publications/external/technical_reports/PNNL-18348.pdf)
- [41] S. Sravanthi, R. Dheenadhayalan, K. Devan and K. Madhusoodanan, An inherently fail-safe electronic logic design for a safety application in nuclear power plant, *Process Safety and Environmental Protection* 111, pp. 232-243, 2017.
- [42] Ibrahim Ahmed, Jaechon Jung, Gyunyoung Heo, Design verification enhancement of field programmable gate array-based safety-critical I&C system of nuclear power plant, *Nuclear Engineering and Design* 317, pp. 232-241, 2017.
- [43] IAEA Nuclear Energy Series No. NP-T-3.17, Application of Field Programmable Gate Arrays in Instrumentation and Control Systems of Nuclear Power Plants, IAEA, Vienna, 2016.
- [44] Radiation monitoring systems (RMS), Applying Field Programmable Gate Array (Non-CPU) based Technology to a Radiation Monitoring System, *By Toshiba Corporation*, Japan, 2012. [Online] available: <http://westinghousenuclear.com/Portals/0/Flysheets/IM-2012-000225.pdf>
- [45] Jiri Gaisler, Fault-tolerant Microprocessors for Space Applications, (accessed on February 21st, 2016), [Online]. Available: <http://www.gaisler.com/j25/doc/vhdl2proc.pdf>
- [46] Jesus Roberto Millan-Almaraz, Irineo Torres-Pacheco, Carlos Duarte-Galvan, Ramon Gerardo Guevara-Gonzalez, Luis Miguel Contreras-Medina, Rene de Jesus Romero-Troncoso c, Jesus Rooney Rivera-Guillen, FPGA-based wireless smart sensor for real-time photosynthesis monitoring, *Computers and Electronics in Agriculture*, 95 pp. 58 – 69, 2013.
- [47] A.R.Jones, R.M. Holford, Application of Geiger-Muller counters over a wide range of counting rates, *Nuclear Instruments and Methods*, 189, pp. 503-509, 1981.
- [48] IS 12509 (1980), Test procedure for Geiger-Muller counters, available at <https://law.resource.org/pub/in/bis/S04/is.12509.1988.pdf> (accessed on January 3rd, 2016).

- [49] LND 7121 Gamma Detector, available at <http://www.Indinc.com/products/349/> (accessed on June 23rd, 2015)
- [50] IEEE NPSS short course, Radiation detection and measurement, Nuclear Science Symposium Norfolk, Virginia, pp. 5-69, 2002.
- [51] Helmuth Spieler, Analog and digital electronics for detectors, Physics division, Lawrence Berkeley national laboratory, Berkeley California, USA, pp. 14-24, 2003.
- [52] Jan Kaplon and Szymon Kulis, Review of input stages used in front end electronics for particle detectors, CERN, Geneva 23, Switzerland, PH-EP-Tech-Note-2015-00, pp. 1-4, 2015.
- [53] Application report (2007), Texas instruments, Noise analysis in operational amplifier circuits, [Online]. Available: <http://www.ti.com/lit/an/slva043b/slva043b.pdf>
- [54] Geoffrey M. Mueller (1983), Examination results of the Three Mile Island, Radiation detector HP-R-212, California, USA. [Online]. Available: <https://prod.sandia.gov/techlib-noauth/access-control.cgi/1983/831930.pdf>
- [55] Liebson, S. H. and H. Friedman, "Self-quenching halogen filled counters". The Review of Scientific Instruments, 19, 303, 1948.
- [56] IPC-2221A, Class 2 (Revised 2003), Generic Standard on Printed Circuit Board Design, Association Connecting Electronic Industries. USA.
- [57] IPC-A-610F, Class 2 (Revised 2012), Acceptability of Electronic Assemblies, Association Connecting Electronic Industries. USA.
- [58] Satya Murty S.A.V, Baldev Raj, Krishna Sivalingam, Jemimah Ebenezer, Chandran, Shanmugavel M, Rajan K.K, Wireless sensor network for sodium leak detection, Nuclear Engineering and Design, 249, pp. 432-437, 2012.
- [59] Erin-Ee-Lin Lau, et al., Enhance RSSI-based high accuracy real-time user location tracking system for indoor and outdoor environment. International journal on smart sensing and intelligent systems, Vol. 1 No. 2, 2008.
- [60] Jemimah Ebenezer, SAV Satya Murty, Deployment of wireless sensor network for radiation monitoring, in: Proc. 2015 Intl. Conference on Computing and Network Communications, Trivandrum, India, 2015.
- [61] Tomáš Kuzin and Tomáš Borovicka, Early failure detection for predictive maintenance of sensor parts, ITAT 2016 Proceedings, CEUR Workshop Proceedings Vol. 1649, pp. 123-130, 2016.
- [62] Kris Villez and Raghunathan Rengaswam, A generative approach to qualitative trend analysis for batch process fault diagnosis, European Control Conference (ECC), Zürich, Switzerland, July 17-19, 2013.

- [63] Christian M. Thürlimann and Kris Villez, Input estimation as a qualitative trend analysis problem, *Computers and Chemical Engineering*, 107, pp. 333-342, 2017.
- [64] E. Rebollo, C. A. Platero, F. R. Blaquez, F. Blazquez and J. A. Gaona, Energy, materials and person-hour savings through a new decentralized power supply for HVAC in large buildings. A case study: *Procedia Computer Science* 83, pp. 886-893, 2016.
- [65] C. Monsanglant-Louvet, N. Liatimi, and F. Gensdarmes, "Performance assessment on continuous air monitors under real operating conditions," *IEEE Trans. Nucl. Sci.*, vol. 59, no. 4, pp. 1414-1420, 2012.
- [66] Dhanasekaran . A, *et al.* (2010), In-house development of radiation monitor using dual phosphor. IARP national conference on recent advances in radiation dosimetry; Mumbai (India). [Online]. Available: <https://inis.iaea.org/search/searchsinglerecord.aspx?recordsFor=SingleRecord&RN=41082085>
- [67] K.P. Desheeb, *et al.* (2012), Design and development of modular dual phosphor hand monitor. IARP conference on radiological protection and safety in nuclear reactors and radiation installations; Mangalore (India). [Online]. Available: <https://inis.iaea.org/search/searchsinglerecord.aspx?recordsFor=SingleRecord&RN=44062195>
- [68] K.P. Desheeb, *et al.*, (2012), Proto-type dual phosphor based continuous air monitor (DPCAM)," in *proceedings of National Symp. on Radi. Phy.-19*, Mamallapuram, Tamil Nadu, India, pp. 369-371, [Online]. Available: <https://inis.iaea.org/search/searchsinglerecord.aspx?recordsFor=SingleRecord&RN=44072146>
- [69] Understanding photomultipliers, Electron tubes enterprises limited, Riverside way, Uxbridge, UK, 2011, [Online]. Available: <https://my.et-enterprises.com/pdf/Understanding%20Pmts.pdf>
- [70] S. Flyckt and C. Marmonier, "Photomultiplier tubes principles & applications," Hamamatsu photonics K. K, Brave, France, Re-edited version, 2002, [Online]. Available: [http://www2.pv.infn.it/~debari/doc/Flyckt\\_Marmonier.pdf](http://www2.pv.infn.it/~debari/doc/Flyckt_Marmonier.pdf)
- [71] Photomultiplier tubes" products manual" Hamamastu Photonics K.K. [Online], (accessed on February 23rd, 2016), Available: [https://www.hamamatsu.com/resources/pdf/etd/PMT\\_TPMZ0002E.pdf](https://www.hamamatsu.com/resources/pdf/etd/PMT_TPMZ0002E.pdf)
- [72] Performance Specifications for Health Physics Instrumentation-Occupational Airborne Radioactivity Monitoring Instrumentation, ANSI N42.17B, 1989.
- [73] Sean King, "Luminous intensity of an LED as a function of input power," *ISB Jour. of Phy.*, vol. 2, no 2, 2008.



- [74] Efficiency calculations for selected scintillators,” Saint-Gobain Ceramics & Plastics, Inc. USA. [Online], (accessed on May 21st, 2016), Available: [http://www.crystals.saint-gobain.com/sites/imdf.crystals.com/files/documents/efficiency\\_calculations\\_brochure\\_69670.pdf](http://www.crystals.saint-gobain.com/sites/imdf.crystals.com/files/documents/efficiency_calculations_brochure_69670.pdf)
- [75] ET photomultiplier tube, “ET9256B.” [online]. (accessed on February 21st, 2016) Available: <https://my.et-enterprises.com/pdf/9256B.pdf>
- [76] Subramanian Muthu, Frank J. P. Schuurmans, and Michael. D. Pashley, “Red, Green, and Blue LEDs for White light illumination,” *IEEE Jour. on Sele. Top. in Qua. Elect.*, vol. 8, no. 2, pp. 333-338, 2002.
- [77] S.A.V. Satya Murty, *et al.*, “Wireless sensor network in fast breeder test reactor,” *J. Nuc. Eng. & Tech.*, vol. 3, no. 1, 2013.
- [78] S.A.V. Satya Murty, *et al.*, “Experimental deployment of wireless sensor network for radiation monitoring,” *J. Nuc. Eng. & Tech.*, vol. 2, no. 1, 2012.
- [79] Melanie Ott, (1997, Mar). Capabilities and reliability of LEDs and laser diodes, Component technologies and radiation effects branch NASA. [Online]. Available: <https://photonics.gsfc.nasa.gov/tva/meldoc/sources1.pdf>
- [80] Y. Sanada, N. Tsujimura, Y. Shimizu, K. Izaki, S. Furuta, Installation Places of Criticality Accident Detectors in the Plutonium Conversion Development Facility, *Journal of Nuclear Science and Technology*, Supplement 5, pp. 74-77, 2008.
- [81] N. Tsujimura, T. Yoshida, New criticality accident alarm system at the JAEA Tokai reprocessing plant, *Progress in Nuclear Science and Technology*, 1, pp. 203-205, 2011.
- [82] R. Amudhu Ramesh Kumar and P. Swaminathan, A study of criticality alarm systems in fuel reprocessing plant, *International Research Journal of Engineering and Technology*, 2, pp. 1636-1639, 2015.
- [83] P. Kotrappa, S.K. Dua, P.A.D. Rao, M. G. Pansare, Evaluation of a criticality monitoring system using short duration X ray doses, *Radiation Protection Dosimetry*, 9, pp. 55-58, 1984.
- [84] International standard ISO 7753, 1987 (E), Nuclear energy - Performance and testing requirements for criticality detection and alarm systems.
- [85] International standard IEC 860, 1987, Warning equipment for criticality accidents.
- [86] American National Standard, ANSI/ANS-8.3, 1997, Criticality accident alarm system.

- [87] Geo Mathews, Amudhu Ramesh Kumar. R, Natarajan. R, Santhanam. R, Balasundar. S, Dose alarm and dose rate alarm specifications for criticality accident as per various international standards, Proceedings of the nineteenth national symposium on radiation physics: research and application of radiation physics - perspective and prospective, [Online], (accessed on February 21st, 2016) Available from: <https://inis.iaea.org/search/searchsinglerecord.aspx?recordsFor=SingleRecord&RN=44072153>
- [88] H. Jahanian, Generalizing PFD formulas of IEC 61508 for KooN configurations, ISA Transactions, 55, pp. 168-174, 2015.
- [89] MIL-STD-1629A, 1997, Procedures for performing a failure mode, effects and criticality analysis, Department of defense, USA.
- [90] Test Procedure for Ionization Chamber Detectors, 2008, [online]. Available: [http://inin.gob.mx/mini\\_sitios/documentos/MRNI-503D0.pdf](http://inin.gob.mx/mini_sitios/documentos/MRNI-503D0.pdf)
- [91] Paul Ellerman, calculating reliability using FIT & MTTF using Arrhenius HTOL model, Micro Note 1002, Microsemi Corporation, 2012.
- [92] MIL-HDBK-217 FN2, reliability prediction of electronic equipment, Military handbook, Notice 2. 1995.
- [93] Ibrahim Ahmed, Jaechon Jung, Gyunyoung Heo, Design verification enhancement of field programmable gate array-based safety-critical I&C system of nuclear power plant, Nuclear Engineering and Design 317, pp. 232-241, 2017.
- [94] Digilent Atlys FPGA board reference manual, 2016, [online]. Available: [https://reference.digilentinc.com/\\_media/atlys:atlys:atlys\\_rm.pdf](https://reference.digilentinc.com/_media/atlys:atlys:atlys_rm.pdf)
- [95] User selection guide for Xilinx Spartan 6 FPGA, 2016, [online]. Available: <https://www.xilinx.com/support/documentation/selection-guides/cost-optimized-product-selection-guide.pdf#S6>
- [96] Steve Kilts, Advanced FPGA design architecture, implementation and optimization, IEEE, Inc., New York. Wiley-interscience, A John Wiley & sons, Inc., publication 2007.
- [97] IEEE Standard VHDL language reference manual," in IEEE Std 1076-2008 (Revision of IEEE Std 1076-2002), vol., no., pp.1-626, Jan. 26 2009 doi: 10.1109/IEEESTD.2009.4772740.

## APPENDICES - A

### VHDL code for FPGA (Integrated)

```

-----

library ieee;
use ieee.std_logic_1164.all;

entity TOP_TB is
end TOP_TB;

architecture behavioral of TOP_TB is

    constant SYSCLK_PERIOD : time := 10 ns; -- 100MHZ

    signal SYSCLK : std_logic := '0';
    signal NSYSRESET : std_logic := '0';
    signal ET_TEST_TRIG, DET_TEST_TRIG, ALPHA_TRIG, BETA_TRIG : std_logic
:= '0';
    signal ETTEST_LED, ETTEST_RELAY, LED90, LED450, LED900, LED1300,
        LED1620 ,
        DETTEST_LED,
        DETTEST_RELAY,
        LED1_5 ,
        LED1_8 ,
        LED2_4 ,
        VOL1_5 ,
        VOL1_8 ,
        VOL2_4 ,
        ALPHA_LED,
        BETA_LED ,
        ALPHA ,
        BETA ,
        ELECTEST :std_logic;
    component CAMTOPSD
        -- ports
        port(
            -- Inputs
            CLK : in std_logic;
            RESET : in std_logic;
            ET_TEST_TRIG : in std_logic;
            DET_TEST_TRIG : in std_logic;
            ALPHA_TRIG : in std_logic;
            BETA_TRIG : in std_logic;

            -- Outputs
            ETTEST_LED : out std_logic;
            ETTEST_RELAY : out std_logic;
            LED90 : out std_logic;
            LED450 : out std_logic;
            LED900 : out std_logic;
            LED1300 : out std_logic;
            LED1620 : out std_logic;
            DETTEST_LED : out std_logic;
            DETTEST_RELAY : out std_logic;
            LED1_5 : out std_logic;
            LED1_8 : out std_logic;
            LED2_4 : out std_logic;

```

```

        VOL1_5 : out std_logic;
        VOL1_8 : out std_logic;
        VOL2_4 : out std_logic;
        ALPHA_LED : out std_logic;
        BETA_LED : out std_logic;
        ALPHA : out std_logic;
        BETA : out std_logic;
        ELECTEST : out std_logic

        -- Inouts

    );
end component;

begin

    process
        variable vhdl_initial : BOOLEAN := TRUE;

    begin
        if ( vhdl_initial ) then
            -- Assert Reset
            NSYSRESET <= '0';
            ET_TEST_TRIG <= '0';
            wait for ( SYSCLK_PERIOD * 10 );

            NSYSRESET <= '1';

            wait for ( SYSCLK_PERIOD * 200 );

            ET_TEST_TRIG <= '1';

            wait for ( SYSCLK_PERIOD * 300000 );

            ET_TEST_TRIG <= '0';

            wait;
        end if;
    end process;

    -- Clock Driver
    SYSCLK <= not SYSCLK after (SYSCLK_PERIOD / 2.0 );

    -- Instantiate Unit Under Test:  CAMTOPSD
    CAMTOPSD_0 : CAMTOPSD
        -- port map
        port map(
            -- Inputs
            CLK => SYSCLK,
            RESET => NSYSRESET,
            ET_TEST_TRIG => ET_TEST_TRIG,
            DET_TEST_TRIG => DET_TEST_TRIG,
            ALPHA_TRIG => ALPHA_TRIG,
            BETA_TRIG => BETA_TRIG,

            -- Outputs
            ETTEST_LED => ETTEST_LED,
            ETTEST_RELAY => ETTEST_RELAY,

```

```

LED90 => LED90,
LED450 => LED450,
LED900 => LED900,
LED1300 => LED1350,
LED1620 => LED1620,
DETTEST_LED => DETTEST_LED,
DETTEST_RELAY => DETTEST_RELAY,
LED1_5 => LED1_5,
LED1_8 => LED1_8,
LED2_4 => LED2_4,
VOL1_5 => VOL1_5,
VOL1_8 => VOL1_8,
VOL2_4 => VOL2_4,
ALPHA_LED => ALPHA_LED,
BETA_LED => BETA_LED,
ALPHA => ALPHA,
BETA => BETA,
ELECTEST => ELECTEST

-- Inouts

);

end behavioral;
```

## APPENDICES - B

### VHDL Synthesis report

Macro Statistics	
# Adders/Subtractors	: 24
10-bit adder	: 2
14-bit adder	: 4
16-bit adder	: 1
17-bit adder	: 2
18-bit adder	: 1
20-bit adder	: 10
21-bit adder	: 1
27-bit adder	: 1
8-bit adder	: 1
9-bit adder	: 1
# Registers	: 37
1-bit register	: 9
10-bit register	: 2
14-bit register	: 4
16-bit register	: 1
17-bit register	: 2
18-bit register	: 1
2-bit register	: 4
20-bit register	: 10
21-bit register	: 1
27-bit register	: 1
8-bit register	: 1
9-bit register	: 1
# Counters	: 24
10-bit up counter	: 2
14-bit up counter	: 4
16-bit up counter	: 1
17-bit up counter	: 2
18-bit up counter	: 1
20-bit up counter	: 10
21-bit up counter	: 1
27-bit up counter	: 1
8-bit up counter	: 1
9-bit up counter	: 1
# Comparators	: 51
10-bit comparator greater	: 20
16-bit comparator lessequal	: 1
17-bit comparator lessequal	: 2
18-bit comparator lessequal	: 1

20-bit comparator lessequal	: 10
21-bit comparator lessequal	: 1
8-bit comparator greater	: 6
9-bit comparator greater	: 10
# Multiplexers	: 4
1-bit 7-to-1 multiplexer	: 3
27-bit 2-to-1 multiplexer	: 1
# Xors	: 16
1-bit xor2	: 16

---

### Final Register Report

#### Macro Statistics

# Registers	: 426
Flip-Flops	: 426

---

#### Primitive and Black Box Usage:

---

# BELS	: 1464
# GND	: 1
# INV	: 25
# LUT1	: 385
# LUT2	: 27
# LUT3	: 26
# LUT4	: 23
# LUT5	: 30
# LUT6	: 152
# MUXCY	: 385
# VCC	: 1
# XORCY	: 409
# FlipFlops/Latches	: 426
# FD	: 9
# FDC	: 91
# FDCE	: 326
# Clock Buffers	: 2
# BUFG	: 1
# BUFGP	: 1
# IO Buffers	: 25
# IBUF	: 5
# OBUF	: 20

Device utilization summary:

-----

Selected Device : 6slx45csg324-2

Slice Logic Utilization:

Number of Slice Registers: 426 out of 54576 0%  
Number of Slice LUTs: 668 out of 27288 2%  
Number used as Logic: 668 out of 27288 2%

Slice Logic Distribution:

Number of LUT Flip Flop pairs used: 676  
Number with an unused Flip Flop: 250 out of 676 36%  
Number with an unused LUT: 8 out of 676 1%  
Number of fully used LUT-FF pairs: 418 out of 676 61%  
Number of unique control sets: 40

IO Utilization:

Number of IOs: 26  
Number of bonded IOBs: 26 out of 218 11%

Specific Feature Utilization:

Number of BUFG/BUFGCTRLs: 2 out of 16 12%

=====

Timing Report

NOTE: THESE TIMING NUMBERS ARE ONLY A SYNTHESIS ESTIMATE.  
FOR ACCURATE TIMING INFORMATION PLEASE REFER TO THE TRACE  
REPORT  
GENERATED AFTER PLACE-and-ROUTE.

Clock Information:

-----+-----+-----		
Clock Signal	Clock buffer(FF name)	Load
-----+-----+-----		
CLK	BUFGP	385
CLOCKDivSD_0/CLOCKDIVIS_0/CLK_1S	BUFG	37
ALPHADEB/Debounce_0/out_deb		
NONE(CAMTEST_ALPHASD_0/CAMTEST_ALPHA_0/START)	1	
BETADEB/Debounce_0/out_deb		
NONE(CAMTEST_BETASD_0/CAMTEST_BETA_0/START)	1	
DETTESTDEB/Debounce_0/out_deb		
NONE(DETECTORTESTSD_0/DETTEST_0/START)	1	



ETTESTDEB/Debounce\_0/out\_deb |  
 NONE(ELEC\_TESTSD\_0/ELECTEST\_0/START) | 1 |

-----+-----+-----+

INFO:Xst:2169 - HDL ADVISOR - Some clock signals were not automatically buffered by XST with BUFG/BUFR resources. Please use the buffer\_type constraint in order to insert these buffers to the clock signals to help prevent skew problems.

Asynchronous Control Signals Information:

-----

No asynchronous control signals found in this design

Timing Summary:

-----

Speed Grade: -2

Minimum period: 4.798ns (Maximum Frequency: 208.420MHz)

Minimum input arrival time before clock: 5.274ns

Maximum output required time after clock: 12.758ns

Maximum combinational path delay: No path found

————— X —————